Handheld Robotic Instruments for Endoscopic Neurosurgery

Emmanouil Dimitrakakis

A dissertation submitted in partial fulfillment

of the requirements for the degree of

Doctor of Philosophy

of

University College London.

Wellcome/EPSRC Centre for Interventional and Surgical Sciences

Department of Computer Science

University College London

August 25, 2023

I, Emmanouil Dimitrakakis, confirm that the work presented in this thesis is my own. Where information has been derived from other sources, I confirm that this has been indicated in the work.

Abstract

The Endoscopic Endonasal Approach, one of the best examples of endoscopic neurosurgery, allows surgeons to access the pituitary gland through the natural orifice of the nose. Recently, surgeons have introduced the Expanded Endoscopic Endonasal Approach for the treatment of tumours around a broader area at the base of the brain. Operating in this way, however, with standard tools which are lacking articulation, is technically very difficult and not widely adopted. Thus, these operations are only performed by few surgeons, in highly-specialised centres, limiting access to most patients. While detection rates have increased due to recent advances in medical imaging, clinical outcome has not improved in the last 20 years. Resultantly, it is widely recognised by patient groups and healthcare institutions that there is an urgent need for surgical innovation to advance clinical outcomes in patients with brain tumours. Robotic-assisted minimally invasive surgery allows for increased instrument articulation and surgeon dexterity in operative workspaces with restricted access. Thus, it could be deemed as a suitable solution for these demanding approaches.

This thesis explores the development of novel handheld robotic instruments for endoscopic neurosurgery. Initial work focused on the design of a miniature spherical-joint, robotic end-effector with the aim to expand the surgeon's operative workspace and enhance their dexterity. To manipulate the end-effector, two concept handle prototypes were developed to cater to a large set of ergonomic literature suggestions. The two novel handles were compared as part of a pre-clinical randomised crossover user-study. This pre-existing work laid the foundation for a robotic system consisting of an ergonomically designed handheld controller, and a series of 3mm detachable end-effectors that was tested in a pre-clinical cadaver study and a multi-surgeon comparison phantom study. Peer-reviewed results on every developmental step suggest that the intended robotic instruments are a promising step towards developing appropriate instruments to drive endoscopic neurosurgery adoption.

Impact Statement

The Endoscopic Endonasal Approach, one of the best examples of endoscopic neurosurgery, allows surgeons to access the pituitary gland through the natural orifice of the nose. Recently, surgeons have also described an Expanded Endoscopic Endonasal Approach which allows access to the entire ventral skull base, from the frontal sinus to the second cervical vertebra. Deploying these approaches has plenty of advantages over traditional open-skull surgery, such as minimised brain-tissue damage and reduced recovery time. However, operating in this way, with non-articulated tools, is technically difficult and not widely adopted. Thus, not many patients enjoy the benefits of minimally invasive neurosurgical approaches, and neurosurgeons often have to resort to more invasive procedures.

A solution to the problem of constrained operative spaces and limited dexterity could be handheld robotic instruments. The enhanced robotic articulation can increase the surgeon's dexterity, allowing them to reach previously unattainable areas and perform delicate manoeuvres that were impossible before. This can increase the tumour resection margins, reduce complications, and improve patient recovery and quality of life. Additionally an ergonomic handheld design can decrease physical fatigue and strain associated with these demanding operations. This addresses an important fact that 80% of surgeons have succumbed to a work-related injury or illness because of sustaining awkward positions throughout lengthy operations.

Handheld robotic instruments are associated with decreased purchasing and maintenance costs, and can be easily incorporated into the operating theatre. Their deployment can result in wider clinical adoption of keyhole techniques something that has the potential to cut down referral costs with more hospitals being able to offer highly specialized keyhole approaches. Additionally, the occurrence of repeat-procedures due to complications or incomplete tumour resection can be reduced, freeing up hospital beds and related resources that could be used for other patients.

The handheld robotic instruments developed in this thesis could also be applied to other surgical approaches that share the same difficulties with minimally invasive neurosurgery such as the constrained operative workspace. These could be neighbouring disciplines, such as Ear, Nose, and Throat surgery, with Functional Endoscopic Sinus Surgery and Trans-oral Robotic Surgery. Simultaneously, these instruments could aid in distant disciplines as well, such as in Transanal Endoscopic Microsurgical procedures.

The technology that is presented in the next few chapters is also the basis for the foundation a UCL spin-out company that develops handheld robotic instruments for minimally invasive neurosurgery. The aim of this start-up is to translate this technology into the operating theatre and increase the clinical adoption of keyhole operative techniques in neurosurgery. For this, a substantial venture capital seed investment has been secured, and a strong advisory network of robotic surgery veterans has been established.

Acknowledgements

First and foremost, I would like to thank my two supervisors, prof. Dan Stoyanov and Mr. Hani Marcus, who have been guiding me throughout this journey. I'll always be grateful to Dan for giving me the opportunity to join this group and for providing the means and access to conduct this research. Even more importantly, his advice shaped my progression, both in research and in skill-set, and drastically improved my ability for problem-solving. I'm also grateful to Hani, it has been a privilege and honour working with him. Hani would always always help me when I asked, and hosted me into his operating theatre more than enough times, giving me insight into the clinical problem that no other resource could ever provide. Finally, to both I want to say a huge thank you for the guidance these past few years, and for trusting me to lead our journey ahead with the commercialization of our research.

Then, I would like to thank all my colleagues and collaborators at the Wellcome / EPSRC Centre for Interventional and Surgical Sciences, and at University College London. This work would not have been possible without them. A special thanks to George, who has been actively contributing to this work from day one, and will continue to do so. The things that George taught me are probably more than the things he didn't. A big thank you also to Lukas, whose help was pivotal at a point in my PhD when I felt there is no light at the end of the tunnel. To my co-authors, Holly, Nicola, Danyal and Petros, thank you for your efforts that significantly improved the quality of this work.

A special thanks to Ago, the first person I met at UCL, and Evans, for the advice they've been giving me ever since I joined. A huge thank you to the WEISS admin team, and especially Clare who at this stage could very well have been a co-PI, for always helping me with every matter I would present to them, no matter how complicated or time-sensitive it was. Last, but by no means least, a special thanks to all the friends I've made within this very sociable group. To Patrick who's been a model to follow, to Claudia and Anita for having shared this experience with me, to Lydia mostly for the memes really, to Krittin,

Dimitris, Keshav, Ema and Bea for spending all these TA hours together.

I would also like to thank my family and friends. My parents, Michael and Popi, who have always believed in me and have provided me with every opportunity to succeed, my sisters Agapi and Rafaella, who will always be there to support me and make me laugh, and my older brother Giorgos, for being my role model from the day I was born. A big thank you to my mates, other Giorgos, Dimitris and Sotiris, whom with I have been memeing since 2013, and to big Chris for always welcoming me in Athens. A special mention should go to my team, Panathinaikos, for teaching me that when you're down, there's no other way to go but up.

Concluding these acknowledgements, I would like to especially thank my partner throughout the PhD Matina, who recently accepted me as her fiancé, with no revisions. We've been through all the ups and downs together, and I could have not imagined it any other way.

Abbreviations

For clarity purposes, this section explains the acronyms used in the next chapters.

- CNC - Computer Numerical Control
- DH - Denavit-Hartenberg convention
- DMLS - Direct Metal Laser Sintering
- DoF - Degrees-of-Freedom
- EEA - Endoscopic Endonasal Approach
- EEEA - Expanded Endoscopic Endonasal Approach
- ENT - Ear, Nose and Throat surgery
- FMH - Forearm-Mounted Handle
- MIS - Minimally Invasive Surgery
- MISTELS - McGill Inanimate System for Training and Evaluation of Laparoscopic Skills
- MRI - Magnetic Resonance Imaging
- NOTES - Natural Orifice Translumenal Endoscopic Surgery
- PLA - Polylactic Acid plastic
- RAMIS - Robotic-Assisted Minimally Invasive Surgery
- RCM - Remote Centre of Motion
- RJH - Rotating Joystick-body Handle
- ROS - Robot Operating System
- RULA - Rapid Upper Limb Assessment
- SLA - Stereolithography
- SURG-TLX - Surgery Task Load Index questionnaire
- TEM - Transanal Endoscopic Microsurgery

- UKA - Unicomparmental Knee Arthroplasty
- UCL REC - University College London Research Ethics Committee

Contents

1 Introduction **24**

1.1 Clinical motivation 24

1.2 Research motivation 27

1.3 Aims and objectives 28

1.4 Thesis Outline 30

1.5 Publications 31

2 Robots for neurosurgery and handheld robotic systems **37**

2.1 Overview of the system 37

2.2 Endonasal approach operative workflow 38

2.3 Robots for minimally invasive neurosurgery 40

2.4 Robotic end-effector for minimally invasive surgery 41

2.4.1 Tendon-driven robotic end-effectors 42

2.4.2 Spherical joint robotic end-effectors 44

2.5 Handheld robots for minimally invasive surgery: Review on Ergonomics . . 46

2.5.1 Optimal design considerations 48

2.5.2 Papers search methodology 49

2.5.3 Handheld robotic instruments for surgery 50

2.5.4 Ergonomic considerations in handheld surgical robots 55

2.5.5 Ergonomically designed tools and procedural ergonomics 58

2.5.6 Bridging the gap between efficacy and ergonomics 59

2.6 Discussion 61

3 A robotic end-effector for the Expanded Endoscopic Endonasal Approach **63**

3.1 Introduction 63

3.2 Proposed tool implementation 64
3.2.1 Design and fabrication 64
3.3 Kinematic analysis 68
3.3.1 Forward kinematics 68
3.3.2 Workspace analysis 69
3.3.3 Inverse kinematics and tendon lengths 72
3.4 Experimental Evaluation 76
3.4.1 Workspace and repeatability study 76
3.4.2 Structural integrity study 80
3.4.3 Preliminary findings 83
3.5 Improvement of the end-effector joint-design 84
3.6 Miniaturization of the tendon-routing system 87
3.7 Discussion 90

4 A handheld controller for the robotic end-effector **93**
4.1 Introduction 93
4.2 Development of a forearm-mounted handle 94
4.2.1 Design criteria 94
4.2.2 Handle design 95
4.2.3 Prototype fabrication 97
4.2.4 Experimental methods 98
4.2.5 Preliminary findings 101
4.3 Development of a rotating joystick-body handle 105
4.4 Comparing the two handles during a randomised crossover user-study . . . 108
4.4.1 Evaluation and preference questionnaire 112
4.4.2 Performance evaluation 113
4.4.3 RULA ergonomic assessment 118
4.4.4 Surg-TLX questionnaire 120
4.4.5 Preliminary findings and concept selection 121
4.5 A functional ergonomic handheld controller 123
4.6 The handheld controller electronics box 126
4.7 Discussion 127

5 Evaluation of the handheld robotic system for Endoscopic Neurosurgery 131

5.1 Introduction . . . 131

5.2 Robotic system . . . 132

5.3 Experimental evaluation . . . 134

5.3.1 Workspace, structural integrity, and force delivery . . . 134

5.3.2 Phantom feasibility test . . . 135

5.3.3 Cadaver pilot study . . . 136

5.3.4 Comparative phantom study . . . 137

5.4 Results . . . 140

5.4.1 Workspace, structural integrity, and force delivery . . . 140

5.4.2 Phantom feasibility test . . . 142

5.4.3 Cadaver pilot study . . . 142

5.4.4 Comparative phantom study . . . 145

5.5 Discussion . . . 148

6 Discussion 151

6.1 Conclusions . . . 151

6.2 Contributions . . . 152

6.3 Limitations . . . 154

6.4 Future work . . . 156

Bibliography 158

List of Figures

1.1 The NeuroMate (top-left), the Pathfinder (top-right), the NeuroArm (bottom-left) and the Neurobot (bottom-right) surgical systems. 25
1.2 The Endoscopic Endonasal Aproach (left), and the Expanded Endoscopic Endonasal Approach (right) 26
1.3 Concept rendering of the proposed robotic tool. The red spheres represent tumors on the pituitary gland (center of the brain) and besides it. The articulation of the robot can aid in the removal of tumors from these areas, besides the centre of the brain, that often are in places where conventional tools have difficulty in reaching, or can not reach. 28
1.4 Diagram of the thesis outline. The indicated numbers refer to the corresponding contributions. 31

2.1 The handheld robotic instrument deploying a grasping tool, alongside three other articulated tools; a flat dissector, a ring-curette, and an endoscope. . . 37
2.2 (a). (Top to bottom) The articulated end-effectors, namely the ring-curette, the grasper, the endoscope, and the spatula dissector, and (b). The articulated endoscope inside a pituitary anatomy phantom at three different angles (top row), alongside the accompanying views from the camera (bottom row). The dark spot seen in the top row of pictures is a magnet used for the phantom assembly, not to be confused with the simulated tumor evident in the bottom pictures. 38
2.3 A concentric tube robotic platform (left), and a 4 DoF elastic elements robotic instrument (right), intended for the endonasal approach. 41
2.4 The ROSA One Brain robotic system intra-op by the patient side. 42
2.5 An articulated tendon-driven surgical end-effector (left), and a continuum tendon-driven surgical end-effector (right). 44

2.6 A surgical end-effector with a spherical joint that is part of a larger continuum body (left), an end-effector with two ball-joints that contribute towards an extended bending radius (middle), and an end-effector with an assembly of ball joints and plates (right). 47

2.7 The search methodology that was followed to find published works on the subject of handheld surgical robotic instruments. 50

2.8 Some of the reviewed robotic systems presented in this chapter. **Added articulation:** A forearm-mounted intuitively controlled handheld robot, a system that enables handheld coordination of both an endoscope and two CTRs, a handheld CTR capable of 6-DOF manipulator, and a handheld robotized needle holder. **Hand-tremor compensation:** The Micron active intelligent handheld microsurgical instrument, a compact fiber bragg grating force-sensing micro-forceps incorporated with the Micron, and a parallel manipulator for the suppression of physiological hand tremor **Force-feedback:** A force-measuring capable handheld robotic tool, a tactile capacitive sensor and tactile display with a dielectric elastomer equipped instrument, and a servo-assisted robotic handle. **Navigation and depth-estimation:** The Navio handheld robotic system, a handheld active steering robotic system for curved drilling and milling, and a handheld steerable surgical drill with a novel miniaturized articulated joint module. 53

2.9 Pie-chart breaking down the number of devices that were ergonomically designed, and the number of devices that lead to improved procedural ergonomics. 60

3.1 The channels that tendons pass through (left) and their termination points (right). Blue is for the pitch axis DoF, red is for the yaw axis DoF and green is for the gripper DoF. 65

3.2 The antagonistic configuration that controls each DoF. The arrows show the tendon movement direction. 65

3.3 CAD renderings (left) and SLA-printed implementation of the end-effectors (right) 66

3.4 CAD renderings of the rerouting mechanism with the tendon insertion points and the actual tendon routing. Red is for the first DoF, blue - light blue is for the second DoF and green - light green is for the third DoF. . . . 67

3.5 Physical relationship between one of the robot joints and its corresponding tendons. . . . 67

3.6 (Left) CAD renderings of the test-bench system and the end-effector. The top-left circled assembly indicates the $3mm$ diameter rigid stainless steel shaft on which the tendons terminate, whereas the top-down circled assembly is an exploded view of the end-effector. (Right) Implementation of the test-bench system and the end-effector. . . . 68

3.7 The robotic end-effector joint frames. . . . 69

3.8 Reaching areas beneath the pituitary gland with a simulated traditional instrument (left), and with the proposed robotic end-effector (right). Red points represent points the conventional tool can not reach whereas the green points represent the points the tools can reach. Red Xs represent no-go areas besides the pituitary gland. . . . 70

3.9 3D model of a cranial CT scan used to determine the available workspaces during EEEA. The artificial channel shown inside the circled areas represents the channel that the surgeon creates during surgery and grants access to the pituitary gland area. . . . 70

3.10 DoF coordinate frames of the traditional non-articulated tool (left), and of the suggested robotic end-effector (right). The robotic end-effector comprises of an additional two articulated joints represented by frames (x_0, y_0, z_0) and (x_1, y_1, z_1). . . . 71

3.11 Workspace comparison between the proposed robotic end-effector (green) and a traditional, non-articulated tool with the same dimensions (blue), from three different viewing angles. . . . 72

3.12 The 6 channels on the spherical joint where the tendons pass through. The exact same pattern is followed on the base of the end-effector, whereas only tendons 5 and 6 arrive at the upper part of the gripper. . . . 73

3.13 Visual representation of how the length of tendon 2 is computed for two different joint-spaces j and j'. . . . 75

3.14 Flow diagram showing the interaction between the two ROS nodes of the tracking experiment. 77

3.15 The robotic end-effector holding the NDI tracking markers attachment (left), and inside a training phantom to illustrate insertion during the robotic EEEA procedure (right). 78

3.16 Comparison between the boundaries of the theoretical workspace (red) and the measured workspace (blue). 79

3.17 The experimental setup to test the end-effector's structural integrity. 81

3.18 (Left to right, top to bottom) The end-effector at its resting position, and supporting objects of 100g, 200g, 500g, 600g and 700g mass. The deflection angle is also evident in the figure. 82

3.19 Design differences between the initial end-effector presented in Chapter 3 and the newly developed end-effector presented in this chapter. 85

3.20 The discrete steps from the initial end-effector design that lead to the finalised end-effector design. 86

3.21 (a). The miniature grasper end-effector, and (b). The tendon-routing of the 3 DoF. 86

3.22 The articulated end-effectors developed as part of the novel robotic system. From left to right, a dissector, an endoscope, a grasper, and a ring-curette. . 87

3.23 Various tendon-routing sub-system designs. (a). System combining bevel gears and capstans, (b) Previous system comprised of a three parts assembly and its tendon-routing paths, and (c). Preliminary differential-drive system and its tendon-routing paths. 87

3.24 (a). The tendon-routing system for a single DoF with the other two DoF tendons following similar routing paths, (b). The differential gearing system, highlighted in grey, with tendons for a single DoF, (c). The coupling on the handheld controller side, and (d). The coupling on the end-effector side. 89

3.25 (a). The routing system inside an open end-effector casing, and (b). The fully assembled grasper end-effector. 90

3.26 Comparison between an end-effector manufactured with DMLS and an end-effector manufactured with CNC machining. 92

4.1 A rendering of the suggested intuitive handle with the coordinate frames of the handle joints (left), and the corresponding coordinate frames of the robot-joints (right). 96

4.2 The coordinate frames of the end-effector that the handle is intended to manipulate (left), and the corresponding frames on the wrist (right). 96

4.3 (a). The hand at its resting position, and (b). The resting position of the handle coincides with the resting position of the wrist. 97

4.4 (a). Exploded view of the proposed handle rendering, and (b). its 3D-printed implementation (right). 98

4.5 (a). Rendering of the modified surgical forceps, (b). Rendering of the endoscope, and (c). Rendering of the physical nasal channel constraint, with the artificial channel circled, a whole skull for reference, and the 3D-printed phantom constraint.. 99

4.6 The custom-built simulated surgical task using the conventional tool (upper row) and the proposed handle (bottom row). 100

4.7 Comparison graph of the success rates and learning curves of the two instruments. 102

4.8 The RULA score decision trees. 102

4.9 The SURG-TLX questionnaire scores. 103

4.10 (a). Rendering of the rotating joystick-body handle prototype with the coordinate frames of the handle joints and the axis of rotation of the rotating body (right), and the corresponding coordinate frames of the robot-joints (left). The roll robot DoF is carried out by the surgeon's hand. (b). The ergonomic specifications analysed in Section 4.3 reflected on the handle design, and (c). A cross-section sketch of the device that reveals its inner structure. 107

4.11 (a). The seven discrete joystick positions on the same 3D-printed rotating joystick-body handle prototype. The axis of rotation of the joystick-body and the angle of each position highlight the rotating function. (b). The hand at its resting position, (c). (left to right and top to bottom) The handle held by a small left hand, a small right hand, a large left hand, and a large right hand, and (d). Thumb adduction (left), thumb abduction (right). 108

4.12 (a). Experimental setup with renderings matched to their respective prototypes. The FMH and RJH are shown on the left side of the image, and the conventional tool that was used as a comparison on the right. Also on the right, the endoscope prototype that was used to manipulate the camera is showcased, alongside the 3D-printed skull constraint. (b). The simulated environment when a researcher is carrying out the peg-transfer task, and (c). The researcher using the prototypes when carrying out the peg-transfer task. 110

4.13 The device sequence for each participant represented by a different color. . 111

4.14 The handle evaluation and preference questionnaire that the participants were asked to fill-in after they inspected the devices and before carrying out the tasks with them. 112

4.15 The completion rate during all 10 attempts for each of the 9 participants, for (a) the conventional tool, (b) the RJH, and (c) the FMH. The red crosses are the outliers of the box-plots, while the black and white x-marks in sub-figures are the mean average values of the completion rate per participant and the completion rate per attempt respectively. 114

4.16 The mean completion rate for all 9 participants for each of the 3 devices. The red crosses are the outliers of the box-plots. 115

4.17 The successful attempt rate for each of the 9 participants, and for each of the 3 devices. 116

4.18 The mean time it took all participants to successfully transfer each ring. . . 116

4.19 The learning curve of (a) the conventional tool, (b) the RJH, and (c) the FMH, presented as the relationship between the completion rate for all 9 participants for each of the 10 attempts. The red crosses are the outliers of the box-plots, while the black and white x-marks in sub-figures are the mean average values of the completion rate per participant and the completion rate per attempt respectively. 117

4.20 The RULA posture scores for all 9 participants for each posture, and for (a) the conventional tool, (b) the RJH, and (c) the FMH. The red crosses are the outliers of the box-plots. 119

4.21 The overall RULA score for each participant, and for each of the 3 devices . 120

4.22 The mean SURG-TLX scores for each individual SURG-TLX dimension, and for each of the 3 devices 120
4.23 Renderings of (a). The concept handheld design suggested in Section 4.3 which was tested in simulation, and (b). The finalised handheld instrument design after electronics, motors, and end-effectors were incorporated to offer functionality. 125
4.24 The rotating joystick-body in its 5 discrete positions with a rotating step of 15^o. 125
4.25 (a). Handheld controller design incorporating a 2-axis rotational joystick module, and (b). Handheld controller design incorporating a 2-axis translational joystick module. 126
4.26 (a). Cross-section of the handheld controller incorporating the motor controllers, and (b). Cross-section of the handheld controller with motor controllers housed outside of the device. 127
4.27 The control box housing all the electronics. 127

5.1 (a). The robotic prototype with the handleld controller and the robotic end-effector disengaged, (b). Various articulated end-effectors, (c). The handheld controller, and (d). The fully assembled robotic system alongside its alternative end-effectors and control-box. 133
5.2 The system context diagram of the robotic system. 134
5.3 (a). Structural integrity test experimental setup, and (b). Phantom feasibility test experimental setup. 136
5.4 The novel robotic instruments that were tested during the cadaver pilot study. Left to right: control box, handheld controller, and articulated tools. . 137
5.5 a) The eTSA phantom tumour, b) the standard instrument inside the phantom environment, and c) the articulated end-effector inside the phantom environment. 138
5.6 The operative setup during the comparison phantom study when using (a) the standard instrument, and (b) the novel handheld robotic instrument. . . . 139
5.7 (a). The grasper end-effector at two different joint-space limits, (b). The ring-curette end-effector at two different joint-space limits. 140
5.8 The overall joint-spaces of both end-effectors. 141

5.9 The ring-curette end-effector maintaining its pose holding a 500g weight. . 142
5.10 The view from the USB-endoscope during the phantom feasibility study where the silicone tumor at the pituitary gland region was removed with the use of (a). The robotic grasper, (b). The robotic ring-curette, and (c). The robotic dissector. 143
5.11 (a). The surgical setup with the introduction of the novel robotic instrument, and (b). (left to right) A standard suction tool, and the robotic curette in different poses interacting with soft tissue. 144
5.12 The miniature end-effector after the completion of the cadaver pilot study. In this figure, a snapped tendon strand can be seen. 144
5.13 The surgical setup with the introduction of the robotic endoscope, alongside endoscopic views. Concurrently with this instrument, a robotic curette as well as a standard neuroendoscope were used. 146
5.14 (a). Concurrent usage of the robotic ring-curette and the robotic endoscope, while in visual guidance from the standard neuroendoscope, (b). View of the sellar anatomy using the articulated endoscope, in its initial pose, and (c). View of the sellar anatomy using the articulated endoscope, having it actuated on the yaw axis. 146
5.15 Primary outcome measure represented by participant performance, grouped by attempt. 147
5.16 Extent of resection on the first and fifth attempts, grouped by instrument. . . 148
5.17 Extent of resection, grouped by attempt and experience. 149

6.1 Renderings of the handheld controller and the articulated instruments. . . . 152
6.2 Design components that could be contributing to the mechanical backlash. . 155

List of Tables

2.1 Design considerations that could lead to an ergonomic handheld surgical robot. 49

2.2 Summary of all reviewed papers, their categories, intended aim, and target surgical operation. 51

2.3 The optimal design considerations, and the papers that presented robotic instruments that were developed following them. 58

3.1 The DH parameters of the 3.6*mm* robotic end-effector. 69

3.2 The STD values of the 19 different joint positions. 79

3.3 The results of the structural integrity study. 82

4.1 Design criteria for the novel forearm-mounted handle prototype. 95

4.2 Comparative table between the conventional tool and the proposed handle. . 101

4.3 Design considerations that could lead to an ergonomic handheld surgical robot. 106

5.1 The measured forces applied at the tip of the end-effectors in the ZZ' and YY' directions while at discrete joint-spaces, at which angular deflection was noticeable. These forces represent the maximum forces each end-effector can withstand at its tip when applied in that particular direction. . . 141

5.2 The forces measured by the F/T sensor when the end-effectors were moved to discrete joint-spaces. 143

5.3 The post-cadaver study questionnaire, and the surgeon replies 145

Chapter 1

Introduction

1.1 Clinical motivation

Robotic-Assisted Minimally Invasive Surgery (RAMIS) has had a great impact in operating theatres since it allows for precise and accurate motions while reducing the surgeons' learning curve [1]. This means that more surgeons can perform RAMIS when they might otherwise resort to open surgery [2]. With the introduction of robotics into the surgical theatre, a number of specialties, such as urology, gynaecology, abdominal and cardiothoracic surgery, have integrated robotic technologies into their procedures augmenting the capabilities of the surgeon while improving patient outcomes. Lately, an increasing amount of surgical procedures have deployed or started deploying robotic devices, with neurosurgery being at the forefront of these advancing technologies.

Due to its delicate subject matter and challenging operations, neurosurgery has always been in need for adapting new techniques and technologies. One such adaptation is surgical robotics, both in brain and spine applications [3]. Especially for brain surgery, a number of commercial robots have already made their appearance in surgical theatres. Such examples are the Neuromate (Renishaw Mayfield, Lyon, France) [4] and the Pathfinder (Prosurgics, High Wycombe, United Kingdom) [5] which are stereotactic robots used for several neurological applications such as deep brain stimulation and endoscopy. Another example of a neurosurgical robot is the NeuroArm (University of Calgary in 2001) [6], which is a magnetic resonance imaging (MRI) compatible robot used in cranial neoplastic cases [7]. All aforementioned systems are depicted in Fig. 1.1.

Although the majority of neurosurgical robots are stereotactic, technological advances in image guidance, endoscopy, and laparoscopic instruments have led into the development of robotic tools for minimally invasive neurosurgery. One such system is the NeuroBot, a

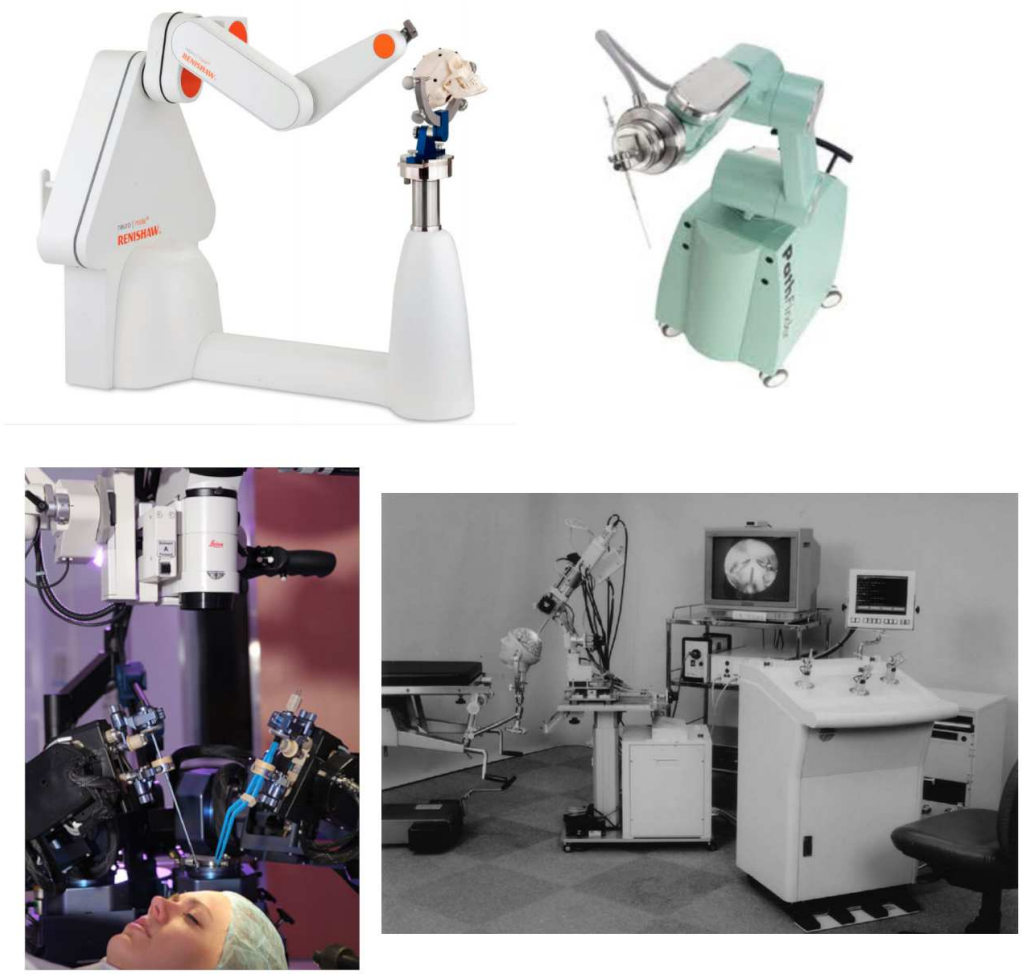

Figure 1.1: The NeuroMate (top-left), the Pathfinder (top-right), the NeuroArm (bottom-left) and the Neurobot (bottom-right) surgical systems.

less invasive and telecontrolled micromanipulator system with a rigid neuroendoscope and three manipulators [8]. However, the use of robotics in 'keyhole' neurosurgical approaches is still rather limited. There are more than 30 systems that have been developed for neurosurgical procedures, but only a few are intended for minimally invasive neurosurgery and none of them enjoys wide clinical use [9].

A procedure that would widely benefit from robotic technology and the enhanced articulation it offers is the Endoscopic Endonasal Approach (EEA), shown in principle in Fig. 1.2. The EEA is a minimally invasive neurosurgical technique that is performed via an anterior sphenoidotomy and aims at the removal of sellar and parasellar lesions [10] with the use of an endoscope and standard rigid instruments.

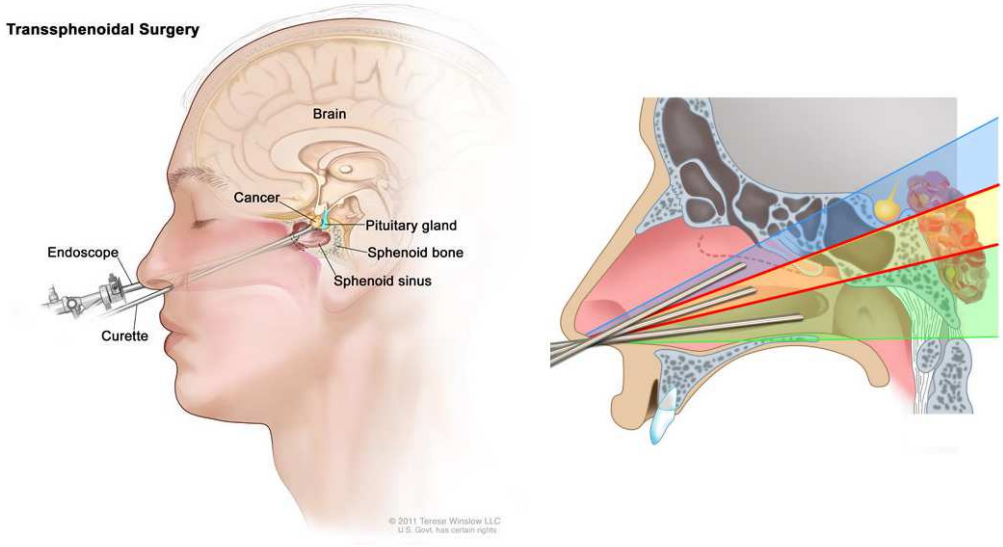

Figure 1.2: The Endoscopic Endonasal Aproach (left), and the Expanded Endoscopic Endonasal Approach (right)

In recent years, there has been an increased interest in the Expanded Endoscopic Endonasal Approach (EEEA), also depicted in Fig. 1.2 that expands the EEA areas of interest to include the regions from the cribriform plate of the anterior cranial fossa to the foramen magnum in the anteroposterior plane [11]. Although a promising alternative to transcranial approaches which require craniotomies and brain retraction, the EEEA comes with its limitations. In [12], a cohort of neurosurgeons were asked about these technical challenges, with 74% of them identifying the limited surgical dexterity that the standard non-articulated instruments offer as the biggest challenge of this procedure.

Fittingly, the EEEA has been described by experts as “operating in a matchbox using chopsticks”, and surgical outcomes have not improved for 20 years [13]. In the case of Cushing’s disease for example, one of the deadliest pituitary tumours, it is found that despite improvements in radiological detection rates, there have been no changes in clinical outcomes for at least the past two decades [14].

Due to the complexity of these operations, they are performed by few surgeons, working in highly specialised centres and in selected geographical regions, limiting access to most patients. It is therefore imperative to find a solution that can aid endoscopic neurosurgery by enhancing the surgeon’s capabilities, and, thus, increasing its efficacy and safety. These minimally invasive approaches will then be applicable to more clinical cases and a larger patient population can enjoy their benefits.

1.2 Research motivation

While robotic surgery has steadily been increasing in popularity, even referred to as the gold standard for some urological operations such as radical prostatectomy [15], use in endoscopic neurosurgery has been very limited [16]. Commercial tele-operated robotic systems which normally enjoy wide adoption cannot cater to the constrained spaces of these advanced operations. As a result, such systems, that can enhance the neurosurgeon's dexterity via remote-control, are not used in neurosurgery [17].

Furthermore, patient involvement has suggested that even if these telesurgical robots could overcome the technical challenges that make them unsuitable for neurosurgery, there are additional considerations that could hinder their deployment. In a survey of patients undergoing cranial surgery, the overwhelming majority expressed a preference towards handheld robotic systems over tele-operated robots [18]. Other than patient preference, a handheld device, when compared with a tele-surgical system, offers similar capabilities at a lower purchasing and maintenance cost, is more easily incorporated into the workflow, and generally is associated with smaller learning curves [19], [20]. Such findings, alongside the notion that robotic technology could aid in endoscopic neurosurgery, defined the requirements of the novel technology developed in this thesis.

To date, no handheld robotic device that can be used in constrained operative workspaces, such as the ones of minimally invasive neurosurgery, exists commercially or in a research context. This could be explained by the technical challenges associated with developing such devices that dishearten the major robotic surgery companies and research centres to endeavour in this development approach.

There are three main technical challenges associated with the development of handheld neurosurgical robotic devices. First, the distal-end miniaturization that the operative workspace requires. Here, the main challenge is reducing the end-effector size, while maintaining the required capabilities such as force-delivery. Second, the compact device form-factor. A balance needs to be maintained between functionality and ergonomics as it's intended to be used in a handheld manner without causing the surgeon any fatigue or strain. Finally, the absence of a trocar-port that is often the case in surgeries that utilise natural orifices. Most surgical robot shafts rest on a trocar-port that provides actuation around a remote-centre-of-motion (RCM). When the entry-point is a natural orifice, this RCM is replaced with the physical channel, in this case the nasal channel, that provides access to the

patient's body. Thus, the shaft cannot rest against this entry-point, but rather requires free space movement.

Coming up with solutions to these problems, especially when introduced into the clinical context of endoscopic neurosurgery, requires invention. To this day, handheld robotic solutions for constrained operative spaces remains a largely unsolved research problem. However, if developed further, they can provide the benefits of robotic surgery at a fraction of the cost and operative burden, and thus, make an immediate impact in the operating theatre. This potential make these devices an attractive research and commercialization proposition.

1.3 Aims and objectives

The aim of this thesis is to address these technical challenges by developing a novel handheld robotic instrument for the EEEA. A concept rendering of this robotic instrument, and how its end-effector could be used to reach multiple areas on the skull-base are shown in Fig. 1.3.

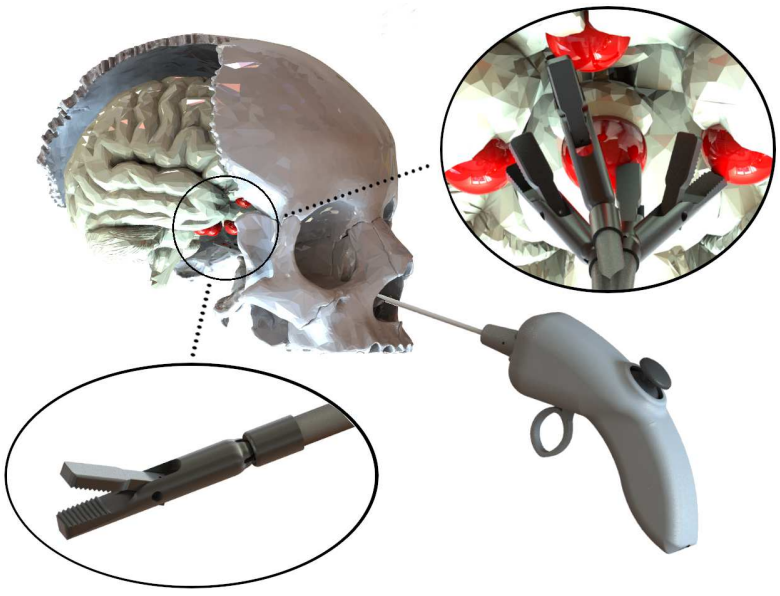

Figure 1.3: Concept rendering of the proposed robotic tool. The red spheres represent tumors on the pituitary gland (center of the brain) and besides it. The articulation of the robot can aid in the removal of tumors from these areas, besides the centre of the brain, that often are in places where conventional tools have difficulty in reaching, or can not reach.

To achieve this aim, the following objectives were identified:

1. The development of a miniature end-effector. This component must provide expanded

articulation, ease of movement, adequate force application and reliable structural integrity.

2. The development of an ergonomic handheld controller to manipulate the end-effector. The controller should incorporate and house all required electronic and conventional components to reliably actuate the end-effector. It should also allow for extended use without causing fatigue or strain.

3. The coupling of the end-effector and the handheld controller. This coupling mechanism should allow for seamless movement transmission between the motors on the controller-end, and the joint actuation system on the end-effector end.

To achieve these three main objectives, the following secondary objectives were identified as the research was progressing.

4. A literature review on existing surgical robotic systems that deploy miniature end-effectors, as well as on systems that are currently used in endoscopic neurosurgery.

5. A literature review on suggestions around what constitutes an ergonomic robot design, paired with a review on state-of-the-art handheld robotic devices, their design and ergonomics.

6. The development of a simulation environment to preliminary test the device capabilities and ease of use.

7. A single participant comparative experiment between one of the proposed handheld controller devices and a conventional tool, to test performance and ergonomics.

8. The design and execution of an expanded multi-participant pre-clinical randomised controlled trial of performance and ergonomics, that tested a broader list of literature suggestion on handheld controller designs.

9. A multi-participant pre-clinical cadaver pilot study that qualitatively evaluated the articulation and force-delivery of the finalised robotic prototype.

10. The design and execution of a multi-surgeon comparative phantom trial that evaluated the performance between the novel handheld robotic system and an equivalent non-articulated standard instrument.

1.4 Thesis Outline

This thesis starts with a brief overview of the novel system in **Chapter 2** to give the reader context of the discussion that is to follow. Then, the most common steps that are followed through the endonasal approach are listed. A synopsis on surgical robots for minimally invasive neurosurgical approaches is presented to showcase relevant technologies, accompanied by a detailed overview of tendon-driven and spherical joint surgical robotic end-effectors. Finally, a review on handheld surgical robots and their ergonomic considerations is outlined.

In **Chapter 3**, a spherical joint robotic end-effector for the EEEA is presented. First, the design and fabrication is discussed, followed by its kinematic analysis. The robotic end-effector was tested for its repeatability and workspace capabilities, as well as its structural integrity. This testing provided some useful insight that lead to further development and miniaturization which produced the finalised robotic end-effector prototype.

In **Chapter 4**, two ergonomically designed handle prototypes for the neurosurgical robotic instrument are presented. Initially, a forearm-mounted handle that maps the surgeon's wrist directly to the robot-joints is developed. To test for the efficacy and limitations of the handle, a preliminary pre-clinical comparative experiment between the suggested prototype and a standard neurosurgical tool was carried out. In that same chapter, an alternative handle design is showcased that employs a trigger and a rotating joystick-body that places the joystick at the position most comfortable for the surgeon. Both handles are evaluated in terms of performance and ergonomics as part of a randomised crossover user study, with the aim to identify the most suitable ergonomic handle design for keyhole neurosurgery. This chapter concludes with the fabrication of a functional handheld controller based on the superior handle concept, intended to actuate the previously developed robotic end-effector.

In **Chapter 5**, the novel robotic system prototype is evaluated in the lab as well as during a series of pre-clinical studies. The robotic instruments were experimentally evaluated for their workspace, structural integrity, and force-delivery capabilities. They then were tested in a pre-clinical multi-surgeon cadaveric pilot study. As a final evaluation of this system, the robotic system was compared with a standard instrument on its ability to resect tumour during a multi-surgeon phantom study.

Finally, in **Chapter 6**, the work presented in this thesis is summarised. This is followed by addressing the contributions of this research, as well as a consideration of its limitations. Before concluding this thesis, future research plans and pathways are presented.

This described outline is highlighted in Fig. 1.4, alongside numbers indicating the corresponding contributions that are associated with each chapter.

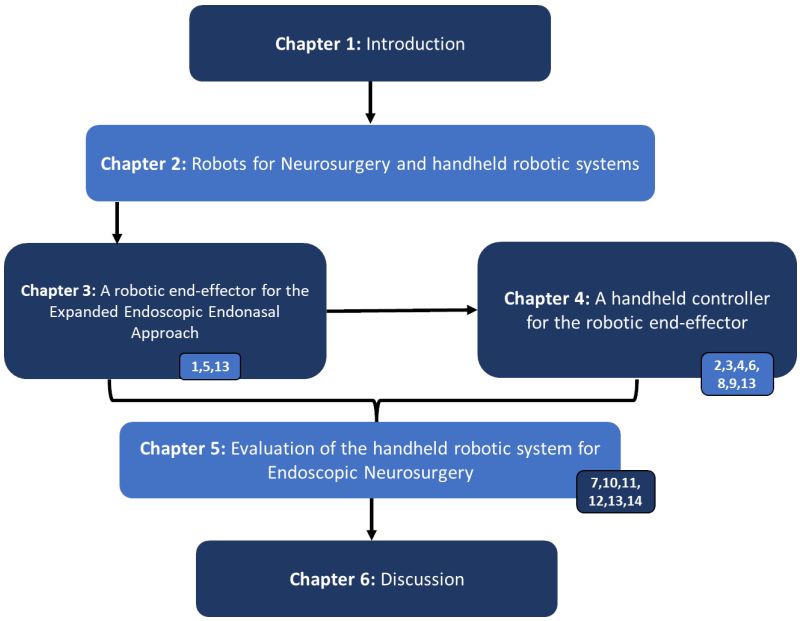

Figure 1.4: Diagram of the thesis outline. The indicated numbers refer to the corresponding contributions.

1.5 Publications

The work described in this thesis has been peer-reviewed and presented in prestigious journals, namely the Annals of Biomedical Engineering Journal (ABME), the International Journal of Computer Assisted Radiology and Surgery (IJCARS), and the Journal of Medical Robotics Research (JMRR).

Parts of the work has been presented in international conferences and workshops. These include the International Conference on Information Processing in Computer-Assisted Interventions (IPCAI), as well as the Conference on New Technologies for Computer and Robot Assisted Surgery (CRAS).

Finally, this work has been awarded during international and domestic competitions by a variety of organisations and committees such as the IPCAI organizational committee, the Institution of Mechanical Engineers (IMechE), and the European Robotics Forum (ERF).

A complete list of all the publications produced by the author about the work presented in this thesis is presented here, followed by co-authored papers and awards. In this list, it is also indicated to which contributions and to which thesis section each publication links to.

Journal Articles

- **Dimitrakakis, E.,** Dwyer, G., Lindenroth, L., Giataganas, P., Dorward, N.L., Marcus, H.J. and Stoyanov, D., "A spherical joint robotic end-effector for the Expanded Endoscopic Endonasal Approach.", Journal of Medical Robotics Research 5, no. 03n04 (2020), 2150002.

  Author contribution: ED conceived the spherical-joint idea. ED, HJM and DS conceived the clinical opportunity. ED developed the technology, conducted the literature search and performed any computations and simulation studies. GD, LL and PG supervised the technology development and helped with ideation. GD, LL, HJM and DS verified the analytical methods. NLD, HJM and DS supervised the findings of this work. All authors discussed the results and contributed to the final manuscript.

  Contribution: 1, Chapter: 3

- **Dimitrakakis, E.,** Lindenroth, L., Dwyer, G., Aylmore, H., Dorward, N.L., Marcus, H.J. and Stoyanov, D., "An intuitive surgical handle design for robotic neurosurgery.", International Journal of Computer Assisted Radiology and Surgery, (2021), pp.1-9.

  Author contribution: ED conceived the handle concept. ED, HJM and DS conceived the clinical opportunity. ED developed the technology, conducted the literature search and performed any simulation studies. HA designed the study protocol and contributed in the literature search. GD, and LL supervised the technology development and helped with ideation. GD, LL, HJM and DS verified the experimental methods. NLD, HJM and DS supervised the findings of this work. All authors discussed the results and contributed to the final manuscript.

  Contribution: 2, Chapter: 4

  Dimitrakakis, E., Aylmore Holly ., Lindenroth L., Dwyer G., Carmichael, J., Khan, D.Z., Dorward, NL. Marcus, H.J., and Stoyanov, D., "Robotic Handle Prototypes for Endoscopic Endonasal Skull Base Surgery: Pre-clinical Randomised Controlled Trial of Performance and Ergonomics.", Annals of Biomedical Engineering, (2022), pp 549-563

  Author contribution: ED conceived the second handle concept. ED, HJM and DS conceived the clinical opportunity. ED developed the technology, conducted the literature search and performed any participants study. HA and DZK designed the study protocol. HA and JC contributed in the literature search and attended the participants

study. GD, and LL supervised the technology development and helped with ideation. GD, LL, HJM and DS verified the experimental methods. NLD, HJM and DS supervised the findings of this work. All authors discussed the results and contributed to the final manuscript.

Contribution: 3, Chapter: 4

Conference and Workshop Proceedings

- **Dimitrakakis, E.,** Lindenroth, L., Dwyer, G., Aylmore, H., Dorward, N.L., Marcus, H.J. and Stoyanov, D., "An intuitive surgical handle design for robotic neurosurgery.", (2021), In The 12th International Conference on Information Processing in Computer-Assisted Interventions (IPCAI).

  Contribution: 4, Chapter: 4

- **Dimitrakakis, E.,**, Dwyer, G., Marcus, H.J., Dorward, N.L., and Stoyanov, D., "Towards the Development of a Novel Handheld Robotic Tool for the Expanded Endoscopic Endonasal Approach.", (2019), 9th Joint Workshop on New Technologies for Computer/Robot Assisted Surgery (CRAS)

  Contribution: 5, Chapter: 3

- **Dimitrakakis, E.,** Lindenroth L., Dwyer G., Holly A., Dorward, NL. Marcus, H.J., and Stoyanov, D., "Towards the Development and Evaluation of a Handle Prototype for a Handheld Robotic Neurosurgical Instrument.", (2020), 10th Joint Workshop on New Technologies for Computer/Robot Assisted Surgery (CRAS)

  Contribution: 6, Chapter: 4

- **Dimitrakakis, E.,** Aylmore, H., Lindenroth, L., Dwyer, G., Marcus, H. and Stoyanov, D., "Towards a Handheld Robotic Instrument for Minimally Invasive Neurosurgery." (2022), 12th Conference on New Technologies for Computer and Robot Assisted Surgery (CRAS)

  Contribution: 7, Chapter: 5

Co-authored journal articles and book-chapters

- Aylmore, H., **Dimitrakakis, E.,** Carmichael, J., Khan, D.Z., Stoyanov, D., Dorward, N.L. and Marcus, H.J., "Specialised Surgical Instruments for Endoscopic and Endoscope-Assisted Neurosurgery: A Systematic Review of Safety, Efficacy and Usability.", (2022), Cancers, 14(12), p.2931.

  Personal contribution: ED contributed in the literature search, the results generation and the paper writing.

- Dietsch, S., McDonald–Bowyer, A., **Dimitrakakis, E.,** Coote, J.M., Lindenroth, L., Stilli, A. and Stoyanov, D., "Localization of Interaction using Fibre-Optic Shape Sensing in Soft-Robotic Surgery Tools.", (2022), In 2022 IEEE/RSJ International Conference on Intelligent Robots and Systems (IROS), pp. 8057-8063

  Personal contribution: ED contributed in the interface coding, the hardware communication setup, the results interpretation and the paper writing.

- McDonald-Bowyer, A., Dietsch, S., **Dimitrakakis, E.,** Coote, J.M., Lindenroth, L., Stoyanov, D. and Stilli, A., "Organ curvature sensing using pneumatically attachable flexible rails in robotic-assisted laparoscopic surgery.", (2022), Frontiers in Robotics and AI, 9.

  Personal contribution: ED contributed in the interface coding, the hardware communication setup, the results interpretation and the paper writing.

- Payne, C.J., Dwyer, G., **Dimitrakakis, E.** and Marcus, H.J., "Basic concepts in robotics.", (2021), Neurosurgical Robotics, pp.3-34.

  Personal contribution: ED contributed in the literature search and the chapter writing.

Awards

- *'Audience award for best innovation: First place'*, In The 12th International Conference on Information Processing in Computer-Assisted Interventions (IPCAI), 2021.

  Contribution: 8, Chapter: 4

- *'Flash talk award: Second place'*, In UCL Institute of Healthcare Engineering Early-Career Researcher Symposium (UCL IHE ECR), 2021.

  Contribution: 9, Chapter: 4

- *'NIHR MIC Prize for Best Biongineering Postgraduate Poster 2022: Finalist'*, In Healthcare Technologies Student and Early Career Awards 2022 by The Institution of Mechanical Engineers (IMechE), 2022.

  Contribution: 10, Chapter: 5

- *'Entrepreneurship Award: 2nd place'*, In euRobotics European Robotics Forum (ERF), 2022.

  Contribution: 11, Chapter: 5

- *'Director's special commendation'*, In Wellcome / EPSRC Centre for Interventional and Surgical Sciences (WEISS) Awards, 2022.

  Contribution: 12, Chapter: 5

  Journal articles: Submitted / To be submitted

- Dimitrakakis, E., Dwyer, G., Newall, N., Khan, D. Z., Marcus, H.J., and Stoyanov, D., "Handheld Robotic System for Endoscopic Neurosurgery", (2023), IEEE Robotics and Automation Letters, (submitted)

  Author contribution: ED conceived the prototype concept. ED, HJM and DS conceived the clinical opportunity. ED developed the technology, conducted the literature search and performed any participants studies. NN and DZK designed the studies protocols and sourced the study equipment. GD supervised the technology development and helped with ideation. GD, HJM and DS verified the experimental methods. HJM and DS supervised the findings of this work. All authors discussed the results and contributed to the final manuscript.

  Contribution: 13, Chapter: 3,4,5

- Dimitrakakis, E., Starup-Hansen, J., Newall, N., Khan, D. Z., Dwyer, G., Stoyanov, D., and Marcus, H.J., "A handheld robotic device for endoscopic endonasal skull base surgery: An updated preclinical validation study (IDEAL-D Stage 0)", (2023), Journal of Neurosurgery, (to be submitted)

  Author contribution: ED, HJM and DS conceived the clinical opportunity. ED developed the technology, conducted the literature search and performed any participants studies. GJH, NN, and DZK designed the study protocols. NN and GJH sourced the

study equipment and contributed in the literature search. GD supervised the technology development and helped with ideation. GD, HJM and DS verified the experimental methods. HJM and DS supervised the findings of this work. All authors discussed the results and contributed to the final manuscript.

Contribution: 14, Chapter: 5

Chapter 2

Robots for neurosurgery and handheld robotic systems

In this chapter, a quick overview of the system and its subcomponents, as well as the surgical operation, is presented to provide context for the subsequent chapters. Then, based on the development roadmap that was followed, pre-existing work relevant to the concepts described in this thesis is presented.

2.1 Overview of the system

Figure 2.1: The handheld robotic instrument deploying a grasping tool, alongside three other articulated tools; a flat dissector, a ring-curette, and an endoscope.

The novel handheld robotic system consists of an ergonomically designed handheld controller with a joystick-and-trigger interface, and a series of $3mm$ detachable end-effectors. It is cabled to connect the controller to the control box, and weighs $247g$. The handheld robotic system, comprised of the handheld controller and its control-box, as well as its various end-effectors can be seen in Fig. 2.1.

The miniature end-effector can be easily detached and re-attached to the handheld controller, which allowed for an expanded portfolio of articulated instruments. Other than the grasper end-effector, The system incorporates a ring-curette, a spatula dissector, as well as an endoscope end-effector. The additional end-effectors that were manufactured as part of the robotic system, alongside the articulated endoscope and its expanded field of view are found in Fig. 2.2.

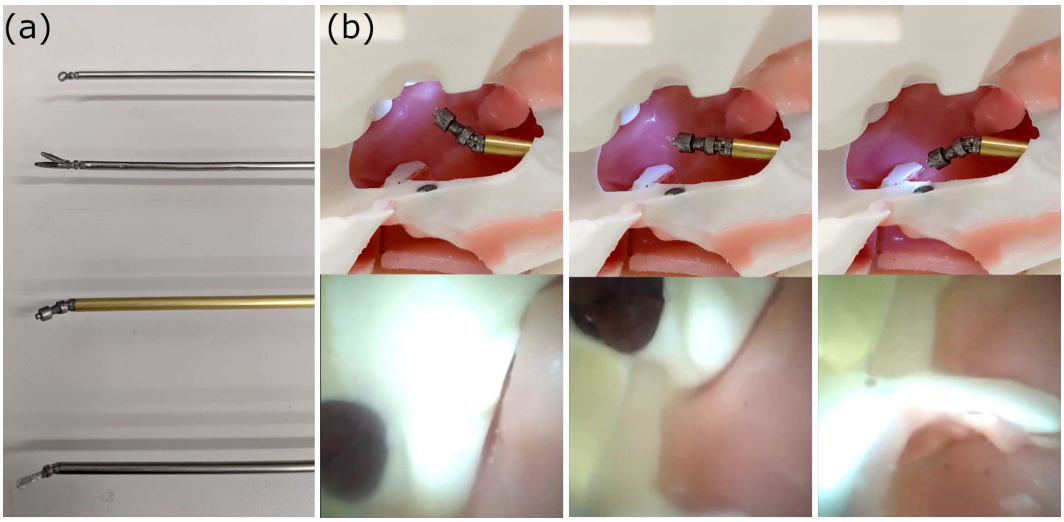

Figure 2.2: (a). (Top to bottom) The articulated end-effectors, namely the ring-curette, the grasper, the endoscope, and the spatula dissector, and (b). The articulated endoscope inside a pituitary anatomy phantom at three different angles (top row), alongside the accompanying views from the camera (bottom row). The dark spot seen in the top row of pictures is a magnet used for the phantom assembly, not to be confused with the simulated tumor evident in the bottom pictures.

2.2 Endonasal approach operative workflow

To better understand the clinical use-case of this novel robotic system, a brief overview of the endonasal surgical workflow is provided in this section. The endonasal approach can be summarised into four distinct phases according to a mixed-methods consensus process composed of a literature review and iterative Delphi surveys that was carried out within the United Kingdom Pituitary Society [21]. These phases are the nasal phase, the sphenoid phase, the sellar phase, and the closure phase, and according to the same study the steps

that the surgeons follow during each phase are outlined below:

Nasal phase

1. Identification of choana, septum, midline, turbinates, anatomic variations

2. Lateral displacement of middle turbinate and superior turbinate

3. Identification of sphenoid ostium and sphenoethmoidal recess

4. Anterior sphenoidotomy

Sphenoid phase

5. Identification of midline, pneumatization of sphenoid and anatomical variants

6. Removal or reflection of sphenoid mucosa (partial or total)

7. Removal of sinus septations

Sellar phase

8. Confirmation of adequate exposure and identification of pertinent landmarks (midline, sellar protuberance, clival recess, tuberculum sellae, optic groove, carotid groove, optic-carotid recess)

9. Sellotomy

10. Confirmation of adequate exposure and identifications of sella limits and neurovascular landmarks (e.g. optic nerves, carotid arteries) with or without adjuncts (micro doppler or neuronavigation)

11. Durotomy.

12. Microadenoma: intracapsular piecemeal or extracapsular en-bloc resection or hemi-hypophysectomy

13. Macroadenoma: piecemeal resection (usually inferior first, then lateral and superior)

14. Confirmation of adequate resection

Closure phase

15. Haemostasis

16. Inspection for occult CSF leak

17. Clearance of debris

The robotic system developed as part of this thesis would aim to mostly enhance the Sellar phase, with steps 9., 10., 11., 12., 13., 14. being especially relevant. The enhanced robotic articulation could potentially aid during the sellotomy (9.) and durotomy (11.) steps by making the cut easier and more precise, whereas during the microadenoma (12.) and macroadenoma resection (13.) steps it could increase the tumour resection margins. An

articulated endoscope could also help with the confirmation of adequate exposure and identification of sella limits and neurovascular landmarks (10.), as well as the confirmation of adequate resection (14.). Finally, and during the closure phase, enhanced dexterity could help with step 17., and the clearance of any debris in the operative workspace.

Before starting the development of a robotic system that would cater to the endonasal approach, it was important to investigate other robotic solution targeting similar procedures. After a research gap had been identified and a novel robotic system concept had been conceived, literature search focused on the state-of-the-art that was relevant to the system development. The implementation of the handheld robotic device can be compartmentalised in two main components. The development of the end-effector, and the development of its actuation handle. For the former component, tendon-driven and spherical joint end-effectors were explored. For the latter, the investigation included handheld robots for minimally invasive surgery and their ergonomic considerations.

2.3 Robots for minimally invasive neurosurgery

One of the main advantages of RAMIS is the small incision size that surgeons operate through. This, of course, comes with the technical challenge of limited workspace. Especially in EEA, the workspace is exceptionally limited and constrained by the nasal access path. In [22], it is found that the surgical workspace is most closely represented by a cylinder with a narrow middle diameter and an average volume of $15.97cm^3$, an average length of $53.9mm$ and an average widest width of $19.08mm$. The fact that multiple rigid manual instruments must work inside such a constrained space, makes the procedure challenging even for expert neurosurgeons.

Motivated by this demanding technical workspace, a number of studies have reported robotic instruments for EEA. Often, studies present concentric tube robots for such approaches. This is due to their ability of navigating inside restricted anatomies [23]. In [24], a prototype concentric tube system for bimanual teleoperated endonasal skull base surgery is developed, and in [25] it is evaluated. A similar platform consisting of concentric tube continuum robots is developed and evaluated in [26] and [27] respectively, where the authors conduct a phantom pituitary tumour removal clinical study. Despite some of the possible advantages of concentric tube robots, there are still major concerns about the distal-end dexterity of these manipulators, and their force-delivery capabilities. Taking a different robotic paradigm, a two DoF robotic tool with elastic elements was partly intro-

duced in [28], whereas in [29] the authors expanded this concept to a four DoF elastic elements robotic instrument implementing a forceps-principle. Limitations arose when the repeated deformation of the tool lead to fatigue and potential breakage. The robotic tools designed for the endonasal approach presented in [26] and [29] are shown in Fig. 2.3.

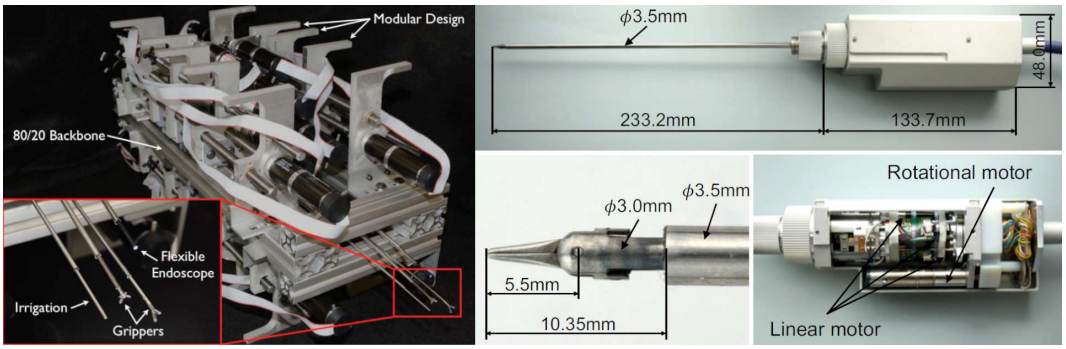

Figure 2.3: A concentric tube robotic platform (left), and a 4 DoF elastic elements robotic instrument (right), intended for the endonasal approach.

On a broader scope, a cable-based actuation method specifically designed for EEA has been reported and tested on a 5.8mm DoF steerable robot in [30]. It is worth mentioning that there have been several reports of instrument holder robots, not articulated surgical tools, for endoscopic endonasal surgery [31, 32]. Finally, there are robots that could be used as holders but can also cater to more surgeries than just the endonasal approach, such as the one developed in [33].

Commercially, the field of minimally invasive neurosurgery is relatively unexplored, with only a few existing solutions. Other than the neurosurgical robotic systems mentioned in the introduction, one of the more notable systems is the ROSA One Brain (Zimmer Biomet, Warsaw, IN, USA), a robotic stereotactic assistance device which can assist surgeons in planning and performing complex neurosurgical procedures through a small drill hole in the skull. This robot has proven to be useful for an array of neurosurgical procedures ranging from Deep Brain Stimulation [34], to Endoscopic Third Ventriculostomy [35] and pediatric neurosurgery [36]. Fig. 2.4 depicts the ROSA One Brain robotic system.

2.4 Robotic end-effector for minimally invasive surgery

Miniature robotic end-effectors for surgery is an extensive research field populated with systems that aim to expand the capabilities of the surgeon through added articulation and enhanced dexterity. From the various end-effector designs found in literature and in commercial systems, such as continuum structures, articulated joints and concentric designs just

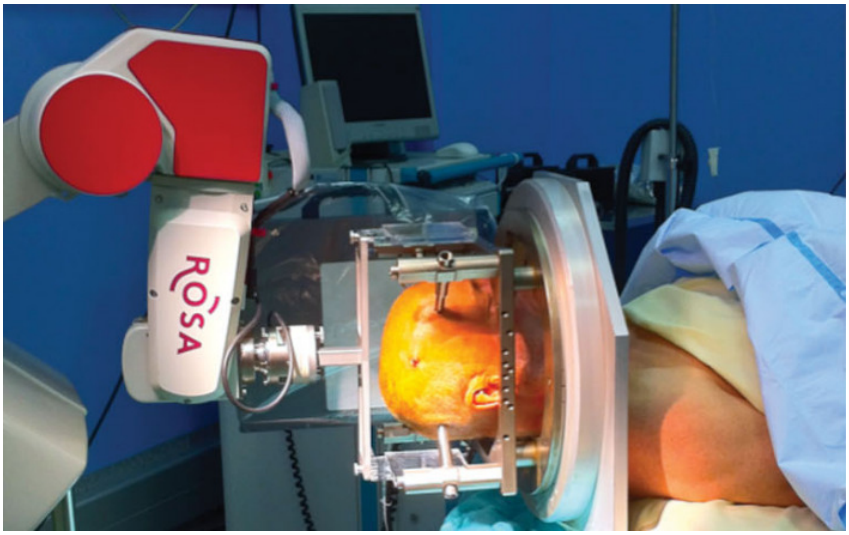

Figure 2.4: The ROSA One Brain robotic system intra-op by the patient side [34].

to name a few, in this thesis, a tendon-driven spherical joint end-effector is developed, as it will be explored in Chapter 3. Thus, in this section, pre-existing work on these specific categories of surgical robotic end-effectors is presented.

2.4.1 Tendon-driven robotic end-effectors

A tendon-driven manipulator has a specific tendon traction force transmission mechanism, in which the joint actuators are located at the base of the robot and a pair of tendons drive the joint by transmitting the actuating power to it [37]. Using tendon-driven robotic end-effectors is popular in RAMIS due to their increased distal dexterity, robust stiffness control and force-delivery capabilities [38].

Tendon-driven robotic end-effectors can vary based on their structural design. One of the most common types of tendon-driven robotic end-effector used in RAMIS is the articulated end-effector. In this category, the end-effector is comprised of a number of small links, with a joint being formed in between two consecutive links. In [39], a novel, modular joint design compatible with the constraints of minimally invasive surgery is presented. A tendon-driven actuation logic was combined with a micromotor in order to transmit the rotary motion of this embedded micromotor to joint rotation. After the authors presented the positioning accuracy as well as the force and torque transmission attributes of the joint, they combined five of these mechanisms to form a 7 degrees-of-freedom (DoF) flexible access robotic platform for Natural Orifice Translumenal Endoscopic Surgery (NOTES). This system was tested in-vivo to demonstrate its feasibility, and it was successfully proven

that it can provide navigation along curved pathways.

An expansion of this joint design, is the robotic platform presented in [40], which aims to improve complex endoscopic procedures. This robotic platform incorporates a snake-like robotic endoscope, two robotic instruments, as well as a robotic arm for global positioning and insertion. Using a combination of tendons and micromotors leads to limited manipulation force at the tip of the instrument, thus the authors chose to incorporate a fully tendon-driven control architecture with the actuation motors located outside of the body of the robotic arms. Thus, each robotic arm is comprised of a total of 13 links with 16mm diammeter bodies. In between each pair of links, a rolling joint is located. In this study, the control workflow of the platform was validated in simulation, and then implemented in a physical experimental setup. The results showcased that the presented robot has clear clinical potential in endoscopy.

Similar to these designs, is the single-port robotic platform for transanal endoscopic micro-surgery that is introduced in [41]. A number of robotic instruments is incorporated in this surgical platform, including energy delivery devices, graspers and needle drivers. The robotic instruments in this study are also fully tendon-driven, with an antagonistic pair of tendons driving each of the articulation joints, and are comprised of an elbow and a wrist. The elbow incorporated two segments moving on perpendicular planes, each featuring two mechanically coupled serially linked joints, while the wrist is driven by three pairs of tendons that are routed through a catheter which ensures that movement of the elbow is not transferred to the wrist. After the design considerations and kinematic control of this platform were analysed, multiple surgical procedures on bovine tissue were performed to showcase that the system is effective during transanal procedures.

A very different approach to these designs is taken in [42], where the authors tackle the problem of yaw and pitch axes coupling, that is often met in commercially available robotic end-effectors, by proposing a novel tendon-driven end-effector that allows the two DoF to be actuated independently. This novel design introduces stationary tendon guides so that the tendons are routed through the plane of symmetry of the tool, and the robotic wrist is decoupled. To evaluate the efficacy of this proposed design, a prototype was implemented. Experimental and analytical results confirm that the end-effector has decoupled actuation capabilities, and suggest that it can be further developed to be incorporated into surgical applications.

Apart from the articulated end-effectors, another popular type of tendon-driven designs is the continuum end-effector. Contrary to articulated types, where the end-effector is comprised of individual links and joints, the backbone of a continuum robot is a continuous structure. In [43], the authors investigate the underlying mechanics of tendon-driven continuum manipulators when applied to a steerable cardiac catheter, and more specifically the forward and inverse kinematic mapping between tendon displacements and beam configuration. The model presented in this study can be used to optimise the performance of tendon-driven continuum robots by means of tendons slacking elimination, and tendon displacement calculation. An articulated tendon-driven surgical robotic end-effector [41], alongside a similar continuum tendon-driven rendition [43] is depicted in Fig. 2.5.

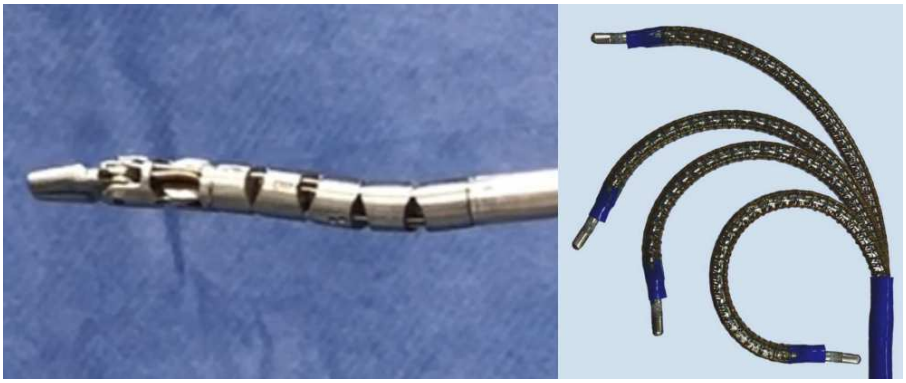

Figure 2.5: An articulated tendon-driven surgical end-effector (left), and a continuum tendon-driven surgical end-effector (right).

Finally, in the study presented in [44], a multi-section continuum robot that focuses on wide-angle visualization and flexible positioning of the distal tip is developed. A kinematic mapping model with tension propagation including friction between the tendons and the robot links was employed for accurate tip position estimation at large viewing angles. This kinematic mapping model was tested in simulation and with a 10:1 scale experimental prototype, resulting into tip-to-tip errors significantly smaller than the errors produced by conventional continuum robot models.

2.4.2 Spherical joint robotic end-effectors

Spherical joints are commonly used in robotic applications, as they can accommodate both the wrist and shoulder configurations of a manipulator, concentrating three DoF in a single-volume device, as opposed to one device per DoF that is usually found in an articulated robotic end-effector. The idea of using this type of joint for robotic applications, also re-

ferred to as a 'ball-joint', is not a new concept. In [45], a spherical induction motor for robotic applications was conceptualised. This new, at the time, robotic manipulator design incorporated a spherical motor capable of three degrees of motion in a single joint, combining pitch, roll and yaw motions. Intelligent planning and control algorithms were designed to guarantee computational speed and robustness.

An alternative spherical actuator based on the operating principle of a stepper motor was introduced in [46]. This type of spherical motor was based on the concept of variable reluctance stepper motors, and would be easier to manufacture than the induction motor previously presented. In this particular study, the authors highlighted the fundamental differences between a three-axes stepper motor and a single-axis stepper motor, since even though the proposed device is based on the conventional variable reluctance stepper motor, its operation differs significantly. The torque and resolution attributes that this sort of device should posses are analysed, before the kinematic and dynamic relationships are discussed. An experimental prototype was developed as part of this study, with its performance validating the suggested proof-of-concept design.

Since the introduction of the spherical joint in robotic applications, technological advancements have made it possible to produce similar ball-joints in miniature size and, thus, make them suitable for surgery. The concept of taking the standard spherical joint and reproduce it in miniature scale for a robotic tool was explored and validated in [47], where a three DoF spherical joint was implemented and evaluated for its control feasibility. After the kinematic and mechanical properties were evaluated and modeled, both open and closed loop control algorithms were developed to control this spherical joint device. By employing a single joint three DoF design, rather than one separate joint for each DoF, the design is simplified, the authors suggest, and the chance that a tendon pair has to be routed through a joint is eliminated. The simulated and experimental procedures conducted in this study showed that a miniature ball-joint can be successfully controlled in all three DoF, and can be potentially incorporated in a surgical robotic tool.

In the study of [48], a $4mm$ spherical joint is used as part of a robotic instrument aimed for general Minimally Invasive Surgery (MIS). In this work the spherical joint is part of a larger articulated robot body rather than being the focal point of the development. The robotic instrument consists of six antagonistically controlled DoF and a wristed gripper. A ball joint enables the wrist to move in two DoF, namely the yaw and pitch, while maintaining

the origin of the wrist joint as close as possible to the end-effector. This robotic prototype was evaluated for its workspace and force-delivery capabilities. As referenced in the study, a limitation of having a spherical joint for wrist dexterity as the last joint of a robotic tool, is that the instrument is compressed under the high tension required to straighten the joint, something not applicable when the spherical joint acts as the sole manipulation means.

These types of configurations, where the spherical joint acts as the common origin for three DoF is only one of the configurations met in surgical robotics. A 2.4mm miniature fetal surgery end-effector with two spherical joints that contribute towards a small bending radius of 2.45mm is implemented in [49]. The mechanism of this end-effector includes two ball joints, each able to bend through 90^o in any direction, that are driven using four tendons. The actuation unit of the prototyped device consists of two ultrasonic motors. Preliminary experimental results suggest that this small diameter manipulator can successfully demonstrate high rigidity. This fact, when combined with the ease of fabrication of the mechanism, showcases potential towards surgical adaptation in fetal and other procedures.

A more complex assembly that takes advantage of some of the spherical joint attributes is presented in [50]. This robotic platform achieves enhanced articulation by using an assembly of ball joints, plates and wires, and antagonistic tendons. The system was tested for its workspace and force-delivery capabilities, while a user study was also conducted where participants carried out two standard surgical training tasks with a conventional non-articulated surgical tool, and then with the proposed robotic system. Results of these aforementioned studies suggest that this spherical end-effector with its actuation unit can offer functionality equivalent to commercially available systems. The spherical joint described in [48], alongside the different configurations proposed in [49] and [50] are shown in Fig. 2.6.

2.5 Handheld robots for minimally invasive surgery: Review on Ergonomics

It is evident that most robotic systems in use or in development for surgery, including the EEEA, are tele-operated. Recently, however, handheld robotic devices have started gaining increased popularity. Depending on the use-case, these devices can offer a series of advantages over the more complex remotely controlled systems. Handheld robotic instruments have a smaller footprint and are associated with smaller purchasing and maintenance costs.

Figure 2.6: A surgical end-effector with a spherical joint that is part of a larger continuum body (left), an end-effector with two ball-joints that contribute towards an extended bending radius (middle), and an end-effector with an assembly of ball joints and plates (right).

Additionally, they can be easily integrated into the surgical work-flow due to their ability of quick instrument change intra-operatively, and they often resemble traditional devices which the surgeons already know how to control, reducing, thus, the surgeon's training period [19].

However, despite these features that handheld devices can bring in the operating theatre, taking the surgeon away from the comfort of their master-console can lead to undesirable results such as fatigue or physical injury. In fact, in a recent study it was found that during minimally invasive approaches, more than 80% of the participating surgeons have succumbed to a work-related injury or illness as a consequence of sustaining awkward or static positions throughout lengthy operations over a career. This important but little recognised fact can lead to operation cancellations due to surgeon unavailability, or even threaten a surgeon's career [51].

Some suggestions to reduce the occurrence of these physiological problems are discussed in the same study. One such suggestion is the formal ergonomic education through tailored training to inform surgeons of subjects such as operative posture, ergonomics, and risk mitigation. Another is the optimization of the operating room ergonomics and equipment placement. Most important, however, is the shift towards designing surgical instruments which have considered procedural ergonomics to reduce the chance of surgeon fatigue and injury.

In this chapter, the ergonomic considerations of some state-of-the-art commercially available and research-stage handheld robotic surgical systems are analysed. First, a research literature on surgical ergonomics is conducted to compile instructions that could lead to an ergonomically-designed robotic device. Then, the state-of-the-art handheld robotic

devices are identified, and based on these instructions, it is investigated whether any ergonomic guidelines were considered during their development. Finally, the chapter concludes with suggestions on engineering solutions that could potentially improve device ergonomics, without sacrificing efficacy.

2.5.1 Optimal design considerations

Long-term use of non-ergonomically designed surgical tools can cause significant physiological problems, such as carpal-tunnel syndrome [52] or pain in the regions of the neck and upper extremities [53]. Ergonomic considerations during device design and development could reduce the occurrence of these problems.

According to [54], it is difficult to define a universal consensus on specific guidelines that make a handle design ergonomic and comfortable to use. Despite this difficulty, there are still some characteristics that are found to be contributing towards an ergonomic device design. In [55], it is found that the size of the surgeon's hand is related to the handle size that they consider optimal, since the optimal diameter of the instrument's handle was different for the four hand size categories that were investigated in that study. In [56], it is proposed that the preferable handle manipulation type is finger-operated, specifically with the thumb and index finger. According to this study, users perceive a finger-operated handle as more precise than an articulated handle. The major reason for this is that with an articulated handle, it is difficult to keep the position of the end-effector steady while changing its orientation. In [57], it is suggested that the thumb should be employed for controlling the robotic joints for manipulation precision, either via joystick, rotary switch or other device as these interfaces were surveyed as the most favorable among the surgeon cohort of this study, while the index finger should actuate a round trigger for the opening and closing of the robotic gripper as was objectively evaluated during an ergonomic video assessment in [58].

In terms of comfort and fatigue, in [59] it is suggested that in order for a handle to feel comfortable, when the instrument is kept at rest, the surgeon's hand should maintain a partially opened pose. When the instrument is maintained by a partially open hand, it is held in place between the thenar eminence and the fourth and fifth fingers, just like the hand is kept at rest, minimizing fatigue. Handle weight has a significant effect on muscle load when performing manual tasks [60], thus transferring the instrument weight that the wrist supports to the forearm could potentially ease the wrist load and reduce fatigue. This would

also create a stable platform for intuitive robot-joint control, something that could increase the chance of developing a surgical instrument with good usability [61].

Finally, regarding the geometry of the handle, an improved ergonomic handle shape could include a large palmar grip surface and the combination of precision and turning ability [62]. This provides a better fit for different hand sizes, and the fingers have a larger contact surface thus reducing the pressure on localized areas, especially the thumb.. In the same study it is also stated that the handle with the shaft should maintain a 45^o angle. This design consideration prevents extreme wrist positions. Ulnar deviation can be prevented by introducing an angle between the handle and the shaft, while maintaining this angle also prevents abduction of the arm. All these design considerations are compiled in the table below:

Table 2.1: Design considerations that could lead to an ergonomic handheld surgical robot.

The same handle design should cater to different hand sizes.
The instrument actuation means should be finger operated.
For precision control, the thumb should control the robot-joints, and the index-finger should operate the robotic gripper.
A resting hand pose should hold the instrument at rest.
The wrist should not support much weight throughout the duration of the procedure.
The instrument should allow for intuitive control.
The handle should include a large palmar grip surface.
The handle with the shaft should maintain a 45^o angle.
The instrument should provide a platform to incorporate complex robotic assistance.

2.5.2 Papers search methodology

Now that the list of design considerations was compiled, the next step was identifying the state-of-the-art handheld robotic systems and investigating their ergonomics. To find published works on the subject of handheld surgical robotic instruments, the systematic approach depicted in Fig. 2.7 was followed.

The following query $\{$*handheld OR hand-held OR portable*$\}$ *AND* $\{$*surgical OR medical OR surgery*$\}$ *AND* $\{$*robot OR* $\{\{$*robotic OR robotized OR smart*$\}$ *AND* $\{$*instrument OR tool*$\}\}\}$ was input into five different research databases to compile a total of 1494 papers. It is worth mentioning that all databases except Google Scholar had search query capabilities, thus for this particular database, all search query combinations had to be input individually.

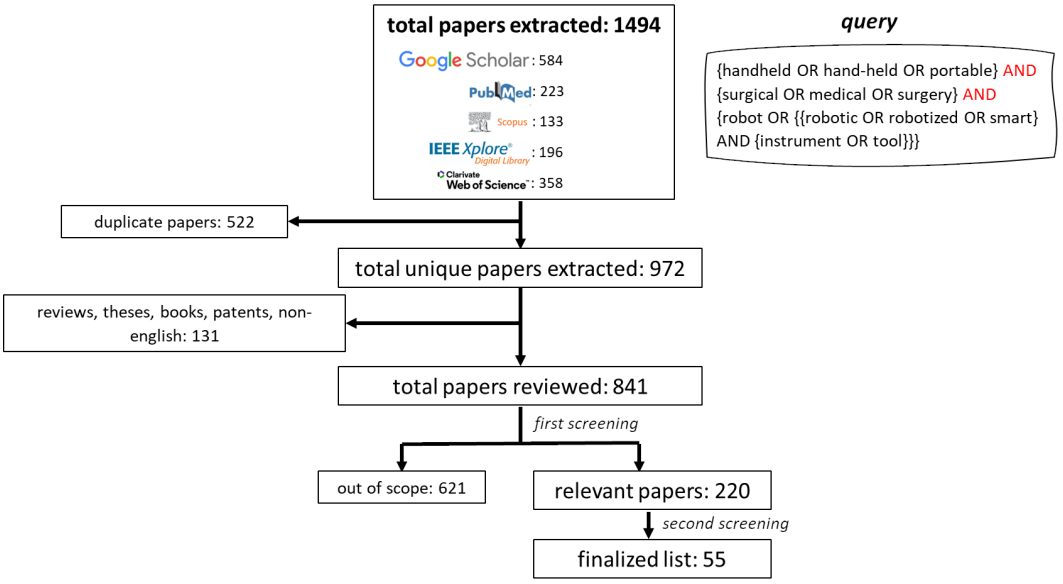

Figure 2.7: The search methodology that was followed to find published works on the subject of handheld surgical robotic instruments.

That preliminary paper list was investigated for duplicate papers, a search that led to 522 papers being discarded bringing the total of unique published works to 972. This number was reduced to 841 papers after reviews, theses, books, patents and non-english works were excluded. Having decided on a curated list of potentially relevant works, each paper was investigated individually to evaluate whether the work presented was introducing or validating a novel handheld surgical robot. This initial screening brought the number of relevant papers down to 220. After a second screening to find works which were evaluating the same device or works which upgraded the device capabilities without any device design changes, the paper search methodology concluded with 55 original works.

2.5.3 Handheld robotic instruments for surgery

The handheld robotic instruments presented in this study were classified into four different categories based on their main functionality feature. These four categories are I. Added articulation, II. Hand-tremor compensation, III. Force-feedback, and IV. Navigation and depth-estimation. A summary of all reviewed papers is presented in Table 2.2, whereas some of these reviewed systems are showcased in Fig. 2.8. Then, indicative systems from each category are presented for a better understanding of their distinctive functionalities.

Table 2.2: Summary of all reviewed papers, their categories, intended aim, and target surgical operation.

Device category	Intended aim in surgery	Target surgical operation	References
Added articulation	Surgeon's dexterity and reachability enhancement.	general laparoscopy, neurosurgery, endoscopy, orthopaedic surgery	[63], [64], [65], [66], [67], [68], [69], [70], [71], [72], [73], [74], [75], [76], [77], [78], [79], [80], [81], [82], [83], [84], [85], [86], [87], [88], [89], [90], [91], [56]
Hand-tremor compensation	Undesired motion filtering, and motion sensing and actuation.	microsurgery, endomicrosopy, vitreoretinal surgery	[92], [93], [94], [95], [96], [97], [98], [99], [100]
Force-feedback	Safety increase with force-measurement and force-thresholding.	microsurgery, general laparoscopy	[101], [102], [103], [104], [105], [106], [107], [108], [109]
Navigation and depth-estimation	Cutting and drilling planning, and penetration-depth estimation.	orthopaedic surgery, neurosurgery	[110], [111], [112], [113], [114], [115], [116]

I. Added articulation

One of the main and most popular features that handheld surgical robotic instruments deploy is the added articulation they offer when compared to traditional non-articulated surgical tools. This robotic component increases the surgeon dexterity and makes distant areas inside the operative workspace reachable. Simultaneously, these instruments can incorporate motion-scaling and assist in complex surgical tasks that require dexterous movements such as suturing.

One such device utilising this enhanced articulation capability is presented in [78]. There, a new hand-held robotic device for laparoscopy is developed to overcome common laparoscopic surgery problems such as the restricted mobility inside the human body. Furthermore, the first fully handheld CTR cabaple of 6-DOF motion was introduced in [73]. A different design philosophy is followed in [88], where a steerable robotic instrument with a curved sliding-joints is presented, and in [83], where a robotic device with a flexible manipulator with intelligent trajectory following for athroscopic interventions is developed.

Combining handheld controllers with endoscopes, the authors in [65] propose four novel designs for a steerable two degree-of-freedom robotic tool body to be deployed through a rigid endoscope and a handheld controller for such a tool body. Similarly, a new system that enables handheld coordination of both an endoscope and two CTRs through a 5mm working channel is presented in [75]. This system aims for seamless integration into the OR by keeping the same surgical setup as the current clinical workflow.

The design feature all these instruments had in common was the use of a standard

actuation means, such as a joystick, rotary switch or trigger. Some handheld devices employ more intuitively designed controllers that aim to map the surgeon's hand movements into the robotic joints. A forearm-mounted surgical instrument handle prototype that maps the surgeon's wrist directly to the robot joints was developed in [68]. In [117], a modular dexterous handheld surgical robot with an ergonomic handle and 4 DoF interchangeable instruments was developed. An instinctive manipulation strategy is also followed in [118], where a dexterous and ergonomic instrument for laparoscopy is presented and in [81], where a master-slave robot is showcased which however has the size of a handheld device.

All these systems, while in various developmental stages, were still presented in a research capacity. There are some handheld robotic instruments, however, that have already been commercialised and used in the operating theatre. [79] is the first study to describe and objectively evaluate the use of the DEX mechatronic system (DEX Surgical, Verrières-le-Buisson, France), a robotic-driven needle holder with an ergonomic handle, during laparoscopic practice. Additionally, the study in [20] assesses the surgeon's performance and ergonomics when using the Kymerax Precision-Drive Articulating Surgical System (Terumo Europe NV) while the robotized needle holder with two intracorporeal DoF Jaimy-en-2 (Endocontrol, La Tronche, France) was compared with a classic needle holder in [63].

II. Hand-tremor compensation

One of the main issues associated with handheld robotic instruments aimed for surgical approaches is the operator's hand-tremor that even at very low magnitudes can be disruptive for some operative tasks that require very high precision, such as those in microsurgical procedures. The high level of accuracy that these operations require shortens the pool of available qualified surgeons to undertake them. Thus, handheld robotic tools that can distinguish between intended and erroneous motion have been developed to increase the efficacy and wide adoption of these highly complex surgical operations. These instruments need to be lightweight and compact so that they resemble the commonly used passive instruments, and able to compensate for hand-tremor movements, cancelling out low-magnitude involuntary hand-motions.

One of the first handheld systems aimed for hand-tremor compensation is the Micron [93]. This active intelligent handheld microsurgical instrument performs real-time tremor compensation, and preliminary laboratory testing showcased significant reduction of simulated tremulous motion. A similar intelligent handheld instrument is the iTrem2 [94] that

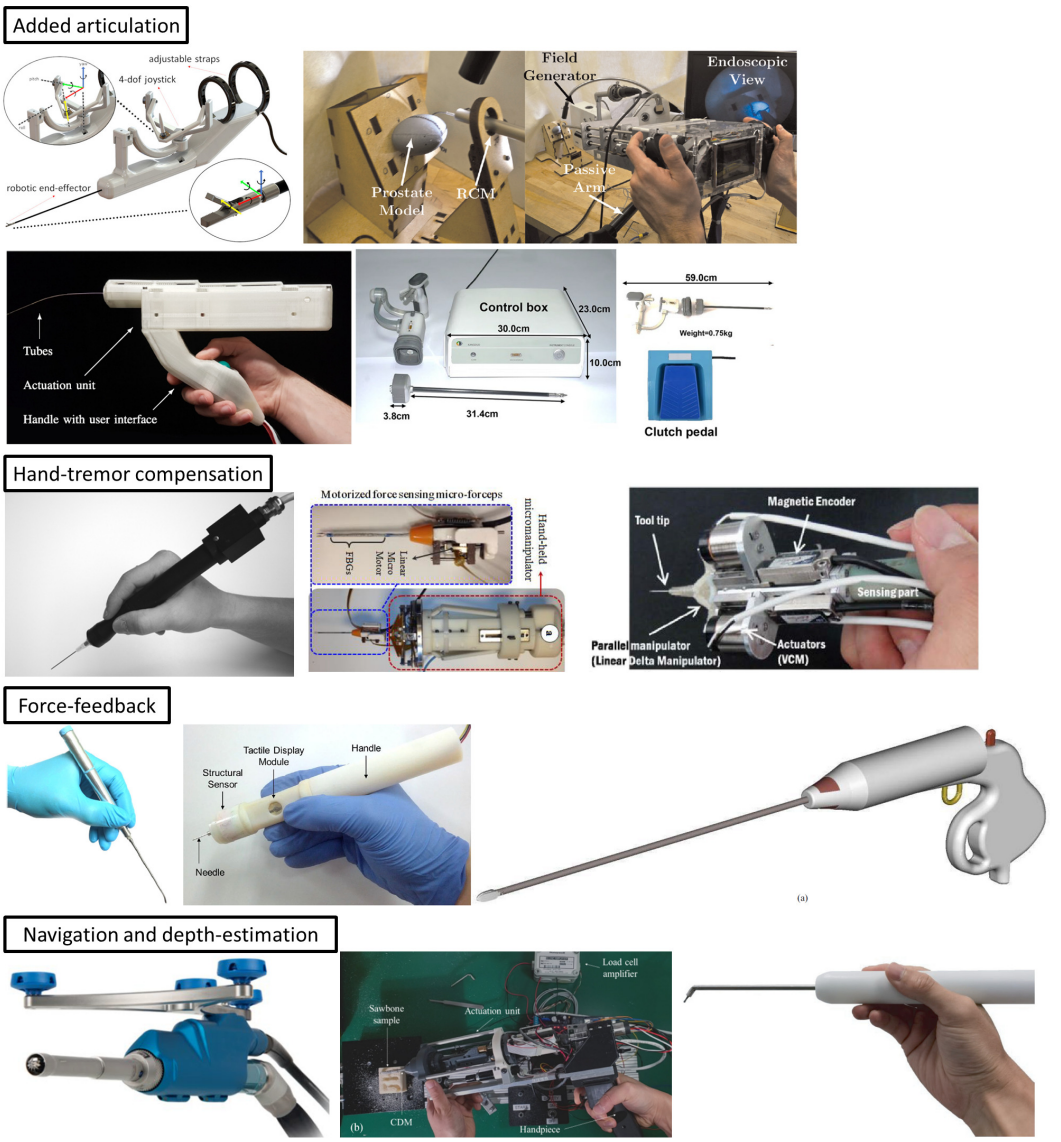

Figure 2.8: Some of the reviewed robotic systems presented in this chapter. **Added articulation:** A forearm-mounted intuitively controlled handheld robot [68], a system that enables handheld coordination of both an endoscope and two CTRs [75], a handheld CTR capable of 6-DOF manipulator [73], and a handheld robotized needle holder [119]. **Hand-tremor compensation:** The Micron active intelligent handheld microsurgical instrument [93], a compact fiber bragg grating force-sensing micro-forceps incorporated with the Micron [96], and a parallel manipulator for the suppression of physiological hand tremor [95] **Force-feedback:** A force-measuring capable handheld robotic tool [106], a tactile capacitive sensor and tactile display with a dielectric elastomer equipped instrument [105], and a servo-assisted robotic handle [102]. **Navigation and depth-estimation:** The Navio handheld robotic system [110], a handheld active steering robotic system for curved drilling and milling [115], and a handheld steerable surgical drill with a novel miniaturized articulated joint module [116].

enhances manual positioning accuracy with hand tremor cancellation. At the same time, it provides automatic micromanipulation functions. Experimental setup showcased 67% amplitude error reduction in 1-DOF tests.

A new design of a parallel manipulator for the suppression of physiological hand tremor in microsurgery was proposed in [95]. This mechanism design is based on the Linear Delta configuration which can compensate for tremor signals in the three translational directions. Concluding with the review of hand-tremor compensation devices, a hand-held instrument that can provide a predetermined contact force to obtain consistent images despite involuntary hand movements that could alter the image quality during probe-based confocal laser endomicroscopy has been developed in [97]. The force control performance of the instrument is evaluated in bench tests and hand-held experiments.

III. Force-feedback

As mentioned before, complex and delicate procedures such as neurosurgery or operations that employ microsurgical techniques require high precision. Another very important skill surgeons need to master is accurate force application. While the forces applied to delicate tissue matter must be adequate to carry out the surgical procedure, excessively applied forces can have a damaging effect on these sensitive structures. The introduction of robotics in microsurgery has allowed for force measuring that can help in improving the tissue interaction consistency, as well as in avoiding the application of excessive forces. This can happen by either implementing force limiters or by providing tactile feedback to the surgeon's hand, informing them that the force applied can potentially be dangerous.

A handheld robotic tool capable of force-measuring is presented in [106]. This work introduces a modified blunt dissector that incorporates sensors which can measure lateral forces applied to its tip. When a force threshold has been exceeded, the on-board actuator produces an easily perceptible vibration. Psychophysical user experiments demonstrated that this approach can limit the amount of force that is applied when users are distracted or when their force perception has been deliberately altered.

Another smart surgical tool for microsurgery was developed in [105], equipped with a tactile capacitive sensor and a tactile display with a dielectric elastomer. The fingertip grasping the tool is stimulated by the tactile display to transmit the contact force information measured by the sensor. The fabricated prototype was experimentally evaluated and showed promise in contributing to the improvement of surgical technologies. Finally, a robotic

instrument aiming to increase safety and dexterity of MIS was developed and tested in simulation, as well as in a clinical environment in [102]. The tool uses servo-assistance to support the surgeon in terms of reduction of fatigue and increase of dexterity.

IV. Navigation and depth-estimation

Orthopaedic and spine surgery are often associated with higher risk, since any bone alteration requires careful handling of the surgical tools to avoid injury. Especially during drilling and cutting, even a slight deviation from the pre-planned trajectory can lead to irreversible damage. This is why the use of robotized handheld drills can be beneficial, aiding the procedure in a variety of ways. These robotic tools can incorporate navigation and increase operational accuracy by restricting drilling and cutting within the confines of the pre-operatively defined resection area. They can also enhance the efficacy of the operation by providing sensory data of the bone temperature, as well as the drill-bit penetration depth.

A system that can restrict the bone cutting into pre-defined areas with the use of navigation, is the handheld robotic system NAVIO (Smith & Nephew, Watford, UK). This tool assists surgeons in planning implant positioning and in preparing the bone surface during unicomparmental knee arthroplasty (UKA). This robotic tool was evaluated for its early implant survivorship results associated with its use in [110]. A similar compact handheld surgical drill is proposed in [112]. A thrust force sensor and an active infrared LED marker are integrated into the portable device in order to enable high accuracy during pedicle screw positioning without permanent X-radiation exposure.

In [114], a compact and patient-safe handheld robotized system for bone manipulation is presented. The system consists of two 2-DoF modules that share a common control block, one for bone drilling, and one for bone cutting. Finally, a handheld active steering robotic system for curved drilling and milling in minimally-invasive orthopaedic surgery is developed by the authors of [115]. This device employs a flexible rotary cutting tool that passes through a continuous dexterous manipulator and is flexible enough to allow for target reachability in constrained spaces, while retaining a sufficiently stiff pose for debriding hard tissue.

2.5.4 Ergonomic considerations in handheld surgical robots

Without a question, handheld robotic surgical devices are used in the operating theatre, and research and development around novel systems is of great interest to the scientific community. The main factors contributing to the popularity of handheld devices, as previously

explained, can be narrowed down to their offering of an increased array of robotic technologies while maintaining a compact form factor that allows for easy integration into the surgical workflow. While the benefits for the patient are clear, it is worth investigating whether these commercially available and research devices have been ergonomically designed to simultaneously aid their operators. In this section, an analysis is carried out to investigate whether the devices presented in the reviewed papers were designed following ergonomic requirements, and if so, which optimal design considerations from Section 2.5.1 were covered.

Of the 55 published papers investigated in this review chapter, a total of 37 devices had been designed following at least one ergonomic suggestion. The remaining 18 bodies of work did not mention any design considerations affecting the human factors of the presented device. The main design requirements met in the reviewed papers were that the robotic instruments should have reduced weight, be compact and miniaturised, they should have an ergonomic and comfortable to use handle shape, if possible maintain a resting hand while holding the hand at rest, and finally allow for intuitive and instinctive control.

Handheld devices are often preferred in the operating theatre because of their reduced weight and overall compactness. That is why a number of the developed devices aimed at an optimal weight. In [73] and in [114], one of the requirements stated is that the device should be compact and lightweight, so that it can be used for standard surgical operations without causing the operator fatigue or pain, whereas in [75] the robotic system employs a spring-loaded counterbalanced arm to assist the surgeon by supporting the weight of the handheld robot. In the same work, the weight reduction is taken a step further, by the construction of a custom 3 DoF orientation frame that allows the surgeon to manipulate the robotic tool without perceiving the weight of the system. Reduction of the device weight was also important in [81], where the pneumatically-driven robotic forceps is supported by a 4-DoF passive holder, and in [112], where the motor actuating the handheld robotic drill is placed outside the device and connected via flexshaft to the rotation shaft.

While some works did not optimize their robotic instrument design to minimize weight, the researchers still appreciated the importance of developing a compact surgical tool. For example in [78], reducing the size and weight of the robotic device for added articulation is presented as part of future work, and in [97], while the current tool is neither too heavy nor bulky, the authors planned on selecting a smaller and lighter actuator to

achieve better miniaturization and thus improved manipulation and ergonomics.

Another popular ergonomic design solution was the development of an ergonomically shaped handle that felt comfortable and provided an easy palmar grip. Such a device is presented in [63] where the instrument possesses two intracorporeal DOF, yaw and roll, controlled by a joystick placed on an ergonomic handle, and in [72], where the developers chose a common ergonomic grip, the foil grip. An innovative handle design is presented in [79], where the instrument ergonomic handle is a grip-type handle which is connected by a mechanical joint to the instrument shaft. This reduces forced wrist movements since the handle works independently from the shaft. Finally, a different suggestion when it comes to designing the robotic handle was presented in [65], where the authors propose that the controller for operating the robotic tool tip must be in the range of existing devices used with commercially available endoscopes in terms of its size.

A more difficult to satisfy but equally important requirement is the incorporation of intuitive control that can reduce the surgeon's learning curve and training period. Such an intuitive control pattern is followed in [117], where the handle is the motion input interface, which converts the attitude of the surgeon's hand into electrical signals and in [96] where the handle mechanism preserves the intuitive actuation mechanism on the existing disposable forceps being actuated simply by squeezing the tool handle. Similarly, the device presented in [102], was required to accurately transmit the interaction forces and reproduce faithfully the mechanical impedance of the tissue so that the surgeon can sense the tissue interaction realistically.

The final ergonomic requirement that was repeatedly met in the reviewed works was the suggestion that in order for the device to not induce strain and fatigue on the surgeon's wrist, it should be mostly maintained by a resting hand. This was met in [88], where after a number of meetings with laparoscopic surgeons it was highlighted that operators should be able to maintain a natural position of the hand with the instrument, and in [68], where the resting position of the actuating gimbal joystick coincides with a resting hand. Concluding, the instrument presented in [118] has a pivot between the handle and the shaft letting the surgeon keep the handle at an angle with respect to the shaft. Table 2.3 below summarizes the optimal design considerations found in Table 2.1, and highlights the papers that follow each one.

Table 2.3: The optimal design considerations, and the papers that presented robotic instruments that were developed following them.

Design considerations	References
The same handle design should cater to different hand sizes.	[93], [65], [68], [69], [71], [72], [75], [112], [76], [92], [77], [78], [98], [79], [83], [106], [86], [87], [107], [88], [108], [90], [116]
The instrument actuation means should be finger operated	[102], [101], [93], [95], [65], [68], [69], [70], [72], [73], [96], [75], [104], [76], [92], [77], [78], [115], [79], [80], [81], [83], [84], [85], [86], [87], [88], [90], [56]
For precision control, the thumb should control the robot-joints, and the index-finger should operate the robotic gripper.	[63], [65], [69], [72], [73], [75], [76], [77], [78], [79], [80], [84], [86], [88], [90], [56]
A resting hand pose should hold the instrument at rest.	[68], [101], [68], [76], [77], [98], [79], [82], [84], [85], [107], [88], [108], [116], [56]
The wrist should not support much weight throughout the duration of the procedure.	[93], [94], [110], [65], [68], [69], [70], [73], [75], [112], [104], [76], [92], [114], [77], [97], [105], [98], [79], [81], [83], [106], [86], [87], [107], [116], [90], [56]
The instrument should allow for intuitive control.	[102], [68], [71], [103], [96], [76], [80], [90], [56]
The handle should include a large palmar grip surface.	[102], [110], [63], [69], [70], [103], [73], [75], [76], [114], [78], [115], [82], [86], [88], [116],[56]
The handle with the shaft should maintain a 45o angle.	[63], [69], [92], [88], [56]
The instrument should provide a platform to incorporate complex robotic assistance.	[110], [68], [69], [71], [103], [112], [76], [77], [97], [105], [78], [115], [87], [90]

2.5.5 Ergonomically designed tools and procedural ergonomics

The majority of the devices presented in this chapter have incorporated at least some of the ergonomic suggestions found in literature in their development. However, only a few of them have been investigated during a pre-clinical, clinical, phantom, or comparative study to effectively validate whether these design choices led to an improvement of the procedural ergonomics associated with the targeted surgical application. Out of all the papers that were reviewed for the purposes of this review chapter, and while all of them were evaluated for their efficacy and performance, the number of papers that evaluated the device they

presented for its impact on procedural ergonomics was only 12, less than 22% of the total number of devices. Out of these 12 studies, 6 reported results on improved procedural ergonomics.

The robotized needle holder presented in [63] was investigated in a crossover randomized study and indicated that it can improve the surgeon postural comfort, whereas the forearm-mounted instinctively controlled handle in [68] outperformed a conventional neurosurgical tool in a preliminary clinical experiment that assessed their performance and ergonomics.

Similarly, the DEX mechatronic system that was evaluated in [79] for the first time, resulted in better ergonomics for the surgeon's hand posture during suturing, even though it did not show significant improvement in terms of precision and quality. Finally, another commercial system that did not necessarily result in better performance was the Kymerax handheld robotic instrument. While execution time as well as precision during a set of basic suturing tasks were superior when using the conventional tool, the robotic instrument can be associated with improved ergonomic body posture [20].

Less encouraging to those ergonomic results are the findings in [78] and [72]. In the former study, while the hand-held robotic device for laparoscopy showed promise by outperforming the conventional tool in some difficult laparoscopic tasks, it left a large space for improvement in terms of ergonomics and comfort. Similarly, in the latter study, the hand-held lightweight dexterous instrument that incorporates end-effectors from the EndoWrist family showcased improved performance to non-articulated tools, but the surgeons that operated the device did not agree with the use of the joystick.

The figure below, Fig. 2.9, breaks down the devices in categories based on whether they incorporate ergonomic suggestions into their design, and whether they were evaluated for their impact on the target application procedural ergonomics.

2.5.6 Bridging the gap between efficacy and ergonomics

All design guidelines suggested in Section 2.5.1 are satisfied at least in four different papers. It is very common for handheld surgical robots to cater to various hand-sizes, to be finger-operated with a large palmar grip surface, and to be compact and lightweight, so that the wrist is alleviated from excess weight and fatigue. All these ergonomic suggestions are met with the use of miniaturized motors and electronics that can be housed inside compact and lightweight handles, that allow for a comfortable palmar grip. When the device is mostly

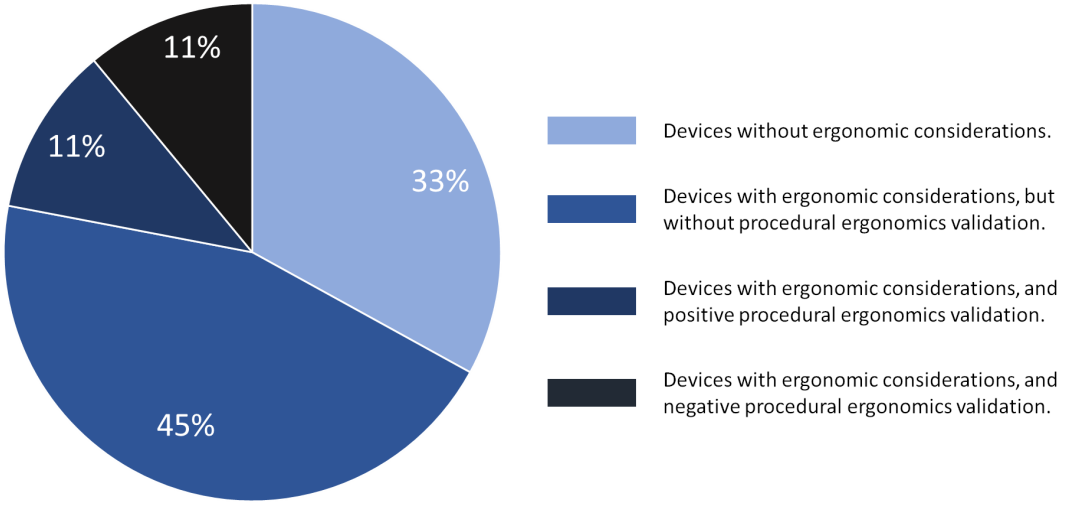

Figure 2.9: Pie-chart breaking down the number of devices that were ergonomically designed, and the number of devices that lead to improved procedural ergonomics.

maintained by the palm and hand, the surgeon is then free to use their fingers to operate the robotic joints of the device with an actuation module, such as a joystick, rotary switch or trigger.

More complex design guidelines, such as the need for instinctive and intuitive control, or trying to maintain the hand at rest, are satisfied with greater effort. To achieve intuitive control, the device should incorporate a manipulation module that can immediately map the surgeon's wrist movements to the robotic joint movements. This module can be a gimbal-joystick, a pointing and control device specialized for movement in 3D environments, or even an array of electromyography sensors that would transfer the surgeon's muscles movement to the robot joints.

No matter the module used, this handheld device would require to have a stable platform around which the operator would actuate the module. In most laparoscopic operations this role could be carried out by the trocar, which functions as a portal for the placement of surgical instruments. However, in surgical operations where these mounts are not used, such as in minimally invasive neurosurgery, the tool itself should incorporate this platform. To achieve that, the tool can be wrist- or forearm-mounted, or in the case of heavier handheld devices, the intuitive control can be aided by the external usage of a robotic or non-robotic holder.

One of the least commonly met ergonomic suggestions in developed handheld devices, is the ability to maintain a resting hand for a significant portion of the operation. This is

because actuation modules such as joysticks are placed at the exact centre of the device as to allow usage by both right- and left-handed surgeons. A potential solution to this problem could be the development of handedness specific tools, that would place the joystick at an angle either to the left or to the right of the device shaft so that the fingers and the thumb can maintain a resting pose. Ideally, the device would employ a movable part that could be placed at the optimal position for each surgeon's hand.

Finally, one crucial step into developing a widely-adopted handheld robotic device is to involve human factors evaluation from the earlier stages of development. Of all the devices presented in this study, 22% had gone through an ergonomic assessment, with only 11% presenting ergonomic improvements. Usability, user experience, as well as ergonomics assessment studies during pre-clinical and clinical studies that evaluate the ergonomics of a device can play a crucial role into its development, and the feedback that comes out of these studies can have a major impact on increasing the chances for a successful clinical adoption.

2.6 Discussion

Technological advancements, combined with the need to increase the efficacy of complex surgical approaches, propelled the development of a plethora of surgical robotic instruments to aid in a variety of operations. Common features incorporated in robotic instruments such as enhanced articulation and force feedback capabilities, have popularised the usage of robotic systems into the operating theatre, and expanded this field of research. In this chapter, work relating to the technologies developed as part of this thesis was presented.

Section 2.3, which introduces a wide range of neurosurgical robots, relates to the thesis in its entirety, since the aim of this work is to develop a novel neurosurgical robot. The miniature end-effector aimed to be incorporated in the handheld robotic neurosurgerical instrument is tendon-driven and employs a spherical joint. This is why studies showcasing tendon-driven end-effectors, as well as spherical joint manipulators were introduced in Section 2.4 and are related to Chapter 3.

Due to the exceptionally limited and narrow workspace of the nasal access path, robotic end-effectors developed for endonasal procedures should be miniaturised. This restricts the usage of traditional robotic end-effectors with diameters close to 10mm in minimally invasive neurosurgery. Concentric tube manipulators have smaller diameters that can reach sub-millimetre scale and thus are perfect for constrained spaces, but their distal dexterity

and force delivery capabilities are limiting for complex surgical procedures. The choice of a spherical joint was based on these findings, and the fact that such joints can concentrate large sums of material in small volumes, increasing the chances for adequate force delivery without fatigue and breakage.

Having analysed pre-existing work on robotic end-effectors, and since the robotic instrument developed in this thesis will be handheld, a review on handheld robots for minimally invasive surgery and their ergonomics considerations was also included in Section 2.5, relating to Chapter 4. Handheld robots are a convenient solution for the operating theatre, since they offer a wide range of robotic features, while maintaining a compact design and resemblance to conventional instruments. This makes their integration into the surgical workflow easier than bulkier tele-operated robotic systems. However, handheld surgical robots are often non-ergonomically designed, and even when they are, it is rare that they have been validated for their procedural ergonomics.

The aim of this thesis is to develop a handheld robotic instrument that can cater both to the patient and the surgeon. To aid the patient, the enhanced articulation of the robotic end-effector aims to expand the operational workspace and surgeon dexterity, and thus, the operative efficacy. To aid the surgeon, the ergonomic design of the handle and related validation studies aim to improve procedural ergonomics, and avoid burdening the surgeon with physiological problems. In the following chapters, the effort to develop such a device is presented.

Chapter 3

A robotic end-effector for the Expanded Endoscopic Endonasal Approach

3.1 Introduction

The first step in developing a handheld robotic tool for the EEEA was the fabrication of a miniature robotic end-effector that satisfies the requirements of this specific surgical procedure. To iterate through the various joint-designs and assembly arrangements, a modular motor test-bench was fabricated that allowed for easy component replacement and expansion. After the joint-design and actuation means were selected to accommodate the articulation and structural integrity requirements, the prototype was investigated for these characteristics to evaluate its efficacy. Preliminary experimental evaluation suggested feasibility and increased capability, but left room for improvement. This is why an iterative development process was followed that produced a more robust articulated end-effector.

In this chapter, the development of a novel, tendon-driven, 3 DoF robotic instrument for the EEEA with end-effector articulation based on a spherical joint design is explored. The end-effector is actuated by a miniautre differential drive tendon-routing system. The joint mechanism has increased distal-tip dexterity and can be fabricated in a small diameter profile. Initial experiments suggest that the tool achieves favourable structural integrity, repeatability and workspace reach. This miniaturised prototype set the foundation for an articulated end-effector that could be fabricated in such a way as to avoid breakage and structural fatigue limitations.

The contributions that are associated with this chapter are:

- Dimitrakakis, E., et al., ”A spherical joint robotic end-effector for the Expanded Endoscopic Endonasal Approach.”, (2020), Journal of Medical Robotics Research

- Dimitrakakis, E., et al., "Towards the Development of a Novel Handheld Robotic Tool for the Expanded Endoscopic Endonasal Approach.", (2019), 9th Joint Workshop on New Technologies for Computer/Robot Assisted Surgery (CRAS)

- Dimitrakakis, E., et al., "Handheld Robotic System for Endoscopic Neurosurgery", (2023), IEEE Robotics and Automation Letters, (submitted)

3.2 Proposed tool implementation

3.2.1 Design and fabrication

When designing the robotic end-effector, the main constraint present was the very limited operative workspace. In endonasal surgery, the main surgical workspace is the sphenoidal sinus which is mostly resembled by a 25mm diameter sphere [120]. This limitation, combined with the narrow passage that the tool must follow to reach the sinus and the fact that more than one instruments are often used through one nostril at the same time, lead to the need for a small diameter. The proposed robot mechanism has a diameter of 3.6mm and a length of 19.4mm. Commercially available tools for endonasal surgery have diameters in the range of 1mm to 7mm, and end-effector lengths in the range of approximately 10mm to 20mm [121], which deem the proposed end-effector adequately small and simultaneously big enough to avoid breakages as discussed in Section 3.4.3.

The end-effector's articulation properties were based around the use of a spherical joint design rather than a more traditional articulated mechanism. This is motivated by using the spherical joint as a platform for easy tool adaptation and also for potentially enhanced robustness since a sphere concentrates a large amount of material and is difficult to break. Furthermore, the spherical joint concentrates both pitch and yaw rotations around the same origin, achieving articulation at a minimum size. Six nylon tendons, two for each DoF, with a diameter of 0.25mm terminate on the distal end of the sphere, passing through 0.5mm diameter channels. The end-effector of the robot is coupled on the distal end of the sphere completing the robot assembly.

The tendons pass through the 6 channels that exist throughout the robot body and terminate at different positions depending on which DoF they actuate. Tendons 1 and 2 actuate the pitch axis DoF and terminate at the distal end of the main body of the robot. Tendons 3 and 4 actuate the yaw axis DoF and also terminate at the distal end of the main body of the robot, but in points whose connecting line is perpendicular to the line that

connects the termination points of tendons 1 and 2. Lastly, tendons 5 and 6 actuate the gripper DoF and terminate on the upper part of the gripper. The tendon channels and the tendon termination points are shown in Fig. 3.1.

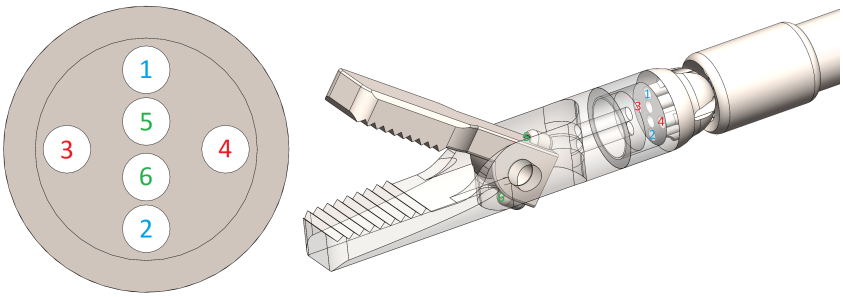

Figure 3.1: The channels that tendons pass through (left) and their termination points (right). Blue is for the pitch axis DoF, red is for the yaw axis DoF and green is for the gripper DoF.

The tendons are fixed to their corresponding termination positions by either tying their loose end in an 8-figure knot, or by crimping a small piece of tubing at the tendon's very end. After tendons $1-4$ are fixed at their termination points, the bottom part of the gripper is coupled with the main body, and the upper part is coupled with the bottom part. The tendons work in antagonistic fashion, meaning that when one of the tendons pulls, the other one lets go, giving, thus, each DoF a two-way actuation capability (up/down, left/right, open/close). This antagonistic logic is depicted in Fig. 3.2. The arrows show the direction towards which the tendon is either pulled or let go.

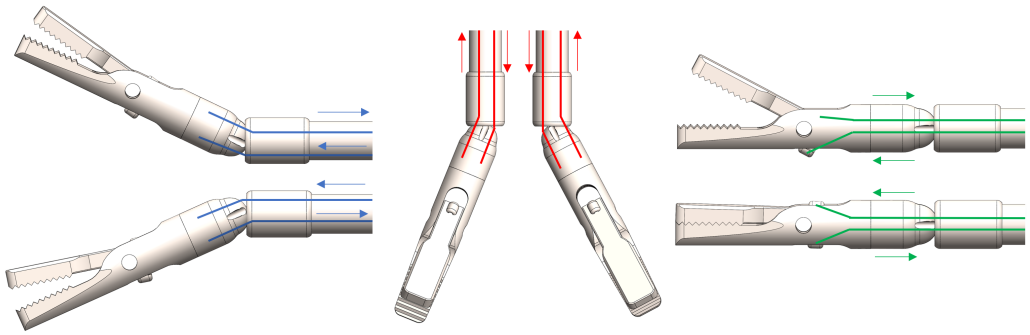

Figure 3.2: The antagonistic configuration that controls each DoF. The arrows show the tendon movement direction.

Additive manufacturing, and more specifically stereolithography (SLA), was used to print the initial implementation of the 3.6mm robotic end-effector. The printing material was clear resin, a type of resin used in fluidics, optics and mold-making. This material was chosen because it allows for printing resolutions as small as 25μm. The printer used

was the desktop 3D printer Form 2 (FormLabs, Somerville, Massachusetts, United States). A number of different end-effectors were designed as part of this study to cover a larger number of tasks during the endonasal approach. These end-effectors are a flat-long spatula dissector, a round spatula dissector, a ring curette and a spring-loaded bone punch that, however, needs further prototyping. Their design and implementation is shown in Fig. 3.3. All these surgical instruments would benefit by articulation capabilities and in large part they share the same kinematic model, which means their kinematics and control were uniform.

Figure 3.3: CAD renderings (left) and SLA-printed implementation of the end-effectors (right)

The robot end-effector is fixed to a stainless steel grade 316 seamless tube shaft of 3*mm* outer diameter and all the tendons pass through 0.457*mm* diameter 304 welded hard drawn stainless steel wire-guiding tubes which do not allow the tendons to get tangled with each other. This 3*mm* shaft is then fixed on a test-bench setup that was used to validate the end-effector's efficacy. The test-bench setup consists of an upper tendon-housing part that contains the axes where the tendons terminate and their rerouting system, and a lower actuation part with all the motors. It was again produced via additive manufacturing techniques, this time in polylactic acid (PLA) plastic using the desktop 3D printer Ultimaker S5 (Ultimaker, Geldermalsen, Netherlands).

The tendons starting from the joints of the end-effector terminate on capstans that lie on three 3*mm* diameter rigid stainless steel shafts on the tendon-housing part, which are co-axially connected with the motor shafts on the actuation part of the system. Each DoF is controlled by two nylon tendons that are fixed on capstans on the same rigid shaft. Since the tendon insertion points from the shaft to the test-bench upper part are not colinear with their corresponding capstans, there is also a rerouting mechanism that uses pulleys to redirect the tendons from their one point to the other in order to reduce their backlash and friction. The rerouting mechanism as well as the tendons insertion points are shown in Fig. 3.4.

For a deeper understanding of how the tendon pulling and pushing leads to robot joint

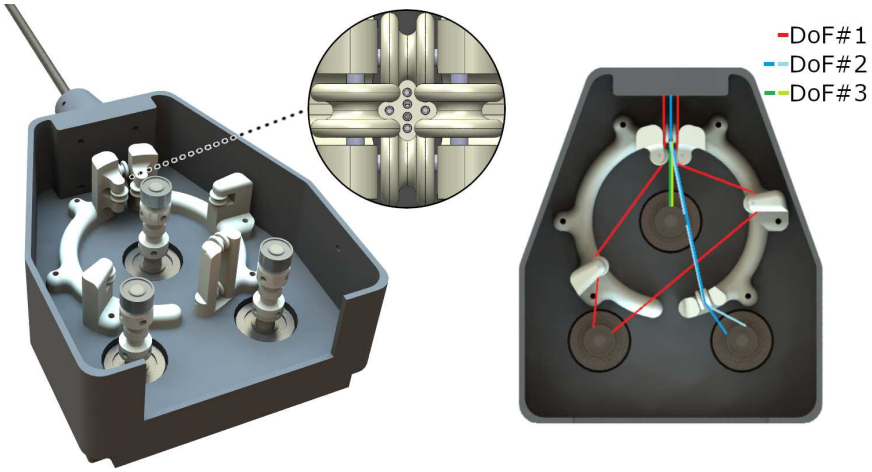

Figure 3.4: CAD renderings of the rerouting mechanism with the tendon insertion points and the actual tendon routing. Red is for the first DoF, blue - light blue is for the second DoF and green - light green is for the third DoF.

movement, Fig. 3.5 depicts the physical relationship between the tendons of one of the robot DoF and their corresponding robot joint.

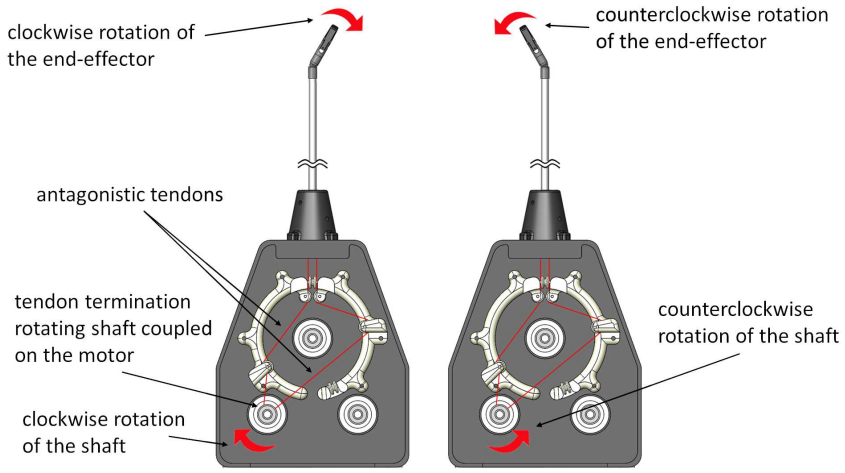

Figure 3.5: Physical relationship between one of the robot joints and its corresponding tendons.

The motors used for the actuation system were three MX-28T Dynamixel Robot Servo Actuators (Robotis CO. Ltd, South Korea) with a stall torque of $25.5 kg \cdot cm$ and an angular step resolution of 0.088^o. Each actuator utilizes an embedded PID-controller and communicates through a USB-to-TTL bus at a rate of $50 Hz$. Motor selection for this setup was based on the torque capabilities of the motors and their seamless integration into the system, a result of their embedded encoders and controllers. The motors are fixed on a PLA-prototyped base and covered by a PLA mount-plate while on the rotating shaft of each motor

an SLA-prototyped coupler is fixed. The mount-plate of the actuation part of the test-bench is equipped with a coupling pattern on which the tendon-housing part is fitted, while the motor shaft couplers connect with the rigid rotation shafts that stand inside the upper part. In this way, the actuation system is separated from the tendon-housing for easy end-effector swapping. A complete overview of the system, both in CAD and its implementation, is shown in Fig. 3.6.

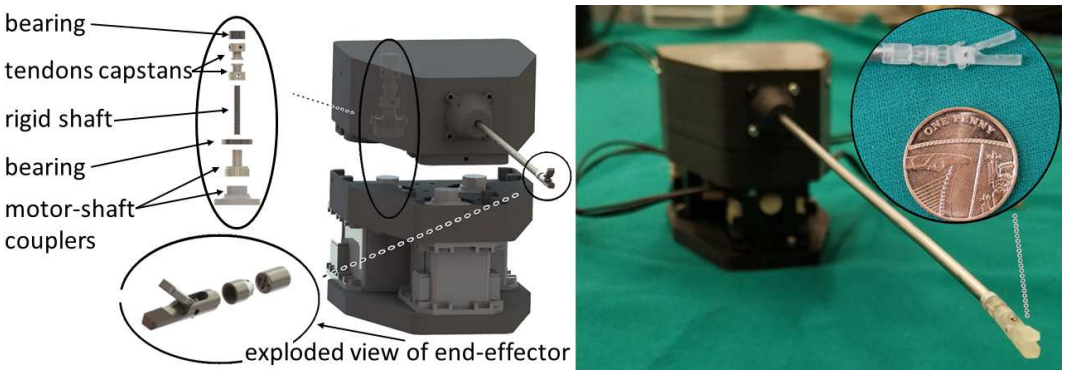

Figure 3.6: (Left) CAD renderings of the test-bench system and the end-effector. The top-left circled assembly indicates the 3*mm* diameter rigid stainless steel shaft on which the tendons terminate, whereas the top-down circled assembly is an exploded view of the end-effector. (Right) Implementation of the test-bench system and the end-effector.

3.3 Kinematic analysis

3.3.1 Forward kinematics

The kinematic model of the robot is extracted using the Denavit-Hartenberg (DH) convention with the frames of the first two DoF located on the middle point at the base of the spherical joint, while the frame of the third DoF is located on the axis of rotation of the gripper end-effector. Although a spherical joint design was used, the joint is rotating over two axes only, namely the pitch and yaw axes, and not over the roll axis since the tendons and antagonistic motion constrain such rotation. The missing roll motion, as well as the translation of the tool, will be carried out by the surgeon's hand when the handheld robotic tool is implemented in future work. The end-effector frame is located on the distal middle point of the robot, namely on the bottom-middle part of the rotating part of the gripper. The joint frames of the robotic end-effector are shown in Fig. 3.7, and the produced DH parameters are found in Table 3.1.

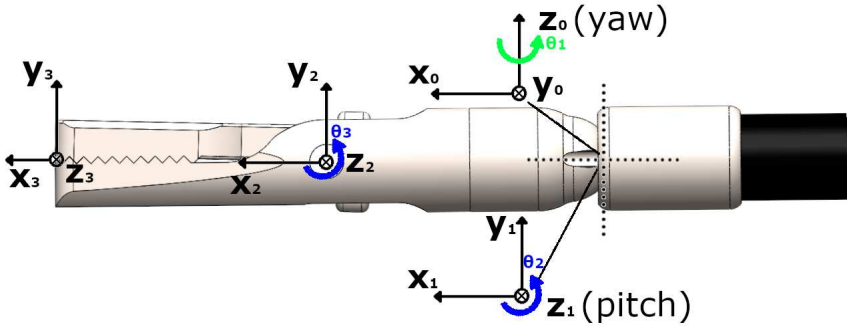

Figure 3.7: The robotic end-effector joint frames.

Table 3.1: The DH parameters of the 3.6*mm* robotic end-effector.

i	$a_i\,(mm)$	$\alpha_i\,(rad)$	$d_i\,(mm)$	$\theta_i\,(rad)$
1	0	$\pi/2$	0	θ_1
2	8.6	0	0	θ_2
3	9.5	0	0	θ_3

3.3.2 Workspace analysis

The end-effector design was produced based on the operative space requirements. It was then important to evaluate its workspace capabilities to make sure that while miniature in size, it would pose a substantial improvement over current non-articulated instruments.

In Fig. 3.8, the target-reaching capabilities of the proposed end-effector are compared to that of traditional tools using the open-source software CHAI3D [122]. This simulator was implemented using the robot's forward kinematics equations and was controlled by a 6-DoF joystick that controls the robot joints and the shaft movement in 3D space.

Alongside the robotic end-effector, a traditional non-articulated tool was implemented in the same framework, again controlled by the joystick. The aim of this simulator was to test the robot kinematics and showcase that some areas besides the pituitary gland and around the base of the brain can be reached with the robotic end-effector but are out of reach with the conventional tool. This is depicted when all three red points can be reached and turn to green with the articulated tool, but only one of them with the traditional non-articulated end-effector.

Expanding on this preliminary proof-of-concept workspace analysis of the end-effector, a more thorough analysis was carried out in the robot simulation platform CoppeliaSim [123]. Both the robotic end-effector and a non-articulated tool with the same dimensions were simulated in this environment.

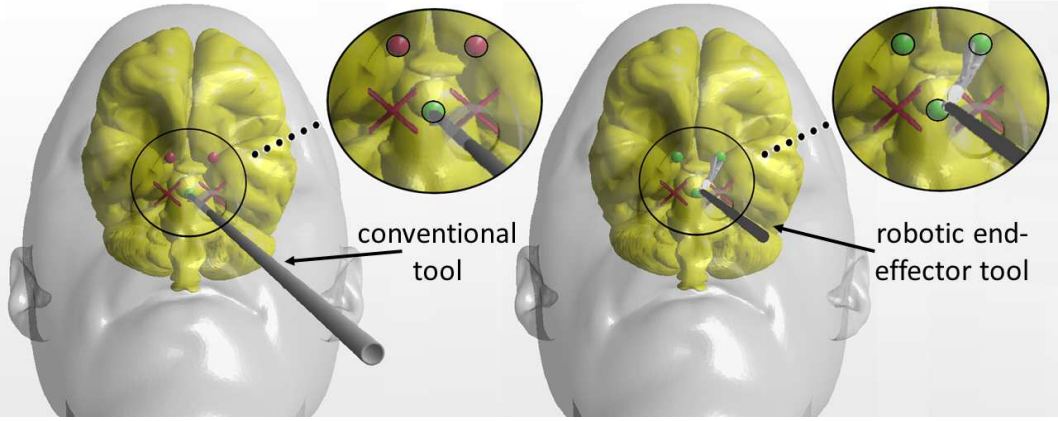

Figure 3.8: Reaching areas beneath the pituitary gland with a simulated traditional instrument (left), and with the proposed robotic end-effector (right). Red points represent points the conventional tool can not reach whereas the green points represent the points the tools can reach. Red Xs represent no-go areas besides the pituitary gland.

To also simulate the physical constraint within which the tools operate during surgery, a 3D model of a cranial CT scan, modified so that it only features the EEEA areas of interest, was also input into the simulation platform. Apart from the cropping of the 3D model to exclude areas of the skull that are out of scope for this procedure and would slow down the simulation, a cylindrical channel was also created starting at the sphenoid ostium, and passing through the sphenoid sinus granting access to the pituitary gland area. This channel is created by the surgeon during the EEEA procedure to access the pituitary gland, and is highly constraining the tool motion. The diameter chosen for the cylindrical channel is $1cm$ [10]. The modified 3D model is shown in Fig. 3.9.

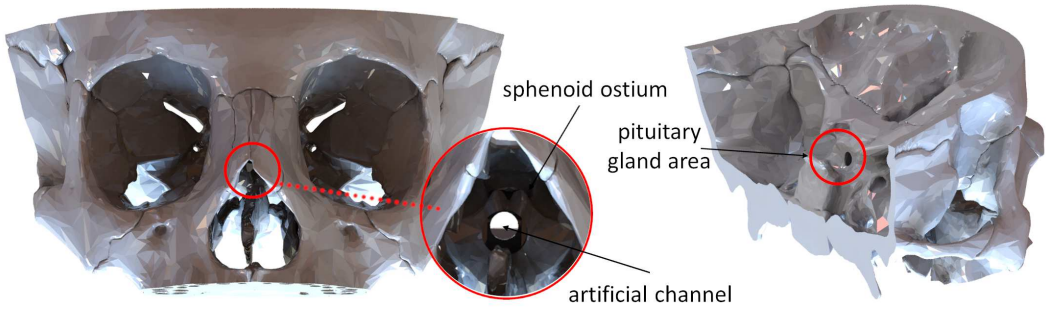

Figure 3.9: 3D model of a cranial CT scan used to determine the available workspaces during EEEA. The artificial channel shown inside the circled areas represents the channel that the surgeon creates during surgery and grants access to the pituitary gland area.

The goal of this workspace analysis was to compare the effective workspace of the

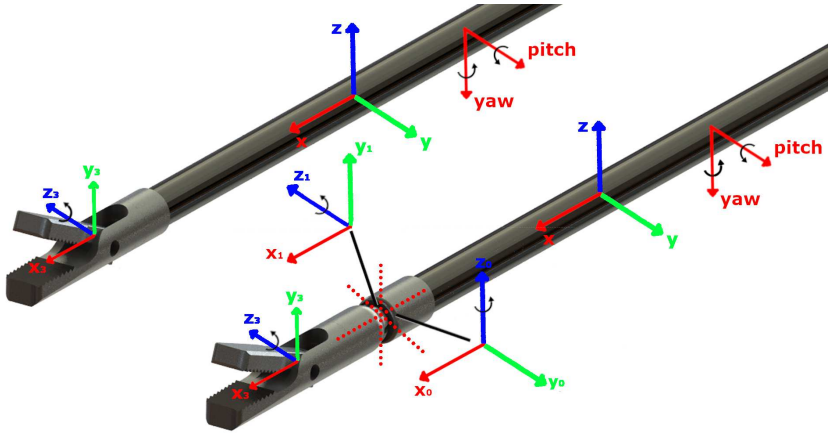

Figure 3.10: DoF coordinate frames of the traditional non-articulated tool (left), and of the suggested robotic end-effector (right). The robotic end-effector comprises of an additional two articulated joints represented by frames (x_0, y_0, z_0) and (x_1, y_1, z_1).

non-articulated tool with that of the suggested robotic end-effector. To calculate both workspaces, a search was carried out that iterated through each tool's various DoF. The non-articulated tool was simulated by a 5 DoF system. 3 DoF for the (x, y, z) translation of the shaft, and 2 DoF for the $(yaw, pitch)$ rotation of the shaft. The robotic end-effector was modelled similarly, with the addition of 2 DoF for the end-effector joints. In both cases the roll DoF, as well as the gripper open and close DoF, were not taken into consideration for simplification reasons. The DoF coordinate frames for both tools on a side-by-side comparison can be seen in Fig. 3.10.

The workspaces were evaluated by accessing a number of different shaft positions, entering from the right side of the nasal cavity, and different shaft and robot-joints orientations. The range of translation of the shaft was $20mm$ with an increment of $0.6mm$ on each axis, the range of rotation of the shaft was 10^o with an increment of 0.5^o on each axis, and the range of the robotic end-effector DoF joint-space angle vector was 70^o, from -35^o to 35^o, discretised by 5^o. These specific ranges and steps were a result of trial-and-error testing to find the most suitable values. The physical constraint was incorporated by determining mesh collision between the tools and the cranial model. An end-effector point was pushed into the point cloud only if no part of the tool was in contact with the physical constraint by employing the mesh collision checking capability of the CoppeliaSim software. The resulting effective workspaces are shown in Fig. 3.11.

It is evident that the robotic end-effector has a broader workspace and can reach a significantly larger amount of points in 3D space, suggesting that it can potentially improve

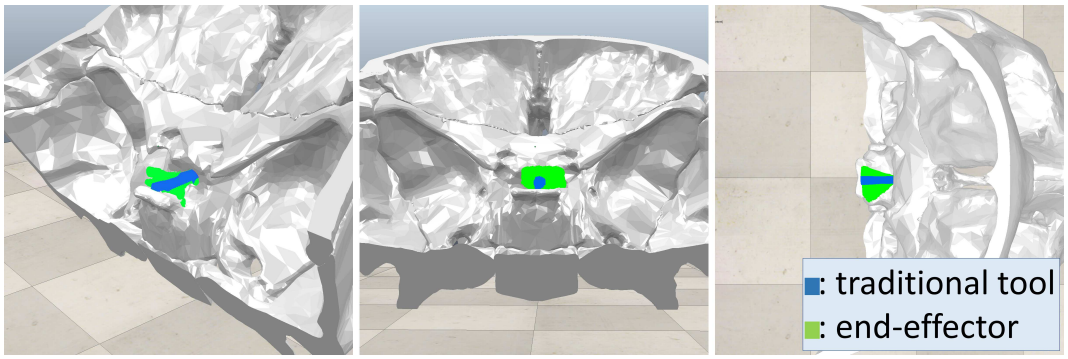

Figure 3.11: Workspace comparison between the proposed robotic end-effector (green) and a traditional, non-articulated tool with the same dimensions (blue), from three different viewing angles.

the efficacy of EEEA. Adding to this analysis, it could be useful to conduct the workspace search in the entirety of the available workspace, rather than just after the sphenoid sinus. This would require a high accuracy 3D model, inclusive of soft-tissue and other structures and could be the scope of future work.

3.3.3 Inverse kinematics and tendon lengths

For the inverse kinematics model of the robot, the forward kinematics equations extracted using the Denavit-Hartenberg convention were used, resulting into closed form solutions for the calculation of $[\theta_1, \theta_2, \theta_3]$ as shown in Eq. 3.1.

$$\theta_i = \begin{cases} \arcsin(r_{13}), & \text{for } i = 1, \\ \pm \arccos\left(\dfrac{y - 0.0098 \cdot \sin(\theta_1) \cdot r_{32}}{0.0096 \cdot \sin(\theta_1)}\right), & \text{for } i = 2, \\ \arcsin\left(\dfrac{r_{31} - \frac{\sin(\theta_2)}{\cos(\theta_2)} \cdot r_{32}}{\cos(\theta_2) + \frac{\sin(\theta_2)}{\cos(\theta_2)} \cdot \sin(\theta_2)}\right) & \text{for } i = 3. \end{cases} \tag{3.1}$$

with the Homogeneous Transformation being: $H(\theta_1, \theta_2, \theta_3) = \begin{bmatrix} r_{11} & r_{12} & r_{13} & x \\ r_{21} & r_{22} & r_{23} & y \\ r_{31} & r_{32} & r_{33} & z \\ 0 & 0 & 0 & 1 \end{bmatrix}$.

Assuming a computed joint-space angle vector, the stroke of each antagonistic tendon pair must be computed in order to control the robot. The method used is similar to the one used in [124]. For each rotational DoF there are two tendons that control the movement of each angle in an agonist-antagonist fashion. The length of the tendon is defined as the

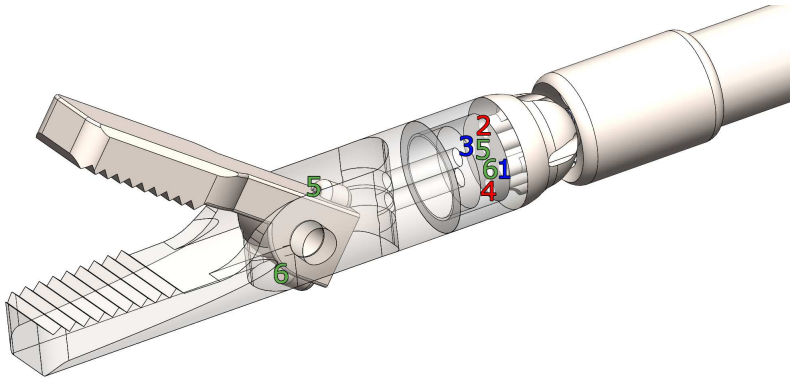

Figure 3.12: The 6 channels on the spherical joint where the tendons pass through. The exact same pattern is followed on the base of the end-effector, whereas only tendons 5 and 6 arrive at the upper part of the gripper.

distance between the base of the robot, rather than the starting point of the tendon on the tool-housing capstan, to the point that each tendon terminates.

The lengths of the tendons are computed by locating the $3D$ positions of the pass-through channels for every tendon and calculating the distance between two consecutive channels. As is evident in Fig. 3.12, the robot has six channels that tendons pass through.

Four of them, channels $i = 1$ to 4, are diametrically positioned at an $1mm$ radius from the centre, terminate on the distal end of the sphere and control the two first DoF. The remaining two, channels $i = 5$ and 6, control the gripper end-effector DoF, are located with a $\pm 0.35mm$ offset from the centre on the z-axis, and terminate on the gripper attachments. On the base of the robot the six holes are positioned as shown in Eq. 3.2 for $r_1 = 1mm$ and $r_2 = 0.35mm$.

$$P_i(x,y,z) = \begin{cases} (x_0, y_0 + r_1, z_0), & \text{if } i = 1, \\ (x_0, y_0, z_0 + r_1), & \text{if } i = 2, \\ (x_0, y_0 - r_1, z_0), & \text{if } i = 3, \\ (x_0, y_0, z_0 - r_1), & \text{if } i = 4, \\ (x_0, y_0, z_0 + r_2), & \text{if } i = 5, \\ (x_0, y_0, z_0 - r_2), & \text{if } i = 6. \end{cases} \tag{3.2}$$

After the channels have been positioned in 3D space using the forward kinematics, the resulting homogeneous transformation matrices are used to calculate the Euclidean geometric distances. Finally, the difference between the lengths of the tendon on the current

joint-space and the desired joint-space is turned into the angle by which the motor should rotate in position control.

The positions of the channels P_i' and P_i'', for channel $i = 1$ to 6, in 3D space for a specific joint-space angle vector $[\theta_1, \theta_2, \theta_3]$ are calculated using Eq. 3.3 and Eq. 3.4. P_i', for channels $i = 1$ to 4, represents the positions where the corresponding tendons terminate, whereas for channels $i = 5$ and $i = 6$, P_i' represents the passing-through channels on the spherical joint for tendons 5 and 6. The termination points of the latter pair of tendons is represented by the P_i'' position pair.

$$P_i'(x,y,z) = A_{0i}^1 \cdot P_i(x,y,z), \text{for } i = 1 \text{ to } 6, \tag{3.3}$$

$$P_i''(x,y,z) = A_{0i}^2 \cdot P_i(x,y,z), \text{for } i = 5 \text{ and } 6, \tag{3.4}$$

where A_{0i}^j is the Homogeneous transformation that corresponds to joint j and channel i. Then, the Euclidean distance L_i between two consecutive channels is:

$$L_i = ||P_i'(x,y,z) - P_i(x,y,z)||, \text{for } i = 1 \text{ to } 4, \tag{3.5}$$

$$L_i = ||P_i'(x,y,z) - P_i(x,y,z)|| + ||P_i''(x,y,z) - P_i'(x,y,z)||, \text{for } i = 5 \text{ and } 6, \tag{3.6}$$

and to compute the displacement of tendon i between two joint-space angle vectors j and j', the tendon lengths L_i^j and $L_i^{j'}$ need to be computed and subtracted.

$$\Delta L = |L_i^j - L_i^{j'}| \tag{3.7}$$

A visual example of how these lengths are computed is shown in Fig. 3.13.

Finally, to compute the angle ϕ by which the motor needs to rotate so that the tendons are pulled/pushed by the appropriate amount, Eq. 3.8 is used:

$$\phi = \frac{\Delta L}{R_c}, \tag{3.8}$$

where R_c is the radius of the capstan on which the tendon terminates. In this case capstans of radius $1.5mm$ were used, and thus $R_c = 1.5mm$. Since ΔL is always positive, the sign

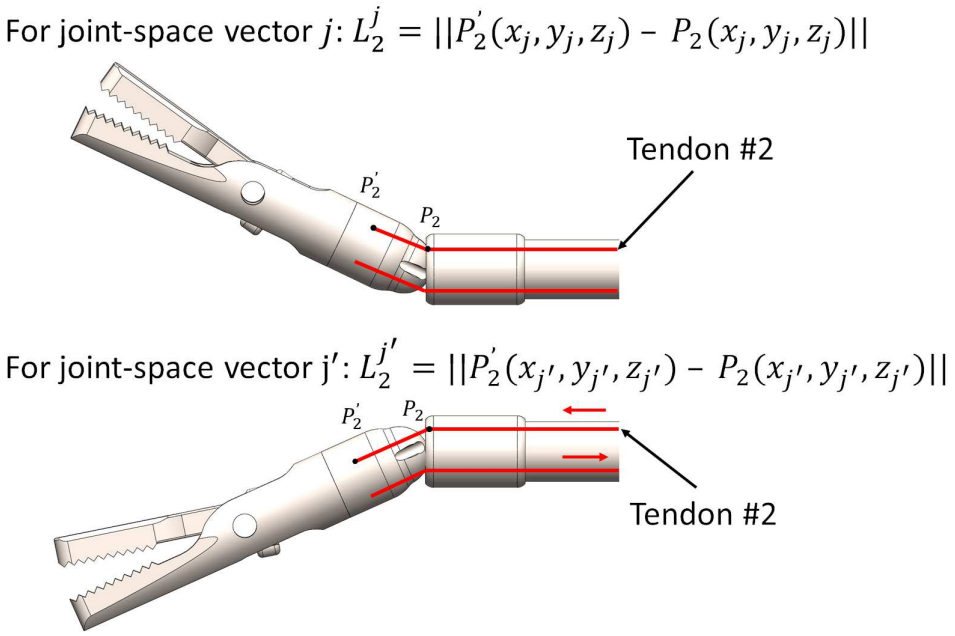

Figure 3.13: Visual representation of how the length of tendon 2 is computed for two different joint-spaces j and j'.

of the angle is decided by a software convention taking into account the direction of joint movement. This joint movement direction is easy to calculate, because both the current joint-space angle vector and the target joint-space angle vector are known. The sign of each motor angle is determined by the sign of the difference between the angle of its corresponding joint at its current joint-space and the angle of its corresponding joint at the goal joint-space.

It is worth mentioning that some simplifications took place during this mathematical process. Each pair of tendons does not always move by the exact same distance because for a spherical joint, movement of DoF 1 results in minor movement of DoF 2 and vice versa. Thus, there is chance that for some joint-space angle vectors one tendon is pulled or pushed more than its antagonist is pushed or pulled. This coupling could potentially vanish by better constraining the spherical joint inside its base, or by placing the tendon channels on different positions on the joint. This difference in tendon lengths between antagonistic pairs, however, and more specifically between tendon pairs 1 and 3, 2 and 4, and 5 and 6, was found out to be very small numerically. Since only one motor per tendon pair is used, this difference was disregarded and the rotation of the motor was based on the average of the two lengths, without trying to build a better base constraint for the spherical joint. Another

simplification is that in this analysis tendon bending radii that would appear in extreme joint angles because of the geometry of the spherical joint were not taken into account.

3.4 Experimental Evaluation

3.4.1 Workspace and repeatability study

The robotic end-effector was tested for its repeatability and workspace capabilities. The focus was on repeatability rather than accuracy since in robotically assisted surgical procedures the robot is either tele-operated via a master console or directly controlled with a handheld mechanism by the surgeon making sure the desired motions are achieved under endoscopic view. For both tests, optical tracking was employed to measure the position of the end-effector. More specifically, two optical markers that were fixed on an SLA-printed attachment were tracked in 3D space. The attachment was again printed in clear resin using the Form 2 desktop 3D printer. The end-effector was firmly gripping the marker attachment so that the tracked positions of the markers could be used to extract the position of the end-effector as detailed later in the section.

For the repeatability test, a vector of 19 desired workspace joint values uniformly generated within the joint-space range between $[-30,-30,30]$ and $[30,30,30]$ was created, with $\theta_3 = 30$ the gripper angle required to get a good grip on the SLA-printed tracking marker attachment. The robotic end-effector was instructed to move between those 19 points, and each time a movement was finished the positions of the markers in $3D$ space were recorded with the NDI Optotrak Certus motion capture system (Northern Digital Inc, Canada). This system has a tracking accuracy of $0.1mm$ and a resolution of $0.01mm$. The robotic end-effector and its test-bench were positioned in front of the tracking system so that the markers are in direct line-of-sight of its three cameras.

Both the robot with its test-bench actuation system, and the capture system were operating within the Robot Operating System (ROS) framework [125]. The application consisted of two nodes. Within the first node, the kinematic computations took place and the motors were instructed to rotate by a specific angle, which corresponded to the desired end-effector position, as shown in Section 3.3. To ensure that the motors had reached their desired position before moving on to measure the position of the tracking markers, a 'do-while' logic was implemented. The desired position was fed into the motors until the current position was measured to be within a threshold of 0.18^o maximum error in motor angle. The capture system was operating within the second node and was constantly pub-

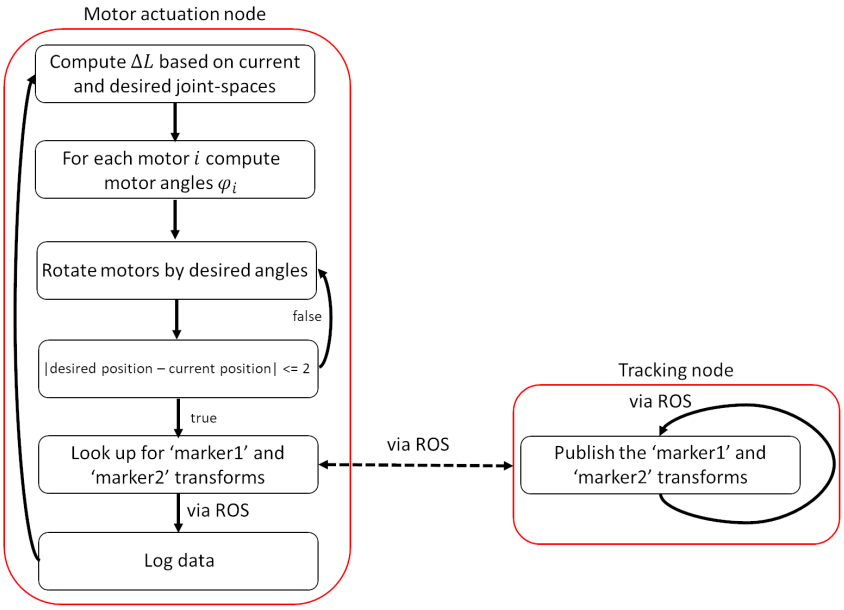

Figure 3.14: Flow diagram showing the interaction between the two ROS nodes of the tracking experiment.

lishing transformations that the first node would look up every time it was instructed. When these transformations were obtained, they would be stored in a rosbag file. The data flow between these two nodes is shown in the flow diagram of Fig. 3.14.

The robot end-effector gripping the marker attachment with the NDI markers on it can be seen in Fig. 3.15. In the same figure, and for demonstration purposes, the end-effector inside a training head phantom is shown. This picture provides an illustration of the robotic EEEA, while simultaneously relating the dimensions of the instrument shaft to those of the head phantom.

The SLA-printed marker attachment was designed in a way so that the line connecting the centres of the two markers passes by the distal point of the gripper, where the last frame of the end-effector was mathematically defined. Thus, the robot end-effector position could be represented by the mean point between the two marker-point positions. Since position is only measured without taking into account the orientation, just the two markers are sufficient. The markers where tight-fitted and hot-glued to the attachment to avoid shifting or falling out of place, and a number of different gripper angle values were tried making sure that the gripper holds on the attachment tightly enough. This was essential to make sure that the measurements kept were indicative of the robot movements.

After all 19 moves were carried out, the vector of points was shuffled and the robot

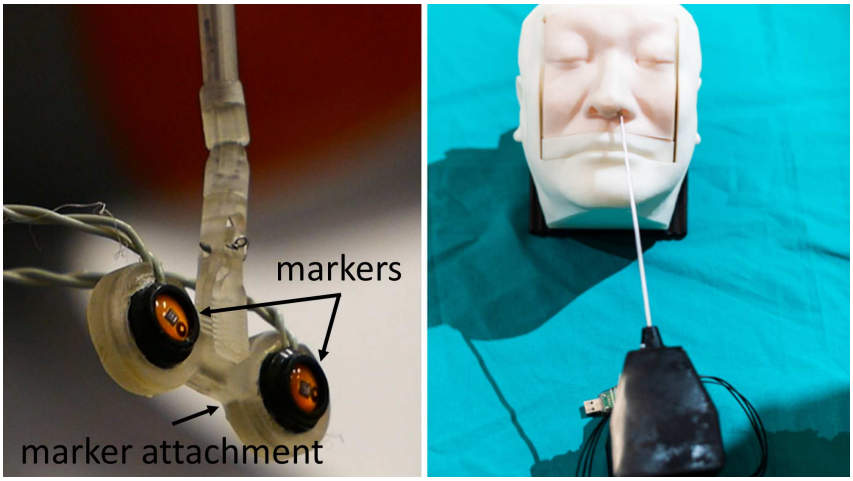

Figure 3.15: The robotic end-effector holding the NDI tracking markers attachment (left), and inside a training phantom to illustrate insertion during the robotic EEEA procedure (right).

was instructed to rotate by the same joint-space values, but in a different order. By shuffling the desired joint-space values the bias in the measurements that following the same order of values every time would produce was reduced. The vector of values was shuffled 19 times, resulting in 20 different sequence groups and 380 moves overall.

To test the workspace capabilities of the robot, it was instructed to move to the boundaries of the joint-space, in the range between $[-30,-30,30]$ and $[30,30,30]$. After the robot reached every position, again the positions of the tracking markers in 3D space were recorded to be used for the construction of the robot end-effector workspace boundaries. Finally, to confirm that the robot is rotating around fixed axes, the end-effector was instructed to move into 1000 random joint values between the same range $[-30,-30,30]$ and $[30,30,30]$. The resulting positions were tracked using the NDI trackers and then organised into a point cloud. The fitted sphere on the workspace point cloud was calculated with the purpose to measure its radius and compare it to the distance between the first and the last frame of the robot end-effector as shown in Fig. 3.7.

To calculate the repeatability value of the robot end-effector, all 19 tracker transformation measurements that correspond to the same joint-space values from each of the 20 iterations are put into a group and their standard deviation (STD) is calculated, resulting in 19 different STD values. Each STD value represents the repeatability of that specific joint-space value and physically corresponds to the positional deviation from the average of displacement [126]. These values rounded up on the second decimal digit, and the joint-space they correspond to, can be seen in Table 3.2. The overall repeatability of the end-effector is

defined as the average of those STD values. With this method, the repeatability of the robot is measured at 0.42*mm*.

Table 3.2: The STD values of the 19 different joint positions.

Joint $(^o, ^o)$	$STD\,(mm)$	*Joint* $(^o, ^o)$	$STD\,(mm)$
$(-21, -29)$	0.29	$(-19, -23)$	0.43
$(18, -27)$	0.21	$(15, -21)$	0.39
$(4, 14)$	1.02	$(-9, 5)$	0.39
$(-12, -1)$	0.48	$(15, -1)$	0.26
$(15, -30)$	0.20	$(-13, 4)$	0.33
$(6, 23)$	0.12	$(-5\ -22)$	0.32
$(-25, 16)$	0.82	$(-12, -22)$	0.23
$(-12, -12)$	0.66	$(24, 18)$	0.94
$(11, -19)$	0.39	$(-19, 29)$	0.26
$(7, -27)$	0.19	**Average**	**0.42**

The boundaries of the workspace of the robot end-effector, as recorded using the NDI tracking markers, compared to the corresponding theoretical boundaries for the joint-space range of $[-30, -30, 0]$ to $[30, 30, 0]$ are shown in Fig. 3.16.

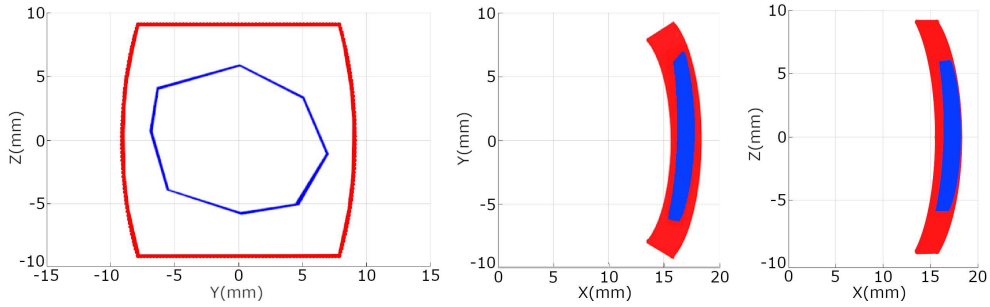

Figure 3.16: Comparison between the boundaries of the theoretical workspace (red) and the measured workspace (blue).

According to these tracking data, the maximum distance that the robot end-effector can cover while constrained to a fixed point, which is the origin of frames 0 and 1 as shown in Fig. 3.7, is 13.1*mm* on the Y-axis, whereas on the Z-axis is 12.5*mm*. The theoretical value for both these axes is 18.5*mm* which means there is an error in movement range of 5.4*mm*

on the Y-axis and another one of 6mm on the Z-axis. It is worth mentioning that although the end-effector has a fixed point where the axes of rotation pass through, its purpose is to be integrated into a handheld mechanism and held by the surgeon that would be moving that fixed point in space, allowing thus for a wider and more sophisticated effective workspace. This is why it was important to verify whether this point was in fact fixed or whether any slides in movement were present that could lead to inaccuracies in the measurements.

As previously mentioned, to confirm that the robot is indeed rotating around fixed axes, the fitted sphere on the point cloud was calculated, which was created by moving the end-effector to 1000 random joint values between the previously specified joint-space angle vectors. The resulting sphere has a radius of 19.6mm and a fitting error of 29.1μm.

The actual distance between the axis of rotation and the distal point of the robot end-effector, the movement of which was tracked, was measured at 19.4mm, using vernier calipers with a resolution of 0.01mm, comparable to the fitted sphere radius, verifying that the rotating axis of the robot is not sliding. The tendons are responsible for keeping the base of the robot end-effector fixed to the distal end of the instrument shaft through tension. The robot end-effector is not otherwise fixed to the shaft.

3.4.2 Structural integrity study

Considering its miniature size, it was important to also test the structural integrity of the end-effector and the amount of load it can support without its gripper or any other part of the robot breaking. To test that, a set of precision weights in the range of 100g to 700g was tied on an SLA-printed attachment using stainless steel wire. Then, a two-pulley system was used to transfer the weight of each object along the wire and change its direction so that the end-effector can grasp the attachment and support the object. The pulleys were of the same size, were placed at the same height and the wire did not wrap around the pulleys, only passed above them. Disregarding the losses generated by the friction on each pulley, it is acceptable to assume that the effort required by the robot to support the object is almost equal to the weight of the object. The experimental setup for the end-effector's structural integrity is shown in Fig. 3.17.

The part of the rerouting system that controls the first two DoF tied to the spherical joint movement was constrained by tying an extra tendon around the capstans that disallowed them to move. This was done in order to make sure that any deflection appearing on the axis of the spherical joint was solely due to the effort created by the weight, rather than a

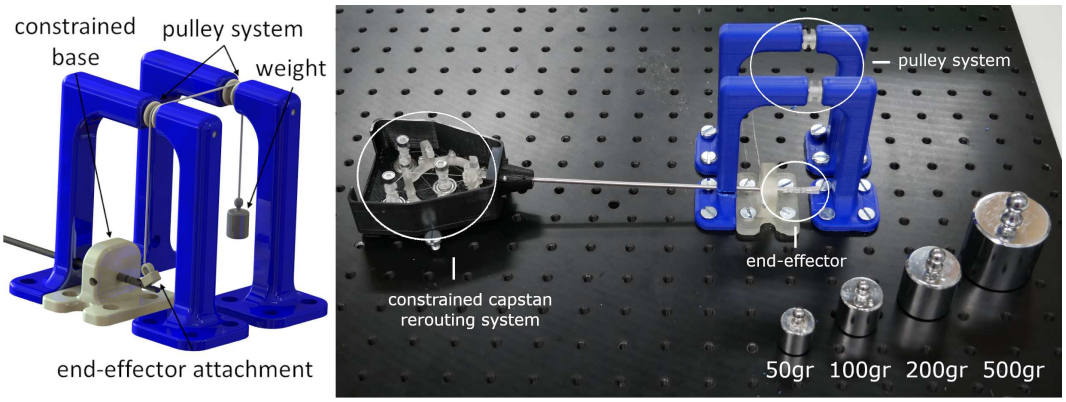

Figure 3.17: The experimental setup to test the end-effector's structural integrity.

normal rotation of the joint. The only DoF that was free to move was that of the gripper. As is evident in Fig. 3.17 the tool-housing is unattached from the actuation system and the gripper was moved manually rather than using its designated motor. This approach was chosen to simplify the experiment design and since the purpose of the experiment is to test the mechanical integrity of the end-effector, the motors are not necessary.

One by one the objects were tied to the attachment and each time the end-effector was tasked with grasping them. The rigid shaft on which the gripper tendons terminate was then manually rotated until the gripper closed and the weight was lifted. Depending on the weight, a deflection angle appeared. Here, the deflection angle is defined as the angle formed on the pitch axis of the spherical joint between the resting position and the final position of the end-effector. This angle is later illustrated as part of the experimental results in Fig. 3.18.

The end-effector was evaluated on its abilities to maintain a grasp on the attachment and support the weight for $15sec$. For each object, the deflection angle was measured. One prototype was used throughout this series of experiments and each weight was tested twice. Between the two series of experiments, the difference in deflection angles for the same weight were negligible.

The end-effector supporting the objects and the corresponding deflection are shown in Fig. 3.18. The end-effector was able to support all the objects up to a mass of $600g$, which corresponds to approximately $6N$, and was able to maintain a grasp up to a mass of $500g$. Here, a successful grasp is defined by the upper part of the gripper not moving from its 'grasping' position for the whole duration of the $15sec$, after the rigid shaft had been rotated. Thus, even though the gripper is not fully closed for some of the weights because

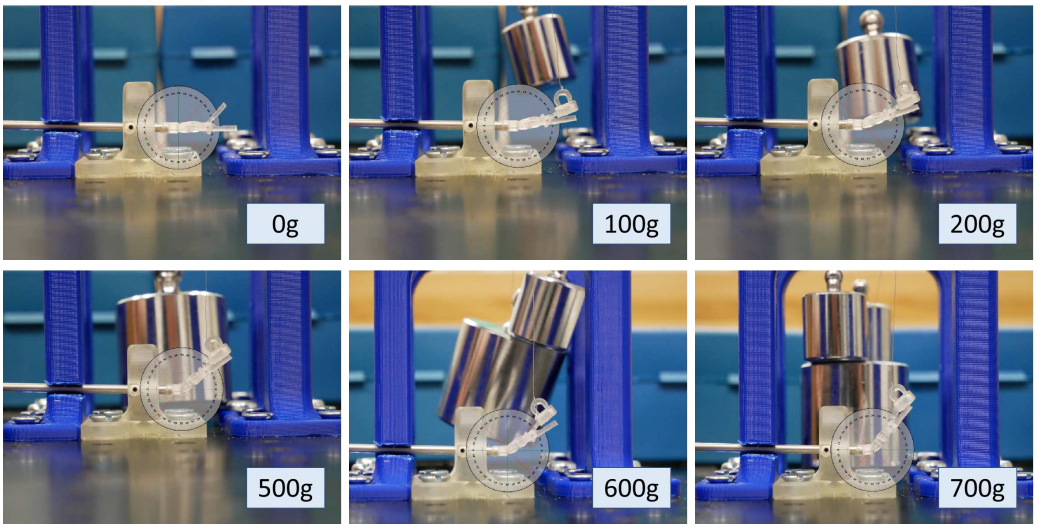

Figure 3.18: (Left to right, top to bottom) The end-effector at its resting position, and supporting objects of 100g, 200g, 500g, 600g and 700g mass. The deflection angle is also evident in the figure.

the rigid shaft was not manually rotated to its full extent, as is evident in Fig. 3.18, the grasping test for these corresponding weights was still considered successful.

For the 600g object it could not maintain a grasp and the gripper was gradually opening as the seconds passed by, even though the capstans and the shaft connected to the gripper-tendons were manually kept still. For the 700g object, the gripper was able to support the weight for barely 3sec before opening and letting go of it. The results of this structural integrity study are concentrated in Table 3.3.

Table 3.3: The results of the structural integrity study.

$Effort\,(\sim N)$	$Deflection\,(^o)$	*Support*	*Grasp*
1	15	✓	✓
2	25	✓	✓
5	35	✓	✓
6	35	✓	×
7	55	×	×

The deflection angle presents a fairly expected behavior. It is relatively small for the 100g object, bigger for the 200g and for the 500g and 600g it reaches and even surpasses the boundaries of the effective workspace as they were calculated in the previous set of experiments. For the 700g object the deflection angle is well over the effective workspace

boundaries and although the end-effector did not break, such a large effort during an operation would significantly weaken the tool. By design, the forces exerted during the endonasal approach are rarely larger than $2N$ [127], on the axis in question in this experiment.

3.4.3 Preliminary findings

During the experimental procedure it was found that the robot has an adequately high repeatability and that the effective workspace, although with boundaries almost 30% more constrained than their theoretical values, is extensive and a clear advancement compared with that of current rigid tools. The repeatability of 0.42mm achieved by the suggested robotic end-effector is low when related to its workspace boundaries. This fact, combined with the very limited workspace of the endonasal approach and the intention for a handheld robotic tool where the surgeon is immediately controlling the robot and can thus provide visual feedback on the goal position, suggests adequate robot repeatability.

In this presented implementation, the joint-space is capped at an adequate but lower than expected $\pm 30^o$ range because it was noticed that in movements beneath this threshold there was a small chance of tendon snapping. The nylon tendons used for this end-effector were not able to withstand the forces required to rotate the joints more than 35^o, thus the movements were capped at a lower and safer value. Another limitation of this study is, of course, the difference between the theoretical workspace boundaries and the tracked ones. This, again, can be traced back to the tendons' elasticity and slipping. It is also speculated that this inaccuracy could be a result of a less sophisticated motor control. When compared with other manipulators intended for the endonasal approach [29], [128], the workspace is smaller, but when combined with the promising repeatability and structural integrity, the end-effector could potentially suggest a substantial improvement over current instrumentation.

For the repeatability test, it is evident that the STD values for some of the joint-space angle vectors are abnormally large, especially the STD value for joint-space angle vector $[4, 14]$ being $1.02mm$. Such a large error could be attributed to various factors. There are some uncertainties concerning the implementation of the mechanism, namely tendon slacking resulting into an accumulated mechanical error, or kinematics simplifications resulting in a slight positioning error. Additionally, another factor that needs to be taken into account is the possible measuring error that appears when the tracker has an unclear view of the markers.

Last but not least, during the structural integrity tests, although the results showed that the end-effector could avoid breakage and support a large amount of weight, a clear limitation appears in the large deflection angle created by the increasing load that would be a drawback during surgery. This deflection angle, that is relative to the weight of the object, could also be one of the reasons contributing to the end-effector's inability to maintain hold of the object attachment, as is evident in Fig. 3.18. However, the weight is most possibly still the main contributor since the deflection angle was the same for both the $500gr$ and $600gr$ objects, with only the $600gr$ object attachment slipping from the end-effector. Using a spherical joint requires careful tendon pre-tensioning since the joint and the base are not physically connected, as they would be in an articulated design. Thus, it is suspected that the large deflection angle could be decreased with a better choice in tendons.

3.5 Improvement of the end-effector joint-design

It is evident from the previous sections that the robotic end-effector located at the distal end of this novel handheld robotic instrument needed further development. While that preliminary work suggested that introducing a miniature robotic end-effector could enhance surgical capability, the joint-space of the end-effector, and more importantly its structural integrity, left room for improvement. This is why following those preliminary experiments, an iterative trial-and-error development process was followed to produce a more robust miniature articulated end-effector prototype.

The two main factors affecting the workspace of the end-effector were the tendon channel placement and the tendon termination points. In the previous design, the tendons were passing through the main body of the spherical joint. Additionally, the tendons were terminating on the inside surface of the joint, facing the distal end of the design. These design choices, while necessary at that exploratory stage of development, were limiting the operative workspace of the device.

The design presented in this section is the natural evolution of this preliminary prototype. The spherical joint has been decreased in size as to not interfere with the tendons, and the tendon channels are now located on the outer diameter of the joint body, increasing the workspace limits of the design. Simultaneouly, and after a series of tendon selection tests where tendons were evaluated for their material properties and endurance during exhaustive actuation tests, the tendon channels have a smaller diameter, which combined with the decreased mass of the spherical joint, allow for a slightly smaller end-effector diameter.

All these design considerations, as well as a direct comparison between the two designs is shown in Fig. 3.19.

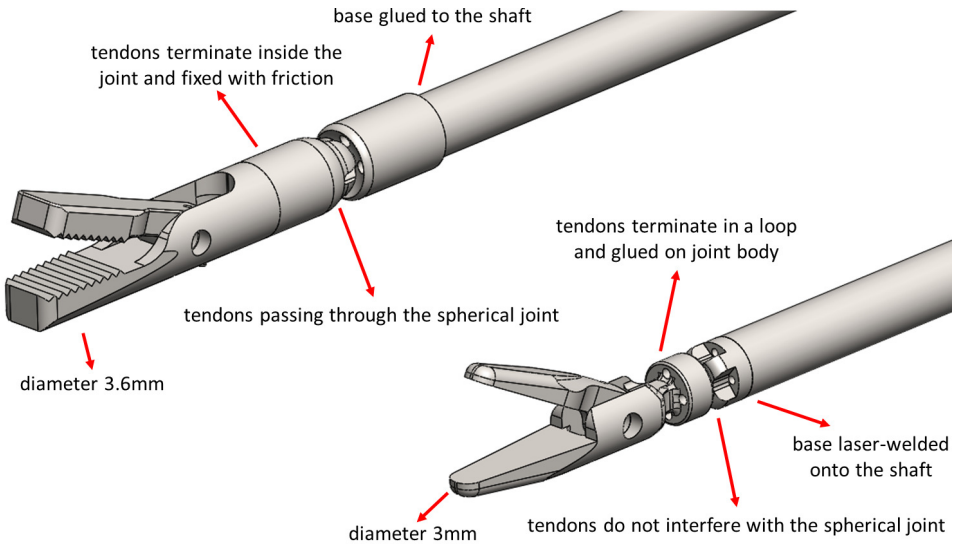

Figure 3.19: Design differences between the initial end-effector presented in Chapter 3 and the newly developed end-effector presented in this chapter.

Starting from the initial end-effector implementation, there was a number of discrete steps that lead to its finalised design. Initially, the spherical joint and the rolling surface were inverted to further increase the workspace. With this inverted design the tendons had more space to translate, and thus, increase the articulation angle. In that design, the tendon-termination points were kept the same. Then, to further increase the workspace, the tendon-termination points were on the outer diameter of the joint, laser-welded on the body itself. This, however, lead to unreliable results, and the design was reverted to have the same termination points as previously, with slightly extended tendon channels. While the workspace was significantly increased with this iteration, the robustness of the device was not adequate.

The next iteration was a combination of the first few iterations, with the spherical joint and rolling surface reverted back to their original configuration, and the tendon routing and termination resembling later implementations. This design combined the increased workspace of the newer prototypes, with the robustness of the original design where the sphere could rotate comfortable around an encompassing rolling surface. All these experimentation lead to the finalised design, and can be seen in Fig. 3.20.

The tendons that were used to antagonistically control the finalised end-effector were 0.3*mm*-diameter stainless steel wire rope (ENGELMANN Drahtseilfabrik GmbH, Han-

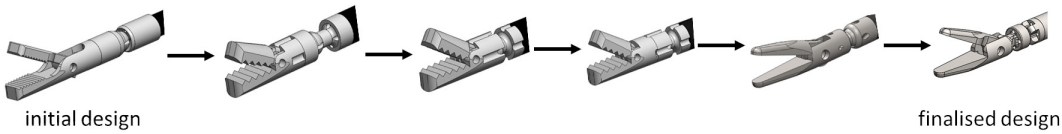

Figure 3.20: The discrete steps from the initial end-effector design that lead to the finalised end-effector design.

nover, Germany). They looped around the spherical joint-body for better grip and were glued to avoid slippage during pre-tensioning. To actuate the grasper DoF, the tendons were passing through a hollow channel in the middle of the spherical joint body and terminating on the moving part of the gripper. Fig. 3.21(b). details the tendon-routing for all 3 DoF of the articulated grasper.

The finalised end-effector has an overall diameter of 3*mm* and deploys a 2 DoF tendon-driven spherical joint that allows movement in the pitch and yaw axes around a rolling surface. The roll axis motion around its rolling surface is restricted by the tendons and can be compensated by the surgeon's hand movement. The third DoF of the end-effector is the opening and closing of the gripper. This articulated grasper was fabricated in stainless steel with additive manufacturing techniques, namely direct metal laser sintering (3DSystems, Rock Hill, South Carolina, United States), and was laser-welded onto a 3*mm*-diameter stainless steel shaft. The fully-assembled grasper is shown in Fig. 3.21(a).

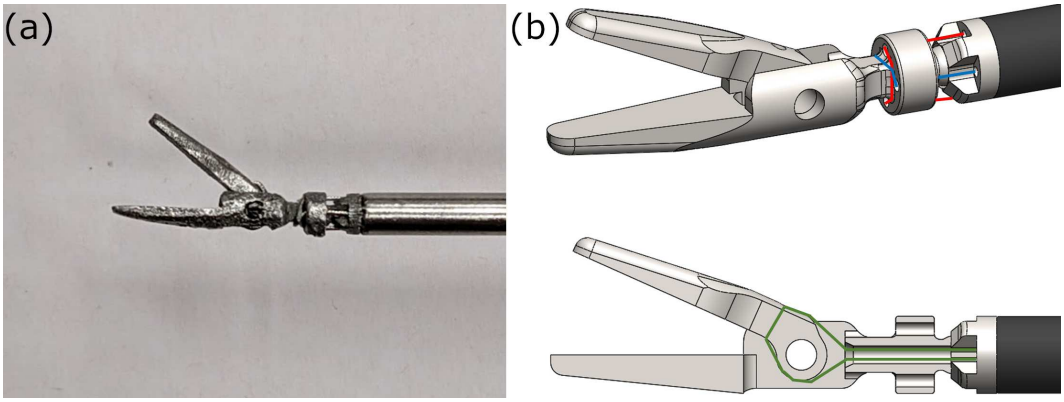

Figure 3.21: (a). The miniature grasper end-effector, and (b). The tendon-routing of the 3 DoF.

To cover a larger set of neurosurgical instruments, and since the end-effector can be easily detached and re-attached to the handheld controller, the grasper end-effector design was amended to enhance other standard instruments with robotic articulation. Namely, these instrument end-effectors were a ring-curette, a spatula dissector, and an endoscope. These instruments do not deploy a third DoF, but rather only need pitch and yaw articulation,

with the endoscope specifically also requiring an expanded hollow working channel with a diameter of 1.8*mm* for the 1.66*mm*-diameter miniature camera to pass through. This increased the overall diameter of the endoscope to 4*mm* to allow for direct metal laser sintering (DMLS) fabrication. The camera used for the endoscope was the MISUMI MD-V1000LH-120 UVC signal camera (MISUMI Electronic Corporation, Taipei, Taiwan). All alternative end-effectors are depicted in Fig. 3.22.

Figure 3.22: The articulated end-effectors developed as part of the novel robotic system. From left to right, a dissector, an endoscope, a grasper, and a ring-curette.

3.6 Miniaturization of the tendon-routing system

After the issue of the limited joint-space had been addressed, it was important to improve the structural integrity of the device. It was quickly evident that the main issue limiting the robustness of the device was mechanical backlash. This could be attributed to the tendon selection, that was solved with the usage of the aforementioned tendons, and more importantly to the tendon routing and pre-tensioning methodology. Fig. 3.23 showcases different tendon routing systems developed that lead to the finalised device design.

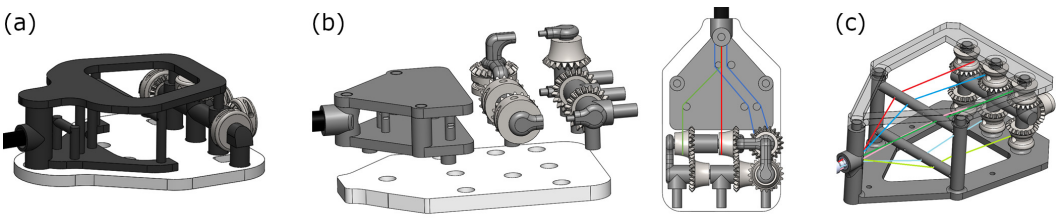

Figure 3.23: Various tendon-routing sub-system designs. (a). System combining bevel gears and capstans, (b) Previous system comprised of a three parts assembly and its tendon-routing paths, and (c). Preliminary differential-drive system and its tendon-routing paths.

The motor placement on the handle design, as discussed in the next chapter, had to be perpendicular to the tendon-termination points on the tendon routing system design. A convenient way to cater to this design consideration is a differential drive bevel-gear

system as this configuration can transfer rotational motor movement alongside one axis, to rotational capstan movement alongside a different axis. The system depicted in Fig. 3.23(a). is the preliminary design of a tendon-routing system that was using bevel gears to transfer the motor movement to the end-effector joints, alongside capstans that were used as tendon-termination components.

An encouraging first step, this design was very difficult to assemble, and more importantly pre-tension, due to the limited access to the capstans, and lack of tendon routing paths. The design in Fig. 3.23(b). built on the previous design principles to allow for tendon-routing through pillars on the distal part, as well as pre-tensioning on the capstans located on the middle part. The proximal part was then the final part of the assembly that would be responsible for the actuation of the whole sub-system.

This design was a clear improvement over the first, but was lacking in ease of actuation, while the modular parts of the assembly decreased the robustness of the structure. The bevel-gear arrangement was difficult to actuate when the tendons had been adequately pre-tensioned. This problem was solved by the differential-drive system design of Fig. 3.23(c)., where two pairs of bevel gears were used per DoF, one for each tendon, rather than a single capstan.

This sub-system was functioning as expected, increasing the robustness of the end-effector while been easy to actuate. It did, however, have one major limitation. The tendon pre-tensioning was done qualitatively and by hand, by rotating the pair of bevel gears in opposite directions. This led to unreliable pre-tensioning with each tendon having different pre-tension values, as well as not adequately robust end-effectors, since the pressure that can be applied by the human hand is limited. These limitations led to the finalised design of the tendon-routing sub-system described below.

To route the tendons from the distal end of the tool, where the robotic end-effector is located, to the proximal end of the tool, at the point where it couples with the handheld controller, a routing sub-system was used. The tendons were terminating on the end-effector socket-joint as shown in Fig. 3.21(b). The termination points were chosen so that they are opposite each other in order to accommodate the antagonistic control methodology of the device. The tendons loop around the gripper body to provide a stable actuation surface, and to minimize complexity.

They were then routed through the stainless steel shaft of the tool and additionally

through a series of 3 contact points before passing through geared capstans. The tendon-routing structure incorporating those contact points was designed based on a few design requirements. The exertion point from the stainless steel shaft was on a different frame of reference than the insertion point on the capstan. Additionally, a pair of antagonistically opposed tendons should terminate on co-axial capstans. Friction at the concact points should be minimal, and finally, the overall size of the end-effector body should be big enough to allow seamless movement, but simultaneously remain reasonably small. The routing structure generated based on these requirements is shown in Fig. 3.24(a).,

To minimise friction, the tendons were passing through small Polytetrafluoroethylene (PTFE) tubing with a diameter of $0.4mm$. They were pre-tensioned at $15N$ using a manual newton-meter, and were crimped to stay in place and at that pre-tension value. This value was a result of trial-and-error testing, where smaller values would lead to an end-effector with inadequate structural integrity, whereas bigger values would lead to tendon snapping. Thus, the result of this experimentation achieved a balance between robustness and freedom to move. Finally, the two capstans were rotating in opposite directions with a perpendicular bevel gear. The differential gearing system with the tendon pre-tensioning mechanism is evident in Fig. 3.24(b).

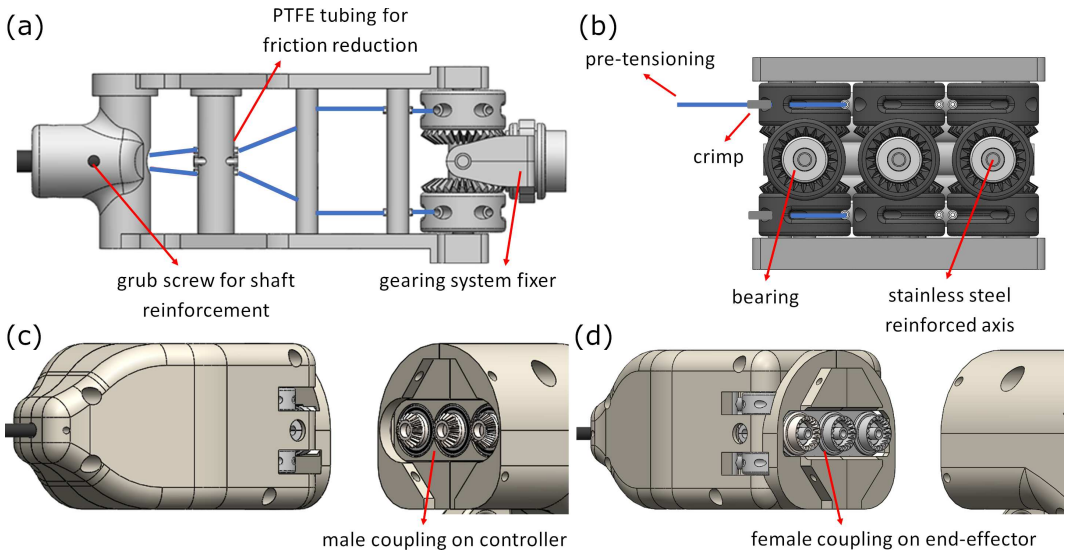

Figure 3.24: (a). The tendon-routing system for a single DoF with the other two DoF tendons following similar routing paths, (b). The differential gearing system, highlighted in grey, with tendons for a single DoF, (c). The coupling on the handheld controller side, and (d). The coupling on the end-effector side.

To couple the end-effector with the handheld controller, a male-to-female connection

is used between the gears that are placed on the motors shafts, and the bevel gears that are part of the differential gearing system. The coupling on both the handheld controller and end-effector sides are depicted in Fig. 3.24(c). and (d). The end-effector and the handheld controller coupling is secured with two alignment pins, one on either side of the instrument. Finally, the tendon routing system is housed inside a two-part casing.

The routing system inside an open casing, as well as the fully assembled robotic end-effector, are shown in Fig. 3.25.

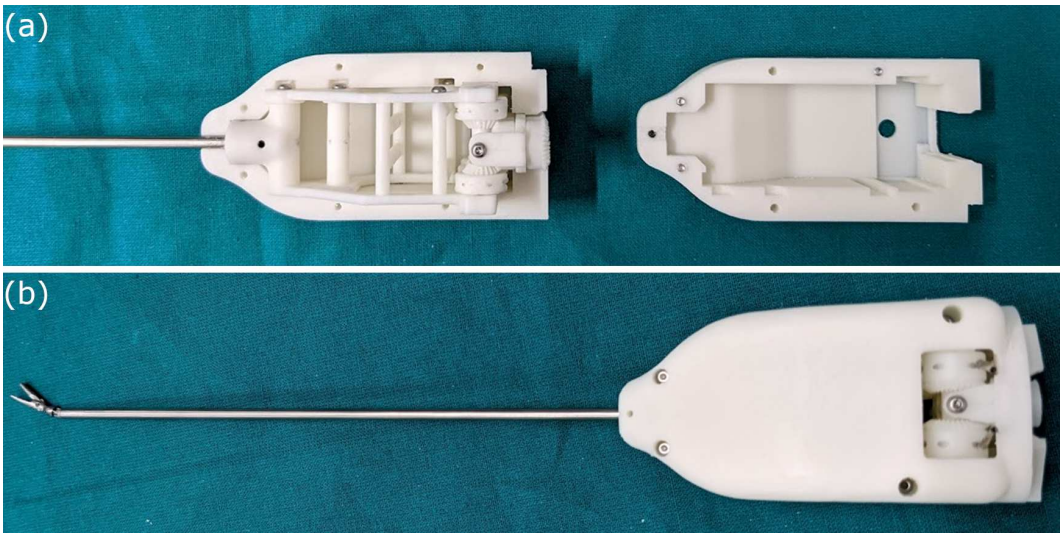

Figure 3.25: (a). The routing system inside an open end-effector casing, and (b). The fully assembled grasper end-effector.

3.7 Discussion

In this chapter, an articulated 3 DoF robotic end-effector for a novel handheld robotic tool intended for the EEEA was presented. Using an actuation test-bench, the design prototype in terms of its repeatability and workspace capabilities was evaluated, as well as in terms of its structural integrity. Preliminary testing showcased potential, with further development leading to a fully functional miniaturised robotic end-effector.

The choice of a tendon-driven mechanism was based on the improved distal point abilities and robustness that such designs offer. To be able to operate inside a very limited workspace, the robot must have a small diameter which often leads to breakages and fatigue. The proposed robot end-effector has a spherical joint in order to create a robust structure by taking advantage of the fact that a sphere can concentrate a large amount of material despite being fabricated in a small size. Other than aiding in miniaturization through increased

structural integrity, the use of a spherical joint can reduce the end-effector size because it concentrates all actuation DoF around the same origin. This minimizes the length of the articulated joint, enabling access even in very narrow corridors and constrained operative workspaces.

A large portion of the development work of this chapter was spent on tendon-selection as well as the tendon routing sub-system. Tendon-driven devices offer plenty of advantages, such as high maneuverability and relatively simple design, but their performance is often limited by nonlinear friction and hysteresis phenomena [129]. An analysis and subsequent mathematical compensation for tendon hysteresis could have improved the performance of this device and could be the scope of future work. Another common issue associated with tendon-driven systems is stretching, which with time could lead to loss of articulation or structural robustness [130]. One way to address that would be be building a capstan test-bench that would pre-stretch the tendons prior to tensioning them.

Reliable tensioning is also very important, and the current methodology left room for human error in pre-tensioning. Active tensioning compensation could compensate for that error. To avoid these errors all together, more sophisticated pre-tensioning methodologies could be deployed by digitally measuring the tension on the tendons, or using strain gauges to extract that information. By implementing such hysteresis, pre-stretching and tensioning methodologies, backlash would be drastically minimised. Finally, in this chapter, friction was addressed by routing the tendons through small cuts of PTFE tubing. Incorporating pulleys on the routing contact points would also reduce friction and allow for smoother motion.

To minimise backlash and increase the end-effector accuracy, new device manufacturing methods need to be explored. The robot joints could be manufactured with subtractive rather than additive manufacturing, namely Computer Numerical Control (CNC) machining, to improve surface finish and smoothness. The difference in surface finish between a prototype manufactured with metal 3D printing and a prototype manufactured with CNC machining is presented in Fig. 3.26.

Then, the gearing system design, as well as the tendon-routing structure and its casings should be amended to accommodate moulding, which will reduce manufacturing inaccuracies that are associated with increased friction and misalignments. Finally, new and more durable materials, such as high-performance engineering plastics or stainless steel, could be

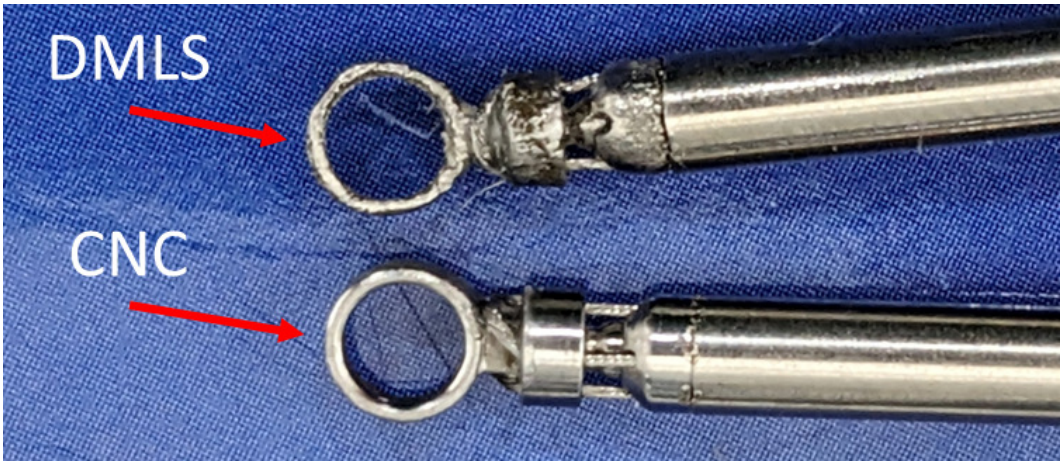

Figure 3.26: Comparison between an end-effector manufactured with DMLS and an end-effector manufactured with CNC machining.

investigated for the manufacturing of the tendon-structure, to increase the device robustness.

Chapter 4

A handheld controller for the robotic end-effector

4.1 Introduction

This chapter aims to continue the development of the novel robotic system by introducing a handheld controller that is intended to actuate the robotic end-effector previously presented. Trying to satisfy as many design requirements from the ones presented in Section 2.5.1, two novel handle concepts were developed. A forearm-mounted handle design and a joystick-and-trigger handle with a rotating-joystick component. These two handles were compared alongside a standard instrument during a multi-participant randomised crossover user-study for their performance and ergonomics. The joystick-and-trigger handle proved superior, which lead to the selection of that handle concept.

In the final section of this chapter, the superior handle concept is further developed in order to produce a functional handheld controller incorporating miniature motors and electronics for the control of the robotic end effector. The produced handheld controller is intended to be paired with the end-effector presented in Chapter 3 to form a functional version of the proposed neurosurgical robotic tool.

The contributions that are associated with this chapter are:

- Dimitrakakis, E., et al., ”An intuitive surgical handle design for robotic neurosurgery.”, (2021), International Journal of Computer Assisted Radiology and Surgery

- Dimitrakakis, E., et al., ”Robotic Handle Prototypes for Endoscopic Endonasal Skull Base Surgery: Pre-clinical Randomised Controlled Trial of Performance and Ergonomics.”, (2022), Annals of Biomedical Engineering

- Dimitrakakis, E., et al., "Towards the Development and Evaluation of a Handle Prototype for a Handheld Robotic Neurosurgical Instrument.", (2020), 10th Joint Workshop on New Technologies for Computer/Robot Assisted Surgery (CRAS)

- Dimitrakakis, E., et al., "Handheld Robotic System for Endoscopic Neurosurgery", (2023), IEEE Robotics and Automation Letters, (submitted)

- 'Audience award for best innovation: First place', (2021), In The 12th International Conference on Information Processing in Computer-Assisted Interventions (IPCAI)

- 'Flash talk award: Second place', (2021), In UCL Institute of Healthcare Engineering Early-Career Researcher Symposium (UCL IHE ECR)

4.2 Development of a forearm-mounted handle

In this section, an ergonomic handle prototype which maps the surgeon's wrist movements to that of the robot-joints is presented. To alleviate the surgeon's wrist of any excessive strain and fatigue, the tool is mounted on the surgeon's forearm, making the shaft of the instrument parallel to the forearm. To evaluate the handle's performance and limitations, a custom 'peg-transfer' surgical task simulator was developed and used to compare the novel handle with a standard neurosurgical tool.

4.2.1 Design criteria

The goal of this section is to develop a safe and effective handle which focuses on ergonomics and comfort. It should also have a fast adoption rate so that it can be easily integrated into the operating theatre.

To design the tool, some of the suggested design considerations presented in Section 2.5.1 were followed. The handle should be designed in a way so that it is indifferent to the surgeon's hand-size [55], and its actuation means should me finger-operated [56]. Additionally, in order for the handle to feel comfortable, when the instrument is kept at rest, the surgeon's hand should maintain a partially opened pose [59].

Handle weight has a significant effect on muscle load when performing manual tasks [60]. Transferring the weight that the wrist supports to the forearm, could ease the wrist load and reduce fatigue. Simultaneously, with this setup, the end-effector is decoupled from the wrist, meaning that any forces applied on the distal-end of the instrument, that would

normally be directly transferred back to the wrist, are now directed to the forearm. Mounting the instrument on the surgeon's forearm creates the possibility to map the surgeon's wrist directly to the robot-joints which could increase the chance of developing a surgical instrument with good usability [61]. Simultaneously, it could potentially ease the realisation of difficult tasks such as suturing by replicating the full range of motion of the surgeon's hand.

All aforementioned instructions and suggestions lead to the following design criteria defined for the proposed handle summarized in Table 4.1. Although, it is evident that these instructions do not describe the perfect ergonomic handle, combining all of them in the same design could potentially prove a substantial improvement over current instrumentation.

Table 4.1: Design criteria for the novel forearm-mounted handle prototype.

The same handle design should cater to different hand sizes.
The instrument actuation means should be finger operated.
A resting hand pose should hold the instrument at rest.
The wrist should not support much weight throughout the duration of the procedure.
The instrument should allow for intuitive control.
The instrument should provide a platform to incorporate complex robotic assistance.

4.2.2 Handle design

A rendering of the suggested intuitive handle, that is based on the design criteria from the previous section is found in Fig. 4.1. The robotic end-effector that this handle is intended to manipulate is the tendon-driven, 3 DoF robot that was presented in Chapter 3. The coordinate frames in 3D space of the end-effector are shown in Fig. 4.2. In the same figure, an added frame for the roll motion is evident which will be carried out by the motorized rotation of the outermost part of the handle body that is connected with the end-effector shaft.

As mentioned before, the handle directly maps the neurosurgeon's wrist motion, including that of the roll axis. This is also evident in Fig. 4.1, where the joint on the handle that corresponds to the roll axis is specified. This additional DoF, has not been implemented immediately on the end-effector, but will rather be included in the final fabrication of the handle.

The handle itself is larger than currently used tools but lightweight, with maximum

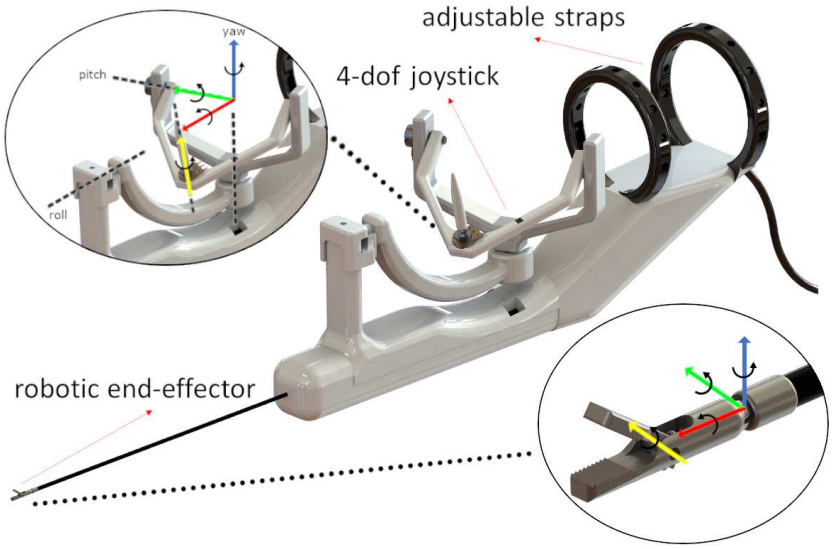

Figure 4.1: A rendering of the suggested intuitive handle with the coordinate frames of the handle joints (left), and the corresponding coordinate frames of the robot-joints (right).

Figure 4.2: The coordinate frames of the end-effector that the handle is intended to manipulate (left), and the corresponding frames on the wrist (right).

dimensions of 42cm length, 16cm height, and a weight of 431gr. Naturally, the weight is subject to change between the handle prototype and its finalised version, with the addition of motors and electronics. It consists of a 4 DoF joystick, that resembles a three axis of rotation gimbal structure, with an additional DoF for the gripper actuation. This gripper DoF is finger operated, namely with the index finger and the thumb, with a rolling pinch motion.

The surgeon's hand rests on the base of the joystick and the three axes of rotation, disregarding the gripper actuation axis, form an imaginary origin in space that coincides with the surgeon's wrist. The angle of each handle joint is measured by a rotary potentiometer and control the end-effector joints in joint-space. The handle is hollow on the inside to allow for cable rerouting and space for electronics. There is adequate space left specifically for any electronics that would need to be used in the future, when this handle is paired with the end-effector to form a finalised surgical robot.

Looking back at the design criteria that were set in Section 4.2.1, the suggested handle is finger-operated in part, and its three axis of rotation immediately map the surgeon's wrist yaw, pitch and roll axes rotations. At a handle resting position, namely when the surgeon is not manipulating the robot joints, the surgeon's hand is also maintained at a resting pose, as is evident in Fig. 4.3 [131].

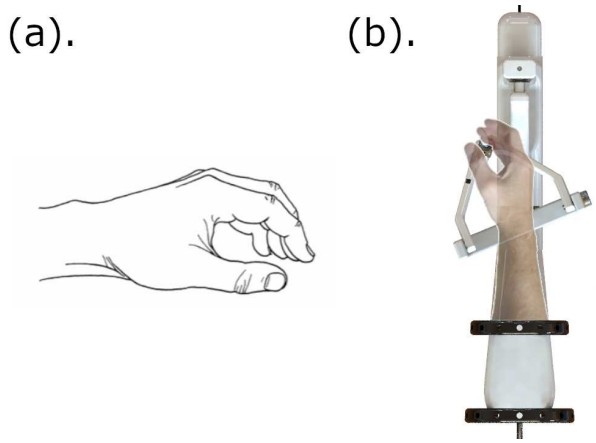

Figure 4.3: (a). The hand at its resting position, and (b). The resting position of the handle coincides with the resting position of the wrist.

The handle is forearm-mounted with adjustable straps, meaning that all weight is alleviated from the wrist, and transferred to the forearm. Since a mounting point, such as a trocar port, is missing during the EEEA procedure, the adjustable straps constrain the handle to the surgeon's forearm creating a stable platform on which the surgeon can freely move their wrist. The base frame of the end-effector is directly manipulated by the surgeon's arm, as the instrument shaft is rigidly fixed parallel to the surgeon's forearm.

4.2.3 Prototype fabrication

The handle prototype was implemented with additive manufacturing techniques, namely 3D printing. All parts of the handle were 3D-printed (Ultimaker S5, Ultimaker BV, Utrecht, Netherlands), using polylactic acid (PLA). For the end-effector shaft, a 3*mm* diameter stainless steel rod was used. The joint angle values were measured with 4 rotary potentiometers, and were read and handled with the use of a miniature single-board microcontroller (Arduino Nano, Arduino AG, Italy). The inside of the handle body contains only the microcontroller, a mini bread-board to connect it with the potentiometers, and the cables. To mount the handle to the forearm, 2 12-inch hook-and-loop adjustable straps were used. An exploded view of the handle with more details on the design, alongside the 3D printed

prototype with its optical marker is shown in Fig. 4.4.

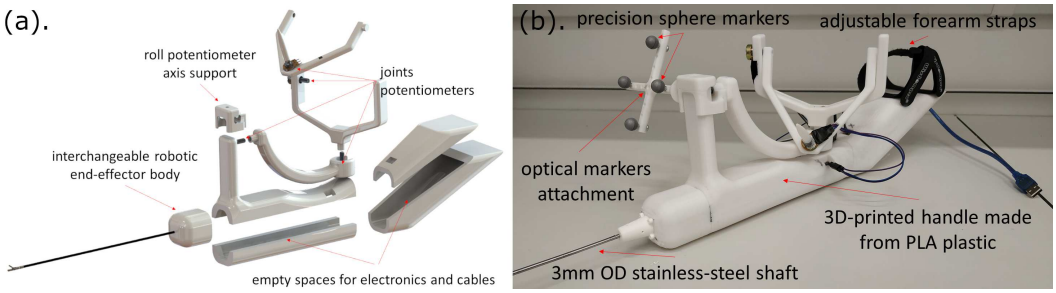

Figure 4.4: (a). Exploded view of the proposed handle rendering, and (b). its 3D-printed implementation (right).

4.2.4 Experimental methods

To evaluate the performance and intuitiveness of the handle, and whether mounting it on the surgeon's forearm would reduce the benefits of the added articulation and ergonomic design as [132] suggests, development of a custom surgical task simulator was needed to compare it with a standard rigid instrument that is commonly used in keyhole brain-surgery. The task chosen to be simulated was a 'peg-transfer' task, taken from the McGill Inanimate System for Training and Evaluation of Laparoscopic Skills (MISTELS) [133].This task was chosen because it was evaluated in [134] as indicative of surgical skill when carried out in constrained spaces, with specific mention to the operative space of keyhole brain-surgery. The added articulation and dexterity required to perform this task could be linked to operative steps 9.-14. as presented in Section 2.2. The focal investigative point of this experiment was whether the proposed handle can out-perform the conventional tool despite being constrained on the user's forearm, while alleviating the wrist of any added fatigue, something that would indicate that there is no loss of robotic dexterity.

To investigate whether that is the case, the simulation platform, and specifically the peg-board dimensions, has been designed in accordance to specifications from [134] that describe an experimental setup that would correspond to the constrained operative workspace of keyhole brain-surgery. Some of the pegs were purposefully positioned in coordinates where it would be difficult for the standard instrument to reach them, to highlight the importance of articulation, and evaluate whether the forearm-mount limits the dexterity of the end-effector.

The conventional tool that was used for the comparative experiment was a 28164TA surgical forceps (Karl Storz SE & Co. KG), on which a push-button and a microcontroller

were placed to simulate the grasping motion. Additionally, a 3D-printed endoscopic device was fabricated to manipulate the camera and its field of view, throughout the duration of the task. The manufactured device was inspired by the 4*mm* Endocameleon Neuro Hopkins Endoscope (Karl Storz SE & Co. KG).

To try and realistically replicate the physical constraint of the EEEA, a 3D model of a cranial CT scan was also prototyped, modified so that it only features the EEEA areas of interest, similar to the phantom used for the kinematic analysis of the previous chapter. This phantom constraint also guides the endoscope to be placed at the angle and distance from the pituitary gland area that the endoscope would be placed in a real surgical operation, providing a similar camera field of view and video feed to that of the procedure. Same as before, this physical phantom constraint included an 1*cm*-diameter artificial cylindrical channel passing through the sphenoid sinus and granting access to the pituitary gland area [10]. The modified conventional tool, the endoscope, and the phantom are shown in Fig. 4.5.

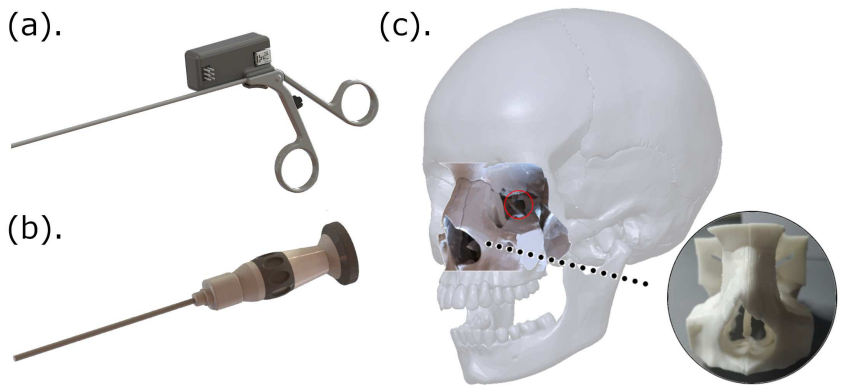

Figure 4.5: (a). Rendering of the modified surgical forceps, (b). Rendering of the endoscope, and (c). Rendering of the physical nasal channel constraint, with the artificial channel circled, a whole skull for reference, and the 3D-printed phantom constraint..

The simulation environment used to develop the 'peg-transfer' task was once again the CoppeliaSim simulation platform. To simulate the conventional tool, the same CAD model as the robotic end-effector was used, but without the robotic-joints, to avoid differences in the surgeon's performance due to difference in tools geometries. Communication between the tools and the simulation environment was achieved through ROS. All prototyped tools, as well as the constraint, were optically tracked using the motion capture system (Optitrack V120:trio, NaturalPoint Inc., Canada) and custom marker attachments. Each rigid body was tracked with four 11*mm* spherical markers. The attachment with all four markers

attached to it, weighed less than $15gr$, deeming the marker-setup weight negligible when compared to the overall device weight. Thus, it can be safely assumed that it did not affect the ergonomics of the device.

The peg base was placed in 3D space at specific offsets from the constraint markers and the tracking for both instruments was calibrated in such a way so that when the shaft of each instrument would touch the desk, that point would correspond to a point just below the peg-board in the 3D space of the simulation, so as to not obstruct the surgeon's motion. This simple solution aimed to give the user-subject of the experiment a hard limit when inserting the instrument's shaft inside the physical phantom constraint, and thus a basic feel for haptics.

The simulation environment, as well as the instruments, constraint, and their markers are shown in Fig. 4.6. The constraint markers are not shown, because they were placed at a position where they would not block the view of the tool markers.

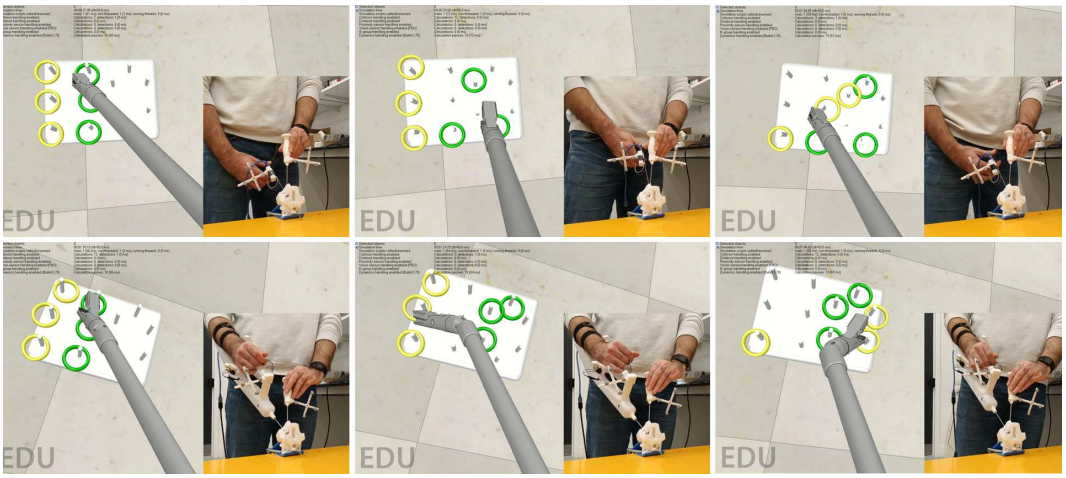

Figure 4.6: The custom-built simulated surgical task using the conventional tool (upper row) and the proposed handle (bottom row).

As previously mentioned, the purpose of this custom simulation environment was to design a comparative experiment to assess the intuitiveness and shortcomings of the proposed handle. To do this, it was necessary to evaluate the behavior of the handles kinematically, rather than to offer a hyper-realistic simulation environment. This lead to some minor inaccuracies in object interaction, such as mesh-clashing, which, however, did not affect the efficacy of the experiment. Since there is no intention for this simulator to be used for training or other demonstration purposes, and since the simulation parameters are the exact same for both tools as to not give advantage to one over the other, it was decided that

hyper-realism in interactions should not be a focal point in development.

An expert neurosurgeon specializing in EEEA procedures was tasked with running the comparative experiment to help evaluate the efficacy of the handle prototype. An initial single minute test-run for each tool was carried out so that the surgeon familiarizes themselves with the simulation environment and handling of the tools. Upon completion of the test-runs, a total of 20 attempts to transfer all hoops from the set of pegs on the left to that on the right were carried out for each tool, with a maximum duration of 2 minutes each. The surgeon carried out all 20 repetitions of the task using the conventional tool, before switching to the proposed handle.

The objective metrics used to compare the two instruments were the number of attempts it took to complete the task for the first time, and the task success rate. Additionally, the learning curve when operating with the handles was investigated. To examine the ergonomics of the proposed handle, a researcher was observing the surgeon during the experiment completing parts of the Rapid Upper Limb Assessment (RULA) [135], a validated measure to assess the ergonomics of operating posture. Finally, and after the experiment was completed, the surgeon was asked to complete the Surgery Task Load Index (SURG-TLX) questionnaire [136] for each of the two tools, the most commonly used subjective assessment of perceived cognitive load among individuals within a surgical team.

4.2.5 Preliminary findings

The number of tries until first completion, the average success rate and the successful attempts rate are summarized in Table 4.2. Here, the success rate is defined as the rate of hoops successfully transferred from one set of pegs to the other, over the total amount of hoops, whereas the successful attempt rate is defined as the rate of completed tasks, with all 6 hoops transferred from one set of pegs to the other, over the total number of tasks.

Table 4.2: Comparative table between the conventional tool and the proposed handle.

Tool	Conventional tool	Proposed handle
Attempts until first completion	NA	2
Average success rate	40.83%	80%
Successful attempts rate	0%	20%

In Fig. 4.7, the graph compares the surgeon's success rate, as previously defined, between the conventional tool and the proposed handle. In the same graph, the learning

curve is visualised as the linear curve fitted to the function of the success rate over the number of attempts. As shown in [137], it is very difficult to define a generally accepted learning curve definition. In [138] and [139], however, 20 attempts were enough to evaluate this measure.

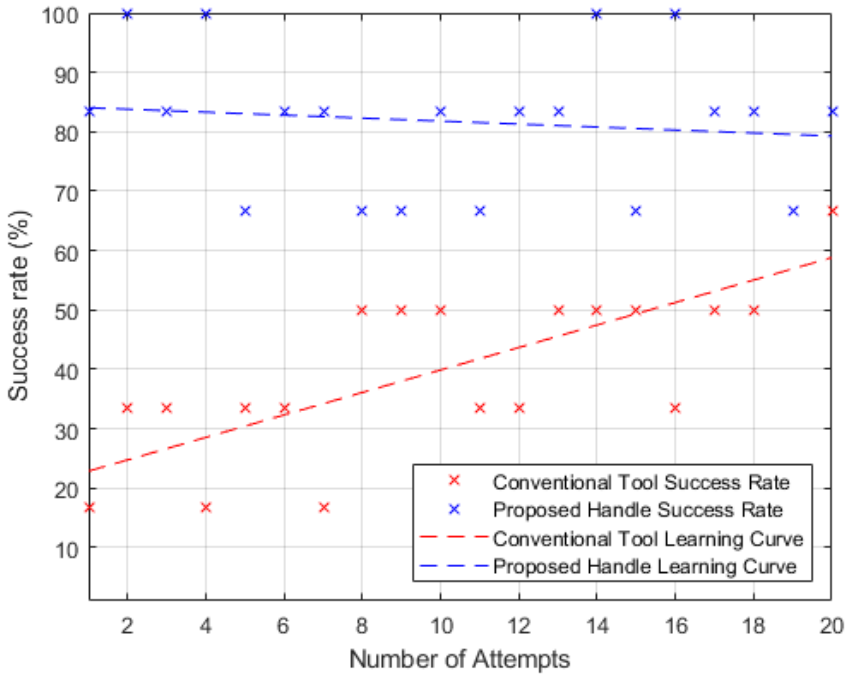

Figure 4.7: Comparison graph of the success rates and learning curves of the two instruments.

On the RULA measure scale, using the conventional tool the RULA score was 3 at the worst posture throughout the procedure, whereas with the proposed handle, the same RULA score was 2. A score of 3 falls under the 'further investigation, change may be needed' category, with a score of 2 falling under the 'acceptable posture' category. The RULA score decision trees are shown in Fig. 4.8.

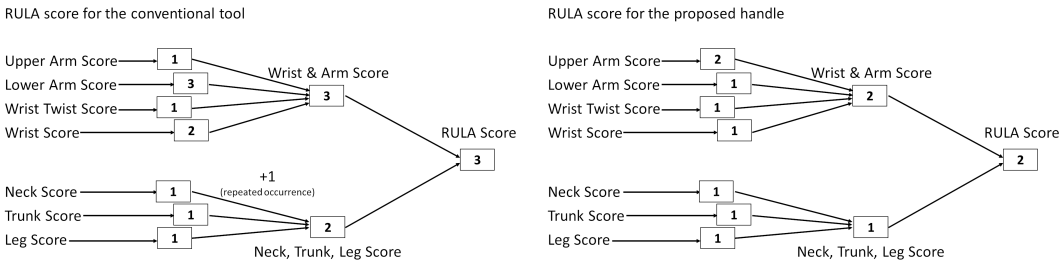

Figure 4.8: The RULA score decision trees.

Finally, the results of the SURG-TLX questionnaire in terms of mental demands, physical demands, temporal demands, task complexity, situations stress and distraction are pre-

sented in Fig. 4.9.

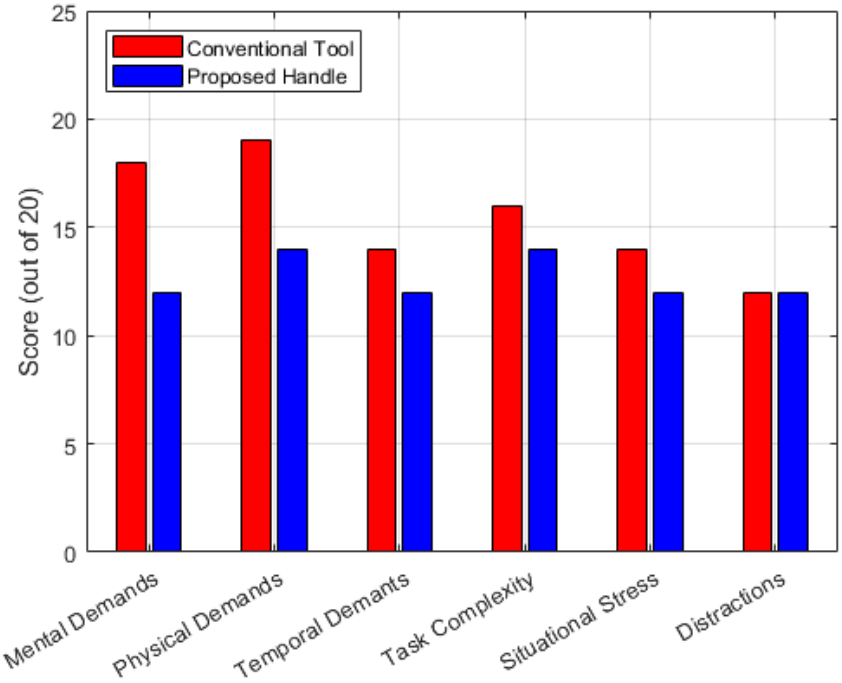

Figure 4.9: The SURG-TLX questionnaire scores.

The suggested prototype outperformed the neurosurgical tool in terms of number of attempts until first completion, average success rate and completed tasks rate. In fact, the surgeon that tested the instruments was not able to complete the task using the conventional handle, even though they had extensive experience using such instruments. This was due to the fact that some pegs were placed outside the effective workspace of the standard tool, but within the normal workspace of neurosurgical procedures.

It is self-evident that an articulated end-effector would result in an expanded workspace when compared to a conventional tool, a trait that could be used by different input devices such as haptic controllers. However, in this chapter the focus is the implementation of a handheld tool that is mounted on the surgeon's forearm, something that could theoretically lead to loss of dexterity. The proposed handle, however, still outperformed the conventional tool, and thus, the results of the experimental study indicate that the slight loss in manipulability from constraining the forearm, does not necessarily lead to loss of robotic dexterity.

The learning curves plotted in Fig. 4.7., showcase that when the surgeon was using the conventional tool, no plateau had been reached by the $20th$ attempt, whereas with the proposed handle, the learning curve is almost non-existent with an immediate improvement

in success rate. Although these findings are promising and could indicate towards fast tool adoption, further investigation with more user-subjects needs to be conducted. This limitation in user-subjects is especially telling in the case of the SURG-TLX questionnaire results, where although the improved evaluation could potentially prove encouraging, its small study size and subjective nature does not allow for concrete conclusions to be reached.

Finally, one of the goals set early on in the development of the handle prototype was the design of an ergonomic and comfortable to use handle. Based on the preliminary RULA scores, the worst posture adopted throughout the test when using the suggested handle was deemed acceptable.

Even though the preliminary results on the proposed handle are encouraging, there are some limitations that need addressing. Of all the design criteria defined in Section 4.2.1, the adaptation for variable surgeons' hand sizes and the potential incorporation of robotic assistance were not addressed in the current implementation. The adjustable straps and large joystick size can potentially cater to different hand-sizes, whereas some handle components, such as the potentiometers, could be replaced by devices that offer force-feedback or gravity compensation.

If this handle prototype were to be incorporated in a final robotic instrument, it is certain that some re-design iterations will be required to address new electronics added and new robotic assistance that is yet to be implemented. Naturally, the weight of the device will also change, although not drastically since miniature motors and electronics will be used to control the miniature end-effector. To validate the robotic prototype, a similar peg-transfer task could be deployed, only this time in a realistic physical scenario with real pegs and rings.

Regarding the simulation, the conventional tool's poorer performance can be attributed in part to the fact that the experienced user-subject has developed a preferred physical operating setup. Simultaneously, the fact that the surgeon used the conventional tool first, could have contributed to the better performance of the proposed handle. However, there is indication to believe that this was not significant. The two simulated tasks differ substantially depending on the tool used because of the distinctively different manipulation means of the tools. The fact that the surgeon could achieve the task with the proposed handle after only two attempts, despite being unfamiliar with how it operates, could still suggest the absence of a learning curve beyond familiarity with the simulation environment.

Finally, despite the limitations of a single surgeon user, it helped to illustrate some of the potential of the proposed handle. The development of a user-facing neurosurgical robotic instrument, however, requires a larger user study where a group of medical trainees and experts test its handle prototype in random repetition patterns as to further investigate whether the familiarity with the setup affects the learning curve. Using the same simulated 'peg-transfer' task developed in this chapter, the results and findings from a larger study can drive the evolution for the design and further verification for the improvement over the state of the art.

4.3 Development of a rotating joystick-body handle

To address some of the study limitations that were previously mentioned, and simultaneously to cater to a larger set of literature suggestions when it comes to ergonomically designed surgical robotic tools, an alternative prototype is presented in this section. This concept follows a drastically different design philosophy than the forearm-mounted concept. This prototype is a joystick-and-trigger handle with a rotating body that places the joystick at the position most comfortable for the surgeon. This handle was also incorporated into the custom-designed surgical virtual simulator previously presented. Alongside with the forearm-mounted handle, they were both assessed for their performance and ergonomics when compared with a standard neurosurgical grasper as part of a randomised crossover user-study, with the aim to identify the most suitable instrument design for the expanded endoscopic endonasal approach.

Similarly to the prototype presented in Section 4.2, this handle was also developed based on design suggestions extracted from the literature. Like the forearm-mounted device, this handle should also be indifferent to the surgeon's hand-size [55], with a finger-operated manipulation means, more specifically with the thumb and index finger [56]. Literature suggests that it is important that the thumb is employed for controlling the robotic joints for manipulation precision [57], either via joystick, rotary switch or other device, while the index finger should actuate a round trigger for the opening and closing of the robotic gripper [58].

Regarding the geometry of the handle, an improved ergonomic handle shape could include a large palmar grip surface and the combination of precision and turning ability [62]. In the same study it is also stated that the handle with the shaft should maintain a 45^o angle. Finally, one of the more important features of an ergonomic handle remains the

general guideline that the instrument at rest should be maintained by a partially open hand, just like the hand is kept at rest [59]. All aforementioned instructions and suggestions lead to the following design criteria defined for the proposed handle summarized in Table 4.3.

Table 4.3: Design considerations that could lead to an ergonomic handheld surgical robot.

The same handle design should cater to different hand sizes.
The instrument actuation means should be finger operated.
For precision control, the thumb should control the robot-joints, and the index-finger should operate the robotic gripper.
A resting hand pose should hold the instrument at rest.
The handle should include a large palmar grip surface.
The handle with the shaft should maintain a 45^o angle.
The instrument should provide a platform to incorporate complex robotic assistance.

Following these design specifications, the handle presented in Fig. 4.10(a). was developed, with its ergonomic design specifications reflected in Fig. 4.10(b). It is finger-operated, employing a thumb-controlled joystick that actuates the robot joints, namely the yaw and pitch motions since the roll motion is carried out by the surgeon holding the tool, and a standard trigger controlled by the index finger that actuates the robot gripper. It contains a large handle surface that provides the surgeon with palmar grip and the handle-shaft angle is 45^o. The robot-joints are controlled by a 2-axis joystick module, while the trigger is controlled by a rotary switch. In this preliminary evaluation prototype, where motors and electronics are absent, the inner structure of the handle consists of the two aforementioned sensory modules, as well as a miniature microcontroller and cabling. A cross-section sketch of the device showcasing these components is presented in Fig. 4.10(c).

All these suggested ergonomic parameters were accounted for with design modifications. The indifference to the surgeon's hand-size, and designing the handle in a way that the instrument at rest is maintained by a hand that is also kept at rest, were bigger challenges. To solve both problems, a rotating joystick-body was introduced. This component is modifiable and can be rotated and tight-fitted into seven discrete positions, in order to be placed at the position that each surgeon feels most comfortable with. Fig. 4.11(a). shows the handle with its rotating body in its different positions. The angles for these positions were $\pm 15^o$, $\pm 35^o$, and $\pm 55^o$, in order to cater to small, medium, and large hands respectively as literature defines them [140].

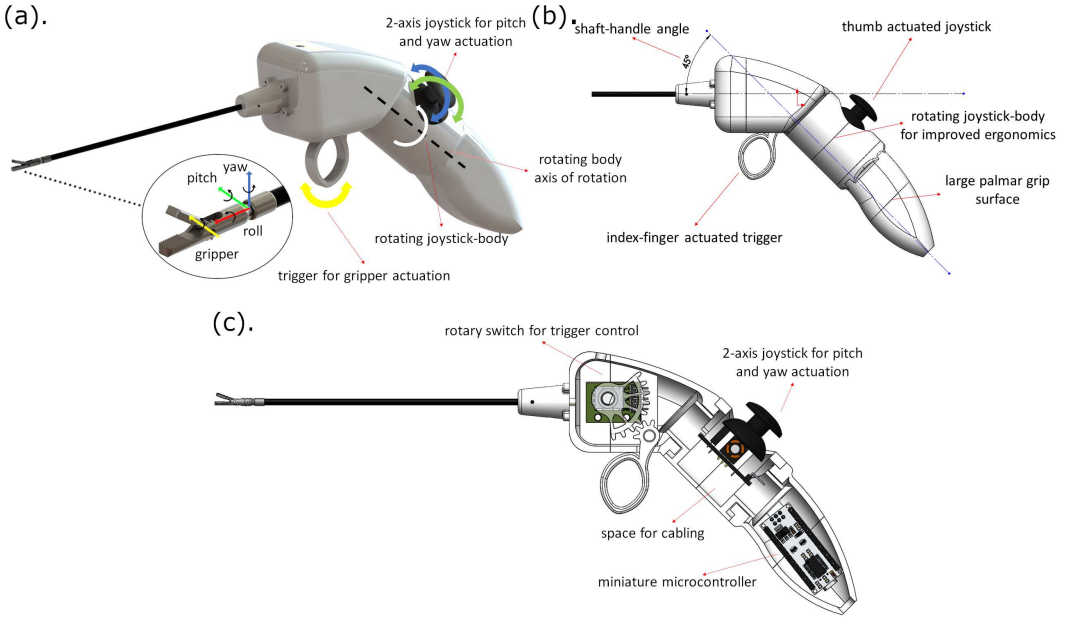

Figure 4.10: (a). Rendering of the rotating joystick-body handle prototype with the coordinate frames of the handle joints and the axis of rotation of the rotating body (right), and the corresponding coordinate frames of the robot-joints (left). The roll robot DoF is carried out by the surgeon's hand. (b). The ergonomic specifications analysed in Section 4.3 reflected on the handle design, and (c). A cross-section sketch of the device that reveals its inner structure.

The level/resting position of the hand is shown in Fig. 4.11(b). and in Fig. 4.11(d)., the thumb is shown in 'adduction' (left) and 'abduction' (right). It is evident from this figure that the resting position of the hand requires the thumb to be in an 'abduction' position.

If the joystick was placed at the exact centre of the handle, the thumb would be at an 'adduction' position and the chance that the surgeon would feel uncomfortable and easily tired could be higher. By placing the joystick on a rotating body, the surgeon can rotate the joystick to the left if they are to use it with their right hand, and to the right, if they are to use it with their left hand. The angle of rotation, namely the angle by which the surgeon needs to rotate the joystick body to feel comfortable, depends on the surgeon's hand-size. In Figure 4.11(c)., it is shown how this handle can cater to different hand-sizes and can be used independently of right- or left-handedness. To cater to the smaller hand, the rotating body has been rotated by 15^o, whereas for the larger hand, the angle was 55^o.

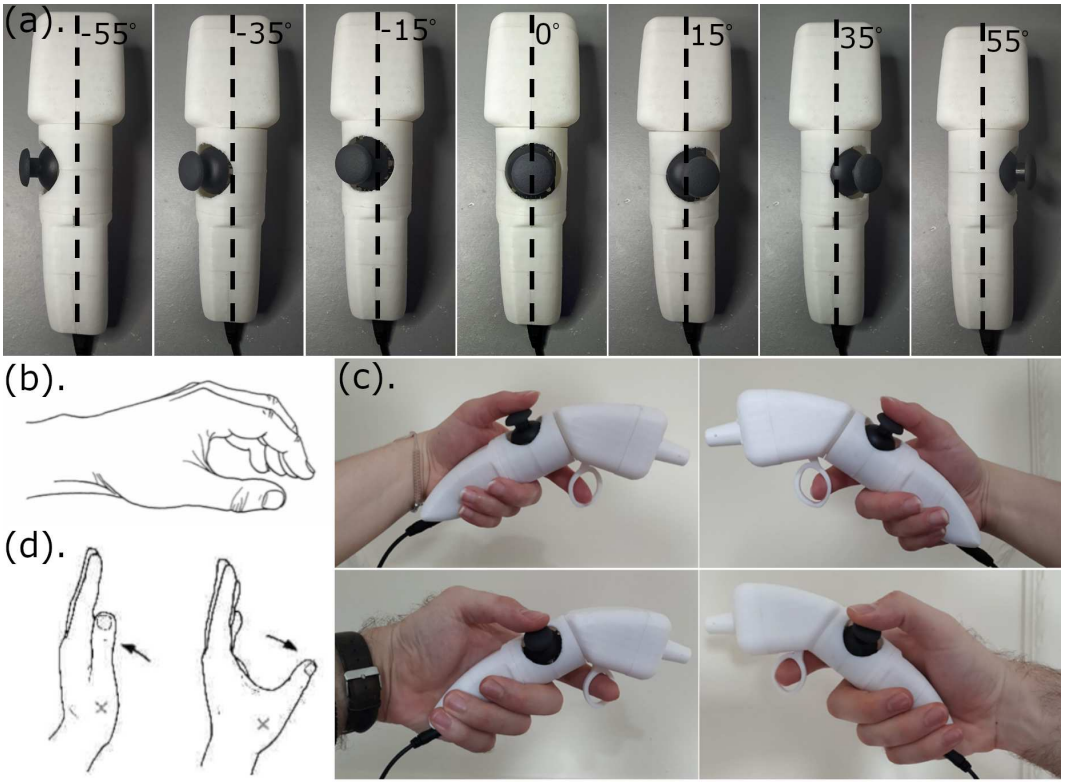

Figure 4.11: (a). The seven discrete joystick positions on the same 3D-printed rotating joystick-body handle prototype. The axis of rotation of the joystick-body and the angle of each position highlight the rotating function. (b). The hand at its resting position, (c). (left to right and top to bottom) The handle held by a small left hand, a small right hand, a large left hand, and a large right hand, and (d). Thumb adduction (left), thumb abduction (right).

4.4 Comparing the two handles during a randomised crossover user-study

The purpose of this study was to expand on the preliminary findings obtained for the forearm-mounted handle (FMH) presented in Section 4.2, to evaluate the newly developed rotating joystick-body handle (RJH), and to investigate if one of the two is superior. To do that, a randomised crossover user-study was organised and ran, where a total of 9 medical students used the novel handles and a standard neurosurgical instrument carrying out a surgical training task inside the previously presented custom virtual simulator. To conduct the study, ethics approval was obtained by the University College London Research Ethics Committee (UCL REC - reference 18035/001).

The simulated surgical training task was again the 'peg-transfer' task, taken from the McGill Inanimate System for Training and Evaluation of Laparoscopic Skills (MISTELS) [133], since it has been validated as indicative of surgical skill during keyhole brain-surgery

[134]. Once again, additive manufacturing techniques were deployed to prototype the RJH, namely 3D printing. All parts of the handles were 3D-printed (Ultimaker S5, Ultimaker BV, Utrecht, Netherlands), using PLA. For the end-effector shaft, a 3*mm* diameter stainless steel rod was used, whereas the end-effector was simulated within the virtual environment. The data from the joystick and rotary potentiometers used in both prototypes were processed using a miniature microcontroller (Arduino Nano, Arduino AG, Italy).

Other than the two handle prototypes, a 28164TA surgical forceps (Karl Storz SE & Co. KG), and a 3D-printed endoscopic device aimed for camera manipulation were used for the comparative experiment. During the endonasal approach, a single surgeon can hold the camera in their one hand and the operating instrument in their other hand, a passive endoscope-holder can be used, or an assistant surgeon can hold the endoscope while the operating surgeon is using an instrument in each nostril [11]. In this study, the first scenario was replicated, with each user-subject of the study manipulating both the prototypes and endoscope, so that they have complete control of the task.

All tools used were optically tracked using a motion capture system (Optitrack V120:trio, NaturalPoint Inc., Canada) and custom marker attachments of negligible weight. The optical markers were placed in positions on the handle body where they would not affect the handling of the instrument. Their physical pose on the handle was transformed in the software environment in relation to the simulated robotic end-effector, and thus the operator manipulation could by realistically replicated inside the simulation environment. To constrain the tools in 3D space, the same physical constraint of a model of a cranial CT was used.

The experimental setup is shown in Fig. 4.12(a)., the simulation environment in Fig. 4.12(b)., and the task being carried out by a researcher holding all the tools with their optical markers is shown in Fig. 4.12(c).

The performance and ergonomic assessment of the participants using this universal experimental setup could be highly affected by the individual surgeon's preferred surgical setup. To alleviate this potential bias, medical students rather than senior trainees or staff neurosurgeons were recruited, who did not have developed an operating preference yet. A total of 9 participants were recruited, with two thirds of them covering the 6 possible combinations between the three devices. The remaining 3 participants used the devices in random sequence. The device sequence for each participant is depicted in Fig. 4.13.

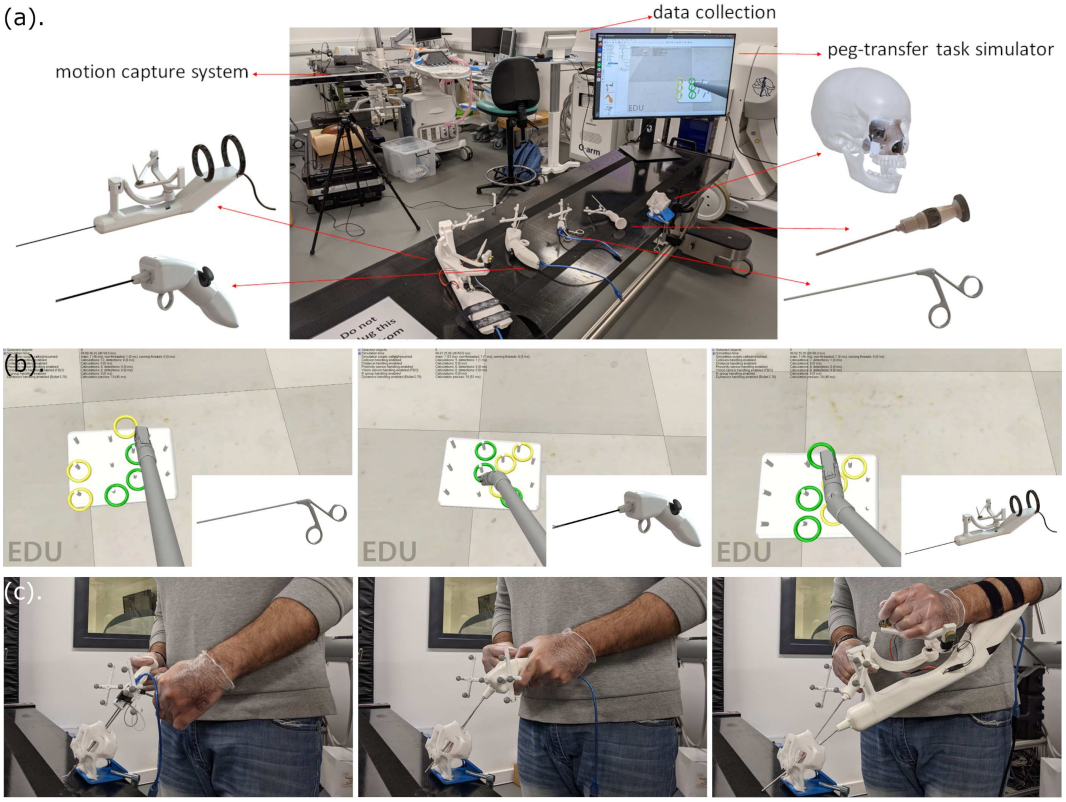

Figure 4.12: (a). Experimental setup with renderings matched to their respective prototypes. The FMH and RJH are shown on the left side of the image, and the conventional tool that was used as a comparison on the right. Also on the right, the endoscope prototype that was used to manipulate the camera is showcased, alongside the 3D-printed skull constraint. (b). The simulated environment when a researcher is carrying out the peg-transfer task, and (c). The researcher using the prototypes when carrying out the peg-transfer task.

At the start of the experiment the participants were asked to complete an adapted version of an already published questionnaire [57] to assess their initial impressions of the three handles. In order to complete this questionnaire, the participants inspected the different prototypes, and briefly used them inside the virtual simulator to get a feel of their operation and control. The aim of this was to assess the face validity of each handle and explore whether there is a general consensus of subjective opinion about each handle between participants. The questionnaire that the volunteers were asked to fill-in is shown in Fig. 4.14.

Then, the following measurements of participants' hands were taken: length of the hand, length of the palm, width of the hand at the metacarpal, length of the index finger, width of the index finger-proximal, width of the index finger-distal, and width of the thumb. The purpose of these measurements was to assess if hand-size impacts the performance of each handle [141].

Using each device in random sequence and whilst wearing surgical gloves, the partici-

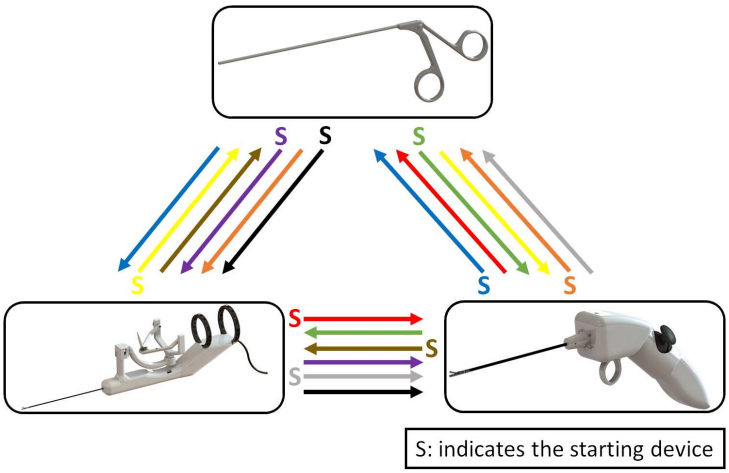

Figure 4.13: The device sequence for each participant represented by a different color.

pants carried out the peg-transfer task. They were maintaining a standing pose and looking at a screen at their eye level, where the simulated task was taking place, and their task was to transfer all rings from one set of pegs to the other, with no particular order. With each device, they attempted the task a total of 10 times, with a maximum duration of 2 minutes for each attempt. No breaks were taken between these individual 2-minute attempts to simulate continuous instrument usage, whereas a 5-minute break was scheduled between tool changes. For each attempt, the time at which each ring was successfully transferred was recorded, something that can give insight on the completion and success rates, as well as the learning curve of the handles.

To investigate the procedural ergonomics, the participants were observed and assessed while carrying out the tasks, completing the Rapid Upper Limb Assessment, a validated measure to assess the ergonomics of instruments [142]. When using this score-based system, lower RULA scores for a procedure are associated with better ergonomic postures. The RULA ergonomic scores throughout the experimental procedure with each device were taken at the participant's worst demonstrated posture.

At the end of the task with each device, the participants were asked to complete the Surgery Task Load Index questionnaire [136]. This questionnaire assesses the mental, physical, and temporal demands of using an instrument, along with situational stress and distractions during the task. Each participant completed this two-part questionnaire for each of the three devices, and based on their answers, 6 weighted SURG-TLX dimension scores for each one of them, and for each device were extracted. The aim of this questionnaire was to assess the ergonomics of the handles from the participants perspective, alongside the more

Handle Evaluation

1. Please look at and touch the handles. Hold each handle, and operate the joysticks and triggers of each one. Then, please indicate a score on a scale of 1 (strongly disagree) to 5 (strongly agree), indicating how much you agree each handle was intuitive, comfortable, precise, and stable.
    a. Rotating joystick-body handle
        i. Intuitiveness:
        ii. Comfort:
        iii. Precision:
        iv. Stability:
    b. Forearm-mounted handle
        i. Intuitiveness:
        ii. Comfort:
        iii. Precision:
        iv. Stability:

2. Would you like to have any additional commands and/or triggers on the handle?
    a. Rotating joystick-body handle: Yes/No

    b. Forearm-mounted handle: Yes/No

Handle Preference

1. Please indicate the instrument handle that you prefer:
    a. Rotating joystick-body handle
    b. Forearm -mounted handle

2. Please could you briefly explain why you prefer this instrument handle:

3. If you have any additional comments about any other handles, please provide them here:

Figure 4.14: The handle evaluation and preference questionnaire that the participants were asked to fill-in after they inspected the devices and before carrying out the tasks with them.

objective Rapid Upper Limb Assessment.

4.4.1 Evaluation and preference questionnaire

For the first question of the 'Handle Evaluation' questionnaire, the participants were asked to rate the two handles on four different categories as shown in Fig. 4.14. Overall, the participants preferred the RJH, which scored mean ratings of 4.1 for intuitiveness, 4 for comfort, 3.8 for precision and 3.8 for stability, with the respective ratings for the FMH being 3.7, 3, 3.6 and 3.8. This preference was also reflected in the 'Handle Preference' part of the questionnaire, where the majority of the participants agreed that the RJH felt easier to use, was less tiresome, and it employed easier gripper control. To improve the design of the handles, it was suggested that the RJH incorporates a clicking joystick rather than a standard trigger, while the FMH would feel better with an articulated trigger or button

	Participant #								
Hand measurement	**1**	**2**	**3**	**4**	**5**	**6**	**7**	**8**	**9**
a.	19	16.5	18	17.5	17	16.5	16.5	20	18.5
b.	10.5	10	10.5	10	10	9	10	11	10
c.	8.5	7.5	8	8	8	7.5	7	9	8.5
d.	7.5	7.4	7	8	7	7	7	9	7.5
e.	2	2	2	1.5	1.5	1.5	1.25	1.75	1.5
f.	1.5	1.7	1.6	1	1	1	1	1.5	1.25
g.	2	1.5	2.3	2	1.75	1.75	1.5	2	2

Table 4.4: The participants' hands measurements with a. length of the hand, b. length of the palm, c. width of the hand at the metacarpal, d. length of the index finger, e. width of the index finger-proximal, f. width of the index finger-distal, and g. width of the thumb.

controlling the trigger, rather than the pen-like rotating trigger that controls it in this current iteration.

The hand measurements a.-g. as mentioned in Section 4.4 taken during this part of the experiment are shown in Table 4.4. The participants' hands were split into categories based on hand length, and following the definition that a hand is considered small when its length is between 16.3cm and 17.9cm, medium when its length is between 17.9cm and 19.4cm, whereas for lengths between 19.4cm and 21.2cm, the hand is considered large [140]. Thus, the study included 5 participants with small-sized hands, 3 with medium-sized hands, and 1 participant with large-sized hands. Resultantly, the respective angles by which the rotating body on the RJH was rotated based on hand-size category were 15^o, 35^o and 55^o.

4.4.2 Performance evaluation

The completion rate, here defined as the percentage of rings that were successfully transferred from one set of pegs to the other out of the total of 6 rings, for each of the 9 participants throughout their 10 2-minute attempts, and for each of the 3 devices is depicted in Fig. 4.15. In the same set of figures, the mean average values of the completion rate per participant are shown.

The median of rings transferred between the 9 participants when they were using the standard instrument was 4, whereas for both the RJH and FMH was 6. With the standard instrument, 2 participants did not manage to transfer any rings at all at least once during their 10 attempts. The least amount of rings that were transferred with the RJH during a single attempt were 2, and with the FMH 3, with the exception of participant #2, who asked to end the experiment early due to shoulder discomfort, as discussed in Section 4.4.5.

Overall, the participants showcased significantly improved performances with the

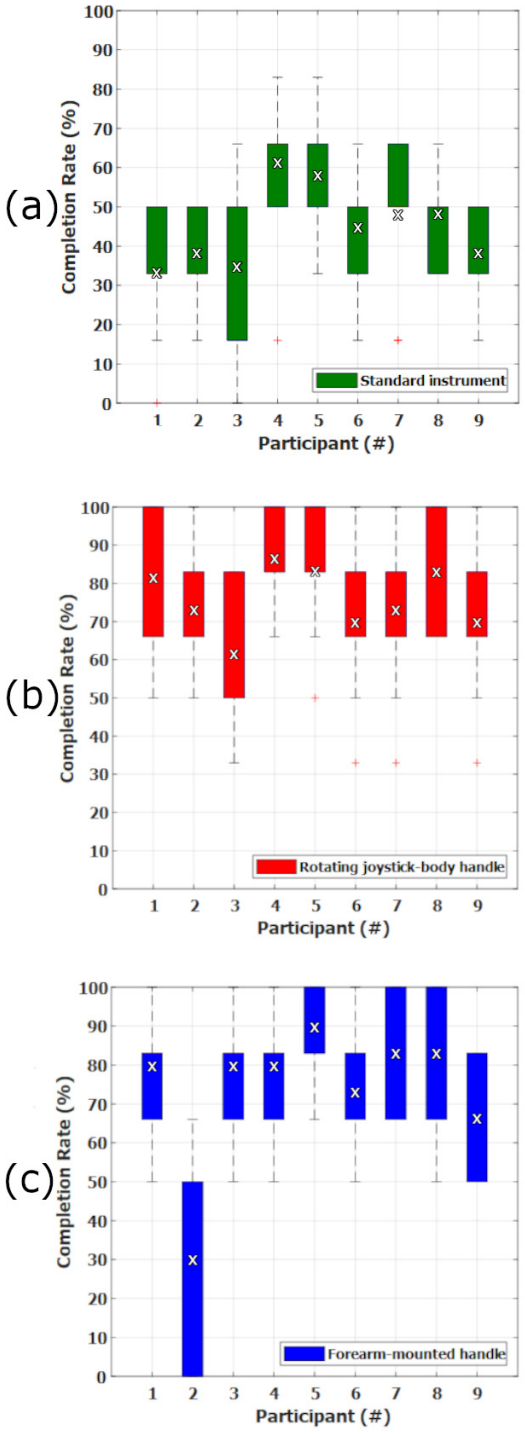

Figure 4.15: The completion rate during all 10 attempts for each of the 9 participants, for (a) the conventional tool, (b) the RJH, and (c) the FMH. The red crosses are the outliers of the box-plots, while the black and white x-marks in sub-figures are the mean average values of the completion rate per participant and the completion rate per attempt respectively.

robotic handles rather than with the standard instrument, with both the lower and upper quartiles of their box-plots scoring higher for the two novel handles. The mean completion rate ($p = 0.44$) , here defined as the arithmetic average percentage of rings that were successfully transferred from one set of pegs to the other out of the total of 6 rings, between all 9 participants, and for each of the 3 devices is depicted in Fig. 4.16.

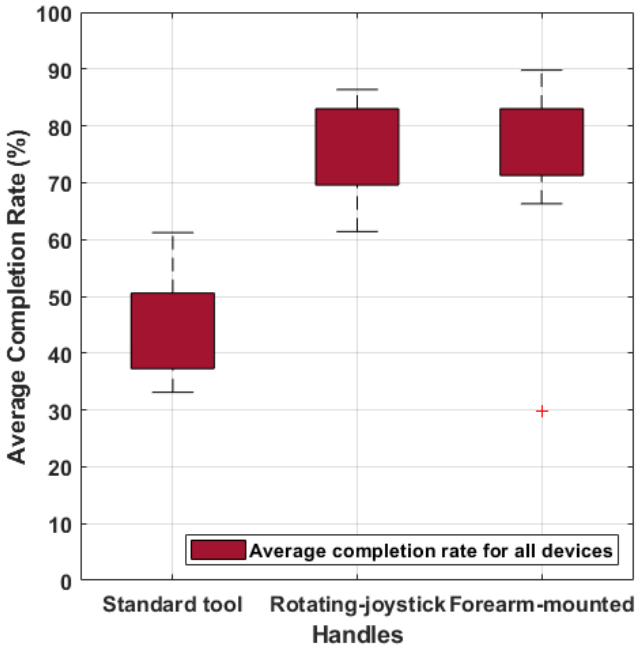

Figure 4.16: The mean completion rate for all 9 participants for each of the 3 devices. The red crosses are the outliers of the box-plots.

It is evident that the two handles clearly outperformed the standard instrument. Fig. 4.17. shows the successful attempt rate ($p = 0.37$), defined as the percentage of attempts out of the 10 attempts when a participant was able to transfer all 6 rings. Once again, the same trend is noticed of the two handles being superior to the standard instrument that had a 0% successful attempt rate throughout.

To have an understanding of the time-efficiency of each handle, the mean time ($p = 0.29$) it took the participants to transfer each one of the 6 rings was calculated. The results are shown in Fig. 4.18. The participants had the most time-efficient performance using the FMH, and managed to complete the task in a mean time of $87.1sec$, almost $20sec$ faster than when using the RJH that had a mean time of successful completion of $106.7sec$.

Finally, in Fig. 4.19, the learning curve of the devices is quantified as the relationship between the completion rate for all 9 participants during each of their 10 attempts. In the same set of figures, the mean average values of the completion rate per attempt are shown.

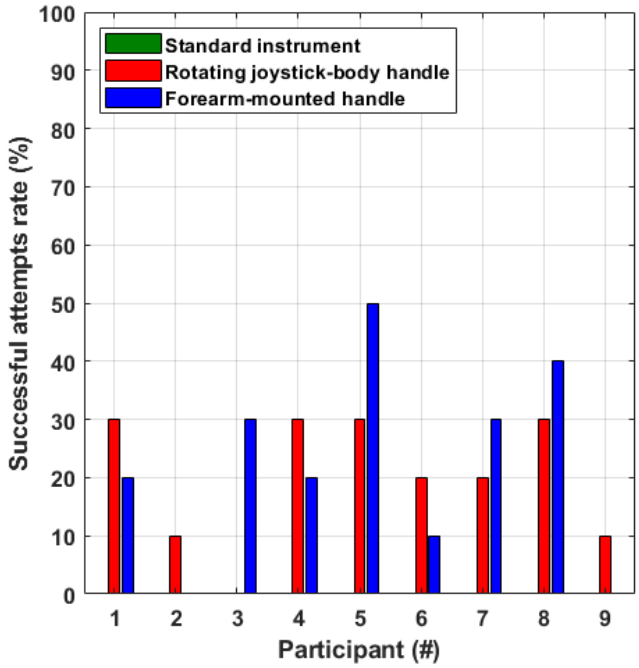

Figure 4.17: The successful attempt rate for each of the 9 participants, and for each of the 3 devices.

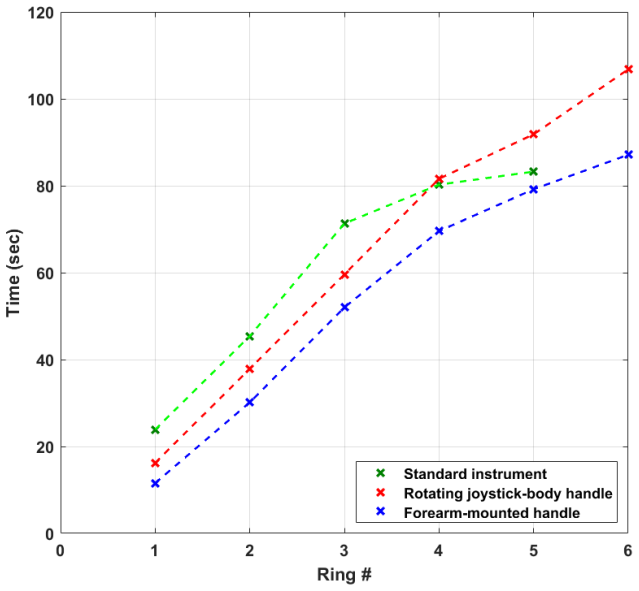

Figure 4.18: The mean time it took all participants to successfully transfer each ring.

When the participants were using the standard instrument, and by the $4th$ attempt, they were confidently achieving 4 rings, a pattern that stayed mostly the same by the end of the experimental session. On the contrary, when participants were using the RJH and the FMH, they achieved completion rates of over 80% early, and after the $5th$ attempt they were regularly successfully completing the task, suggesting that the novel handles have small learning curves. Between the two handles, the RJH seems to present a more consistent

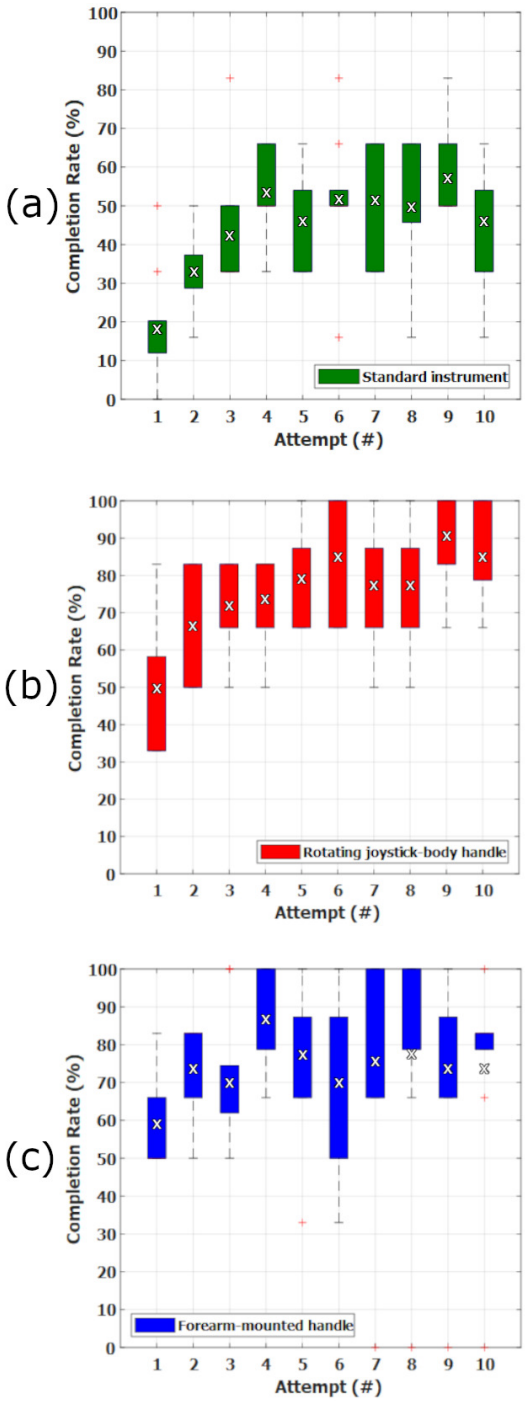

Figure 4.19: The learning curve of (a) the conventional tool, (b) the RJH, and (c) the FMH, presented as the relationship between the completion rate for all 9 participants for each of the 10 attempts. The red crosses are the outliers of the box-plots, while the black and white x-marks in sub-figures are the mean average values of the completion rate per participant and the completion rate per attempt respectively.

learning curve with less noise in each attempt compared to the FMH.

4.4.3 RULA ergonomic assessment

The RULA survey method posture scores for all 9 participants, and for each individual posture of the upper limbs, neck, trunk, and legs are shown in Fig. 4.20., whereas in Fig. 4.21., these scores are used to calculate the overall RULA ergonomic score for each individual participant when using each device. Compiling these individual posture scores into overall RULA scores for each participant, the RJH had a mean RULA score of 3.2, followed by the FMH with a mean score of 4.3, and the standard instrument that scored 5.4.

The upper arm posture was worst for the FMH, where the participants had to raise their shoulders to translate the simulated robotic end-effector, followed by the standard instrument, and then by the RJH. The lower arm posture was similar for the first two devices with the participants occasionally working across the midline of their bodies, and again best performance occurred with the RJH.

As expected, wrist posture was worse with the standard instrument, with extreme angles occurring and participants having to bend their wrist away from the midline. When using the FMH, participants needed to often employ mid-range and extreme angles, while bending their wrist, and when using the RJH they were mostly within a healthy angle range. The final parameter for the RULA posture group A, which includes the arms and wrists, was the wrist-twist, that was almost always near the end of the twisting range for the standard instrument, mainly mid-range for the RJH, and always at the natural wrist twist position for the FMH.

As far as the RULA group B is concerned, namely the neck, the trunk and the legs, participants seemed to struggle more to find a comfortable neck position when using the standard instrument, and they would often twist their neck. The corresponding behavior with the two novel robotic handles was similar between each other, and slightly better than with the standard instrument. When using the RJH the participants would mostly maintain a well-supported trunk and would rarely flex forward, twist or bend it. The same cannot be said for the other two devices, where the participants showed similar behavior that included all flexion, twisting and bending. Finally, throughout the experiment the participants' legs and feet were well supported and in an evenly balanced posture, meaning that no participant scored more than a score of 1.

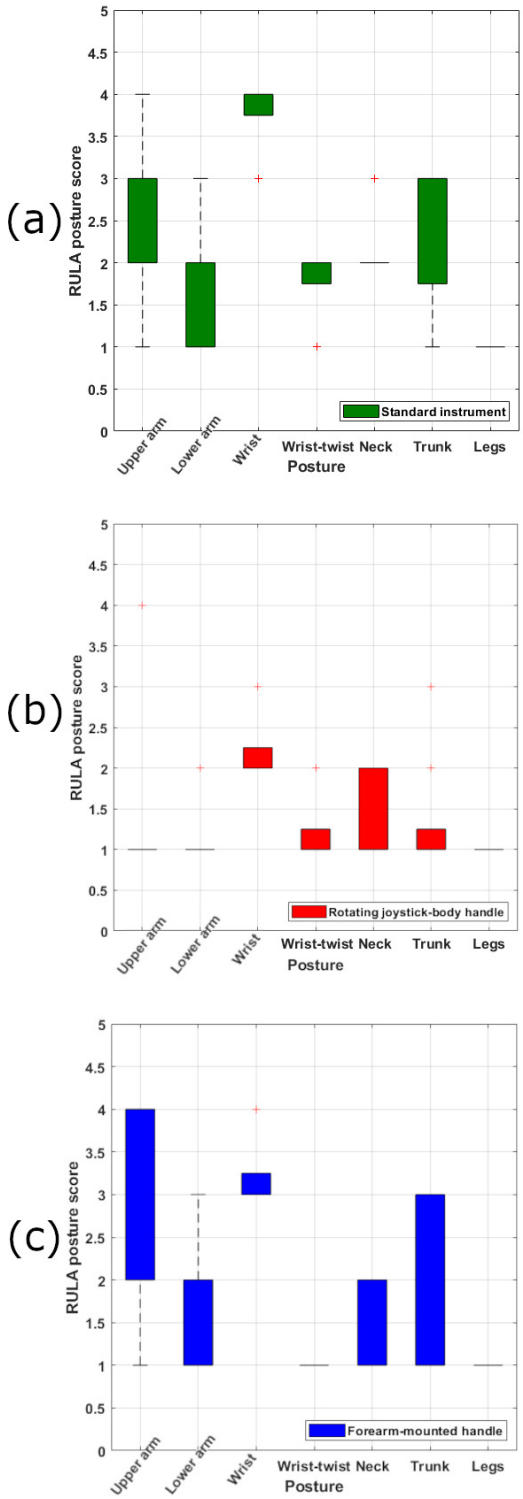

Figure 4.20: The RULA posture scores for all 9 participants for each posture, and for (a) the conventional tool, (b) the RJH, and (c) the FMH. The red crosses are the outliers of the box-plots.

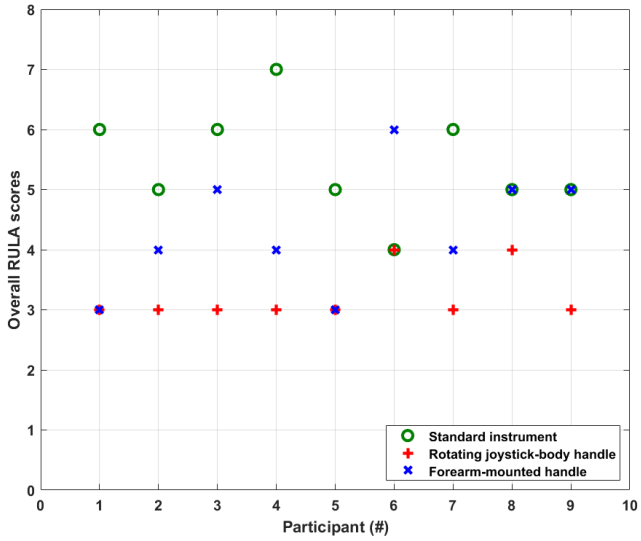

Figure 4.21: The overall RULA score for each participant, and for each of the 3 devices

4.4.4 Surg-TLX questionnaire

The final measure to assess the participants' ergonomic behaviour was the SURG-TLX questionnaire, a subjective questionnaire that aims to assess the participants' mental, physical, and temporal demands while using an instrument, alongside with situational stress and distractions during the task. The mean of the weighted SURG-TLX scores, for each dimension and for each device are shown in Fig. 4.22.

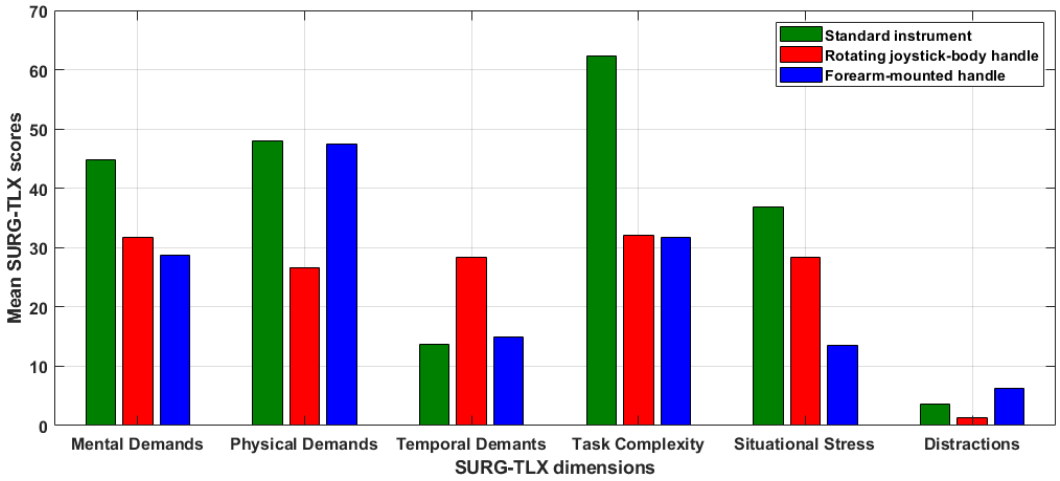

Figure 4.22: The mean SURG-TLX scores for each individual SURG-TLX dimension, and for each of the 3 devices

Summing up all the individual scores for each participant, the total SURG-TLX workload for each participant and for each device can be calculated, shown in Table 4.5. The smaller the workload, the more favorably in terms of ergonomics the device has been per-

Participant #	Total SURG – TLX workload		
	Standard instrument	Rotating joystick-body handle	Forearm-mounted handle
1	230	186	99
2	205	10	197
3	209	192	157
4	188	124	127
5	236	123	124
6	221	212	223
7	171	160	132
8	193	187	142
9	230	143	81
Average	209.22	148.55	142.44

Table 4.5: The total SURG - TLX workload for each participant, and for each of the 3 devices, as well as the mean SURG - TLX workload for each device.

ceived by the participant. The subjective opinions of all 9 participants about their own perceived ergonomics agree that the two novel handles impose a smaller workload than the standard instrument, with a single exception. Participant #6 preferred the standard instrument over the FMH. Out of 9 participants, 6 preferred the FMH, and 3 preferred the RJH. Finally, and on average, the former outscored the latter in terms of mean total SURG-TLX workload.

4.4.5 Preliminary findings and concept selection

In terms of performance and efficacy, the two robotic handles clearly outperformed the standard neurosurgical instrument. Although an expected result, since a tool with added articulation is designed to have a larger workspace than a non-articulated instrument, performance was still an important aspect to investigate. The ergonomic design considerations implemented in the two designs, namely the forearm constraint of the one handle, and the moving joystick-body of the other, could potentially lead to declined performance because of dexterity loss or imprecise control. The fact that both handles outperformed the standard tool suggests otherwise.

When comparing the performance of the two novel handles, the two devices had very similar behaviours. The RJH showcased a slight edge in the categories of completion rate per participant and mean successful attempt rate, while the FMH performed slightly better in terms of mean completion rate. These differences, however, are small and thus are not adequate to confidently suggest which one of the two novel devices is the most suitable for the EEEA.

Both handles seem to have similar and small learning-curves, with the RJH being associated with a more consistent learning curve, and the participants were able to perform very well or even complete the task very early in their 10 attempts sequence. The one category where one handle clearly outperforms the other is time-efficiency, with participants being able to successfully complete the task using the FMH approximately 22% faster than with the RJH. A final note on performance is that a correlation between hand-size and handle performance could not be immediately identified since participants of all three hand-sizes had similar outcomes in terms of completion and successful attempt rate.

Much clearer conclusions can be drawn from the ergonomic assessment. The RJH is the safest handle to use for an extended amount of time according to the RULA survey, since it only scored 3 and 4, both scores falling into the 'low risk' category. On the contrary, the FMH scored both 3 and 4, but also 5 and even 6 once, deeming it low to medium risk. As far as the standard instrument is concerned, and with the exception of one 'low risk' score and one 'high risk' score, it was deemed medium risk.

Finally, when participants were able to voice their opinion at the start of the experiment, the majority preferred the RJH. This consensus was inverted after the experimental procedure took place with the majority of the participants favoring the FMH in terms of total mental, physical and temporal workload. This preference contradicts the RULA assessment outcomes, with the most probable explanation being that the participants highly valued the intuitiveness of the handle, but only used it for a limited amount of time. Had they used the handle for an extensive period, the RULA assessment suggests that there is a higher likelihood for discomfort.

Despite the low mental demands and situational stress associated with the FMH, as well as its time-efficiency, the poor ergonomic results and the similar performance, combined with the increased time and effort it would take to switch between instruments during the endonasal approach, indicate that the more favorable handle for the EEEA, amongst the two investigated with this comparative experiment, is the RJH.

The increased time and effort would be evident in instances when non-robotic tools would need deploying for the operation. To un-mount the FMH from the surgeon's forearm, the operating surgeon would need to leave whatever tool they hold with their other hand to untie the straps, or a second clinician would need to be involved. With the RJH, on the other hand, the operating surgeon would just need to leave the tool on the operating tray and

pick-up another tool. Thus, it is deemed that the RJH offers a more complete solution than the FMH with similar increased joint articulation, while simultaneously maintaining low ergonomic risk. Simultaneously, deploying two forearm-mounted instruments at the same time, when the surgeon would need to use articulated instruments through two insertion points, would be very complicated and technically challenging due to the very constrained access pathway. This is why the joystick-and-trigger handle was chosen as the more suitable handle concept for endoscopic neurosurgery.

While the forearm-mounted handle was deemed less suitable than the alternative design for the endonasal approach, there are some surgeries that could benefit from its introduction into the operative workflow. Microsurgical procedures such as foramen magnum decompression surgery or micro-incision cataract surgery could benefit from the use of an intuitive handheld controller that can scale the end-effector motion. During these operations the surgeon is deploying a high-magnification microscope and handheld tools to visualise and manipulate small structures such as nerves or vessels. A handle concept like the one presented initially in this chapter, with an easy-to-learn manipulation method that directly maps the surgeon's hand movements to the robot joints could make that tissue manipulation easier, while the surgeon is comfortably controlling the device with potential robotic capabilities such as enhanced articulation, motion scaling, and tremor compensation.

As far as the rotating joystick-body handle is concerned, the design presented in this chapter will have to be altered to incorporate motor electronics as well as the robotic end-effector. It will, thus, have to be re-validated for its ergonomics, because while the weight distribution of the functional device will be similar to the suggested prototype, the weight itself will increase with the addition of motors and cables, and the geometry will have to be amended.

4.5 A functional ergonomic handheld controller

Having suggested a suitable handle concept for the endonasal approach, that design then needed to incorporate motor and electronics to form a functional handheld controller that could control the robotic end-effector. While the concept design showed promise, it needed modification in order to form a working prototype. In this section, the work that was undertaken to develop this handheld controller while maintaining its ergonomic characteristics is presented.

The handheld controller was aimed to be ergonomically designed to not cause the

surgeon strain or fatigue, while also being easy to use and associated with small learning curves. In Sections 4.2 and 4.3, two drastically different handheld controller concepts covering a wide array of ergonomic design suggestions found in literature were designed. The two design concepts, as well as a standard instrument, were compared for their efficacy and ergonomics during a pre-clinical randomised controlled trial, with the design shown in Fig. 4.23(a). proving superior.

According to literature suggestions [69], this finger-actuated handheld controller should cater to different hand sizes, and include a large palmar grip surface that would allow a comfortable and robust grip. To achieve the former ergonomic requirement, a rotating joystick-body was designed, which could be placed at a position most comfortable for the surgeon depending on their hand size and handedness.

The handle with the shaft should maintain a 45^o angle to avoid wrist-strain when maintaining it, and to make the control instinctively easy to adopt, the thumb should control the robot-joints, and the index-finger should operate the robotic gripper. After this concept design was preliminarily validated in previous work, the next developmental step was to incorporate motors and electronics to turn it into a fully-functional handheld robotic controller. Fig. 4.23(b). showcases a rendering of the finalised instrument design.

One of the main challenges in incorporating the electronics into the previously suggested design was the rotating joystick-body. It was a core element of the ergonomics of the device, thus, it was important that its functionality was maintained. A translational 2-axis joystick offers a small footprint and alongside the compact rotating platform accommodates the motor placement inside the device, a component that was previously absent in the concept implementation. To fix the rotating platform in the desired position, a multi-pin that fixes it in place was introduced . The rotating joystick-body in its 5 discrete positions is depicted in Fig. 4.24.

The handheld device presented in this thesis is lightweight and compact so that it does not cause the surgeon any physical harm from repeated use. It is also 3D-printed with resin, similar to the end-effector casing, and the motor drive unit housed inside the handle consists of 3 lightweight and compact motors. These motors are brushed DC-motors with an outer diameter of 8mm and a 2.34mm shaft diameter (FAULHABER, Schönaich, Germany). Gears are fixed on the shafts of the motors that are then coupled with the gears located on the proximal end of the end-effector tools as previously described in Section 3.6. That way

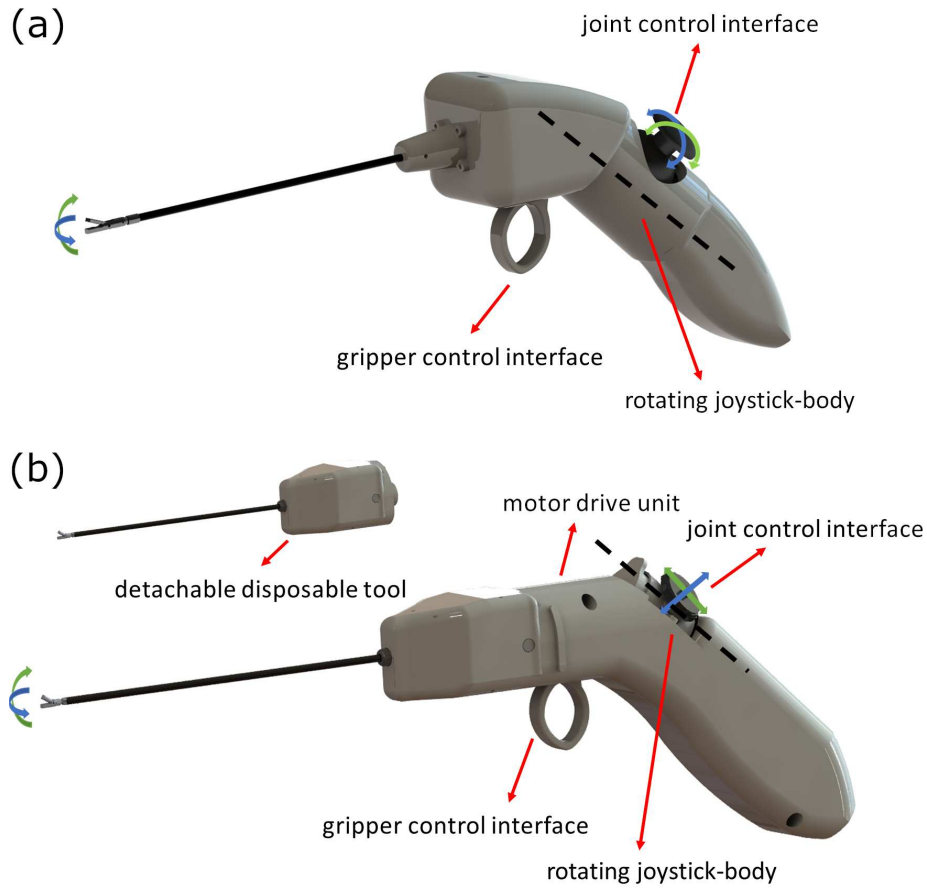

Figure 4.23: Renderings of (a). The concept handheld design suggested in Section 4.3 which was tested in simulation, and (b). The finalised handheld instrument design after electronics, motors, and end-effectors were incorporated to offer functionality.

Figure 4.24: The rotating joystick-body in its 5 discrete positions with a rotating step of 15^o.

the motor movement is transmitted over to the robot joints. Finally, other than the motors, the handle houses the 2-axis joystick for joint control and a $10K\Omega$ trimmer potentiometer for trigger control.

Before reaching this final handheld controller design, a number of considerations took place. An important implementation choice, was the electronics that would be used to interface with the end-effector. The handle prototype developed in Section 4.3 was deploying a

2-axis rotational joystick module for the end-effector joints movement, and a trigger for the grasper actuation. Naturally, the initial design of the handheld controller was incorporating the same 2-axis rotational joystick, as seen in Fig. 4.25(a).

This, however, resulted in a large device that felt uncomfortable regardless of the operator's hand-size. The next iteration of the handle design incorporated a 2-axis translational joystick module that was smaller in size and was placing the operator's thumb at a comfortable position. Simultaneously, the size of the device was decreased, and operation was easier and more comfortable. This iteration of the handheld controller can be seen in Fig. 4.25(b).

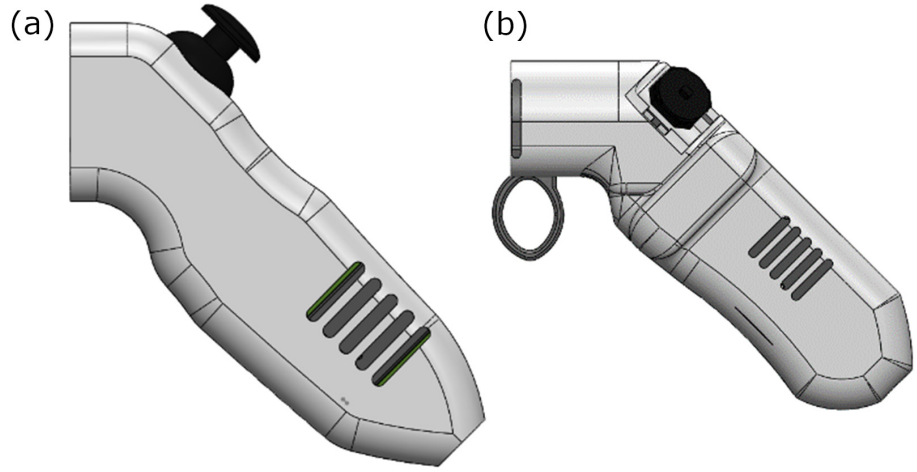

Figure 4.25: (a). Handheld controller design incorporating a 2-axis rotational joystick module, and (b). Handheld controller design incorporating a 2-axis translational joystick module.

At that developmental stage, the electronics driving the motors, namely the motion controllers and motor cable adapters, were still housed inside the handheld device. Fig. 4.26(a). shows that arrangement. This increased the device size, and more importantly its weight, and was deemed as an unsuitable solution. Fig. 4.26(b). depicts a sketch were the only components left inside the device are a breadboard and the cables connect to the motors and interface electronics. All these cables were lead to a 12-core cable that was connected with the device control box.

4.6 The handheld controller electronics box

To keep the device lightweight, all electronics driving the motors and control interfaces, as well as the microcontroller implementing the control operation, are placed outside of the handheld controller. The motor drivers used for this prototype are the DRV8876 single

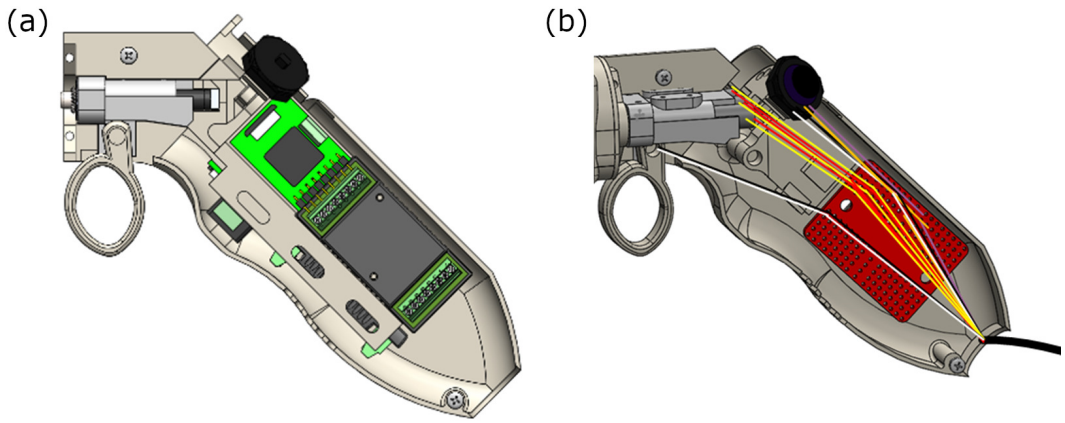

Figure 4.26: (a). Cross-section of the handheld controller incorporating the motor controllers, and (b). Cross-section of the handheld controller with motor controllers housed outside of the device.

brushed DC-motor driver carriers (Pololu, Las Vegas, NV, USA) with integrated current-threshold measuring that was used for the robot control methodology. The motors were moving the robot-joints in velocity domain, until a current threshold was reached. This threshold indicated that the joints had reached their joint-space limits, and thus the motor would stop rotating. The microcontroller interfacing with all motors and electronics was a Teensy 4.1 (PJRC, Sherwood, Oregon, USA), with all these components resting in a custom-designed circuit board made with the Voltera V-One PCB printer (Voltera, Kitchener, Ontario, Canada). An opened control box, the cabling, as well as the electronics can be seen in Fig. 4.27.

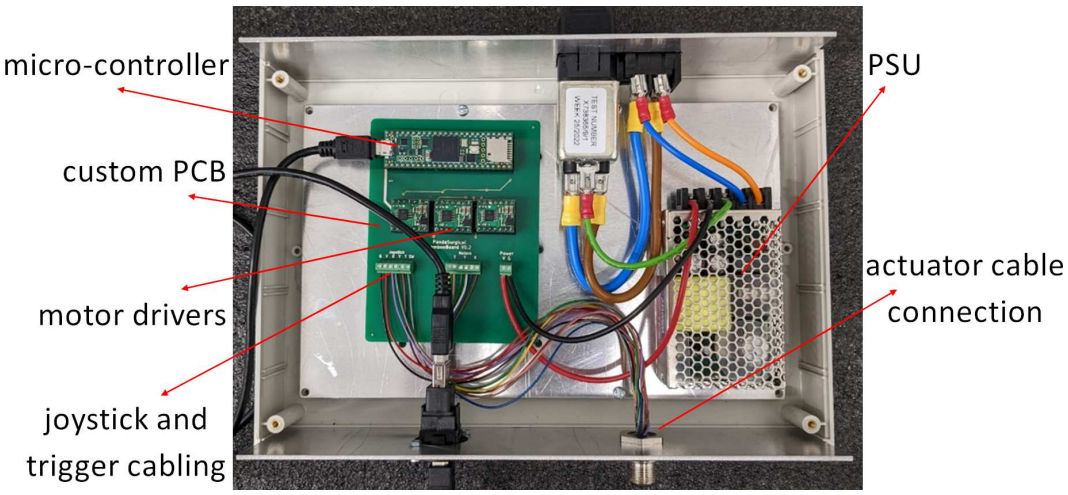

Figure 4.27: The control box housing all the electronics.

4.7 Discussion

In this chapter, a functional handheld controller to manipulate the robotic spherical-joint end-effector is developed. Two novel handle concepts were conceptualised based on ergonomic suggestion found in literature, and were then compared for their performance and ergonomics. The superior concept was re-designed while maintaining its ergonomic characteristics to incorporate motors and electronics and form a functional handheld controller.

The two ergonomic handle concepts that were developed during this thesis had both advantages and disadvantages. While the simulation study which compared them provided enough insight to choose the superior handle, there were some limitations that need addressing. During the study design, it was decided that the operator would control both the instruments and endoscopic device. While camera control does not immediately affect the perceived ergonomics of each device, since the mock endoscope and instrument did not collide inside the operative workspace, it could affect the performance of the operator. The more time the operator would spend manipulating the camera, the better depth-perception inside the simulated environment they would develop. To try and alleviate this risk, randomized tool sequences between the participants were deployed. However, different camera setups could showcase interesting results and their exploration could be scope of future work.

Another limitation of this study design was the decision to not include expert neurosurgeons in the experiment. The reason behind avoiding mixed cohorts for this specific comparative experiment between all three instruments, was that the preferred surgical setup that expert surgeons have developed over the years, would probably lead to a non-representative performance when using the conventional tool, introducing bias to the comparative experiment. However, understanding how helpful the opinion of an expert neurosurgeon cohort would be towards the device development, as part of future work, a human-factors workshop consisting of expert neurosurgeons will be organised, that will validate the performance and ergonomic behavior of the fully-functional handheld prototype. In that study, the number of participants should also be increased to improve the statistical significance of the findings, as showcased by the associated p-values.

One of the main points of concern was that despite the fact that most participants preferred the FMH during their SURG-TLX evaluation, one participant could not manage to finish the part of the experiment with this handle due to shoulder discomfort. This happened even after the surgical table was lowered as to fit the participants height, and suggests that

this forearm-constraint can be affected by the surgical setup, and thus will not always be suitable depending on the surgeon's preference and also the operating theatre arrangement. Changes in the operating theatre setup based on preference is not a strange concept to surgeons. An instrument, however, that would be deemed unfavourable by even a small portion of a surgeon cohort would not be an efficient solution.

The same participant evaluated the RJH an order of magnitude lower than the other participants in the SURG-TLX scale. If this outlier value is omitted from the average, the FMH would score significantly lower than the RJH. More specifically, the average total SURG-TLX score for the RJH would be 165.87, while for the FMH would be 135.62. While the difference between the two scores would be much clearer, the outcome of this part of the experiment remains the same, ie the participants preferred the FMH over the RJH. Still, the objective RULA evaluation suggests that the chance of them feeling discomfort would be higher with the FMH than with the RJH were they to use the robotic instrument for an extended amount of time.

Operative times for endonasal approaches vary depending on the complexity of each case and the surgeon experience, ranging from one to two hours for routine cases [143], up to more than ten hours for more complex ones [144]. A variety of different tools are used for each stage of the procedure, with frequent tool changes [145]. While the indication is that each 20-minute session with each handle would be sufficient to give us representative information on ergonomics about shorter approaches with frequent tool changes, more complex procedures would necessitate more elaborate phantoms, tasks, and also the allocation of time from participants.

Finally, while the 'peg-transfer' task that was chosen to evaluate these two handle concepts has been validated as indicative of surgical skill during keyhole brain-surgery [134], there are alternative simulation studies that could provide further insight into the comparison. An example would be a cutting task, where the participants are asked to use the handle concepts, as well as the standard instrument, to cut a pattern constrained by the sphenoid phantom. An even more representative task of a realistic scenario would be a simulator where the participants partake in tumour resection, but this would require extensive software development time.

A final limitation that needs addressing is the fact that while the handle concepts were extensively evaluated for their ergonomic behaviour, this did not happen for the final hand-

held controller prototype. While this device component has been designed with ergonomic considerations and is lightweight by housing its electronics and micro-controller outside of the casing, it has not been specifically evaluated for its ergonomic performance. A multi-participant study similar to the one presented in this chapter could provide useful feedback for this aspect of the robotic system.

In the next chapter, the robotic end-effector presented in Chapter 3 is paired with the handheld controller of this chapter to form the handheld robotic system. The prototype is then put through engineering as well as preclinical testing to be evaluated for its performance as well as clinical feasibility potential.

Chapter 5

Evaluation of the handheld robotic system for Endoscopic Neurosurgery

5.1 Introduction

In Chapter 3, a 3*mm* miniature end-effector for endoscopic neurosurgery was developed [67]. This manipulator deployed a tendon-driven spherical-joint design and was evaluated for its extended workspace and structural integrity. Then, preliminary work on pairing this end-effector with an appropriate handheld controller in Chapter 4 included the design and fabrication of two concept handle prototypes that were compared in terms of performance and ergonomics, with the superior handle concept being a joystick-and-trigger actuated concept [68] [69].

In this chapter, the development of the handheld robotic system for endoscopic neurosurgery concludes with the assembly of the functional robotic prototype [146] and its experimental engineering and pre-clinical evaluation. The robotic end-effector and handheld controller prototypes are combined to create a full assembly of the robotic system. This system was then experimentally evaluated for its operative workspace, structural integrity, and force-delivery capabilities. After its engineering evaluation, the robot was put through a pre-clinical series of testing during a phantom feasibility test, as well as during a cadaveric pilot study by a cohort of surgeons of varied clinical experience. Finally, both novice and expert surgeons compared their performance with manual tools and robotic tools during a comparative phantom study. Results from this series of experiments showcased enhanced dexterity and adequate robustness that could suggest feasibility in a clinical context, as well as improvement over current neurosurgical instrumentts.

The contributions that are associated with this chapter are:

- Dimitrakakis, E., et al., ”Towards a Handheld Robotic Instrument for Minimally Invasive Neurosurgery.” (2022), 12th Conference on New Technologies for Computer and Robot Assisted Surgery (CRAS)

- Dimitrakakis, E., et al., ”Handheld Robotic System for Endoscopic Neurosurgery”, (2023), IEEE Robotics and Automation Letters, (submitted)

- Dimitrakakis, E., et al., ”A handheld robotic device for endoscopic endonasal skull base surgery: An updated preclinical validation study (IDEAL-D Stage 0)”, (2023), Journal of Neurosurgery, (to be submitted)

- ’NIHR MIC Prize for Best Biongineering Postgraduate Poster 2022: Finalist’, (2022), In Healthcare Technologies Student and Early Career Awards by The Institution of Mechanical Engineers (IMechE)

- ’Entrepreneurship Award: 2nd place’, (2022), In euRobotics European Robotics Forum (ERF)

- ’Director’s special commendation’, (2022), In Wellcome / EPSRC Centre for Interventional and Surgical Sciences (WEISS) Awards

5.2 Robotic system

The robotic system developed in this thesis is a handheld robotic device comprised of a series of exchangeable articulated surgical instruments, an ergonomically designed handheld controller with a rotating joystick-body that can be placed at the position most comfortable for the user, and their accompanying control box. The robotic prototype with the handleld controller and the robotic end-effector disengaged is depicted in Fig. 5.1(a). Then in Fig. 5.1(b) and (c) the end-effectors and handheld controller are shown respectively, with Fig. 5.1(d) presenting the fully assembled robotic system alongside its alternative end-effectors and control-box.

To best understand how this system would be used in the clinical context of the endonasal approach, the system context diagram is presented in Fig. 5.2. The neurosurgeon operator would use the joystick and trigger to manipulate the end-effector of the handheld device and perform tasks that could be enhanced by robotic articulation. As previously mentioned, such tasks could include tumour resection and cutting, such as the operative

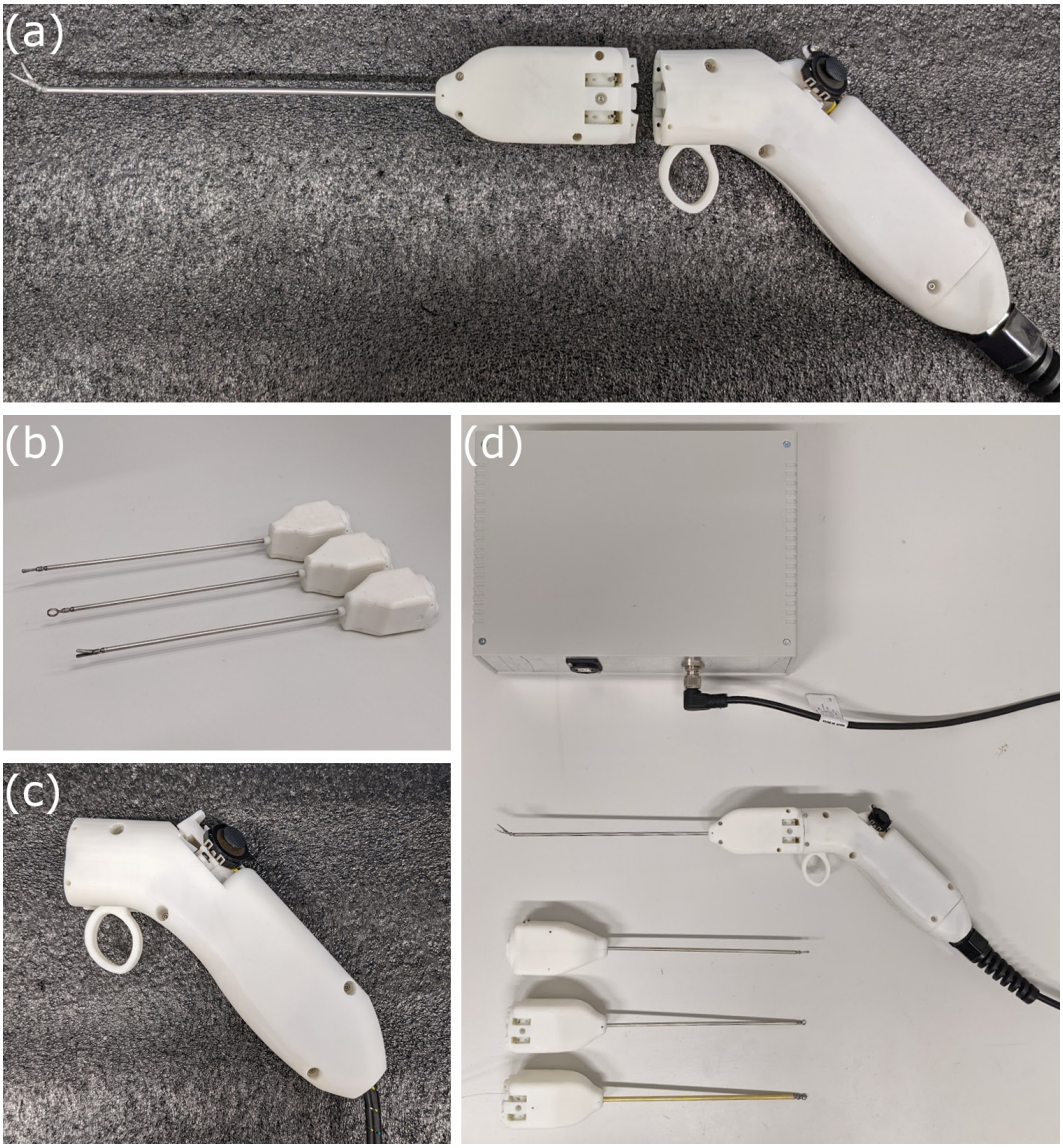

Figure 5.1: (a). The robotic prototype with the handleld controller and the robotic end-effector disengaged, (b). Various articulated end-effectors, (c). The handheld controller, and (d). The fully assembled robotic system alongside its alternative end-effectors and control-box.

steps 9., and 11.-13. of Section 2.2 or enhanced visualisation for steps 10. and 14. in the case of the articulated endoscope.

The operator would change end-effectors depending on the task. Steps 9. and 11. that describe cutting the sella and the dura would require a dissector or scissors end-effector, whereas steps 12. and 13. that undertake the tumour resection component of the operation would require the ring-curette to manipulate and gain access to the tumour, and the grasper to collect the resected tumour parts. Finally, steps 10. and 14. associated with visualisation would required the endoscope end-effector.

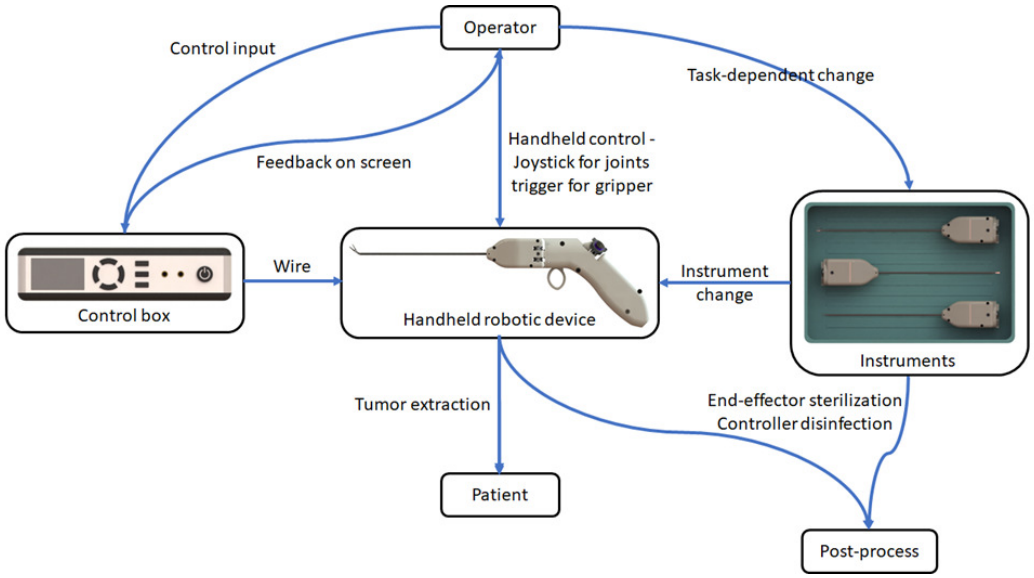

Figure 5.2: The system context diagram of the robotic system.

In the system developed as part of this thesis, the control-box included the electronics, the power-supply and the micro-controller that implemented the control implementation of the device. In a more advanced iteration of this system, the control box is envisioned to also provide a control input interface to the operator so that they can tune some device features. It can also incorporate a small screen that provides the surgeon with visual feedback on the device status.

5.3 Experimental evaluation

In this section, the novel robotic system prototype is evaluated in a series of engineering and pre-clinical studies. The robotic instruments were experimentally evaluated for their workspace, structural integrity, and force-delivery capabilities. They then were tested in a pre-clinical multi-surgeon cadaveric pilot study. Finally, the robotic prototype was compared with a standard instrument during a multi-surgeon phantom tumour-resection study.

5.3.1 Workspace, structural integrity, and force delivery

During these experimental procedures, only the grasper and ring-curette end-effectors were investigated, since the ring-curette and dissector share the same joint design. The grasper end-effector, however, has a hollow middle channel for the DoF that actuates the gripper at the distal end.

To identify the joint-space of the robotic end-effector of the handheld instrument, a protractor was used. The end-effectors were moved to their joint limits until the motor

would stop outputting torque. The end-effectors were actuated on each axis individually, as well as simultaneously.

Then, to investigate the end-effectors' structural integrity, the grasper and ring-curette were moved to a range of joint-spaces, namely in $[0,0]$, $[\pm jointlimit/2,0]$, $[0,\pm jointlimit/2]$, $[\pm jointlimit,0]$, $[0,\pm jointlimit]$, and $[\pm jointlimit,\pm jointlimit]$, and forces were applied with a Newton-meter at the tip of each respective end-effector in the Y and Z directions, with the shaft supported. The value at which angular deflection was noticed on the joint was recorded as the maximum force the end-effector can withstand at its tip when applied in that particular direction. This experimental setup can be seen in Fig. 5.3(a).

Finally, the two end-effectors were tested for their force-delivery capabilities with the use of the 6-axis F/T sensor ATI Nano17 (ATI, Markham, Ontario, Canada). With their shaft supported, the end-effectors were actuated on each axis individually, pushing against the force sensor until the motor would stop outputting torque, at which point the force measurement on the sensor was recorded. This procedure was repeated 5 times, and the average measured force was kept as the maximum output force delivered in that direction. In the case of the grasper end-effector, its grasping force was also measured with the use of a force-sensitive thin film sensor and an Arduino Uno microcontroller (Arduino AG, Italy).

5.3.2 Phantom feasibility test

The first pre-clinical experiment aimed at validating the feasibility of the novel device. To do that, a tumor extraction procedure was simulated using the handheld robotic instrument inside the TNS box (UpSurgeon, Milan, Italy), a phantom model for the endoscopic endonasal approach to the pituitary fossa. This model was chosen because it has been validated as a potentially useful surgical skills training tool for its face, content, and construct validity [147]. The phantom feasibility test setup is shown in Fig. 5.3(b).

A silicon tumor was inserted in the pituitary fossa region, and in combination with a USB-endoscope, a non-clinician participant, familiar with the TNS box and the device, was tasked with extracting the tumor using the articulated grasper, the ring-curette, and finally the spatula dissector. The scope of the experiment was to investigate preliminary feasibility. More specifically, to understand whether the miniature end-effectors could maintain their pose when interacting with the tumor in order to successfully remove it from the skull-base cavity.

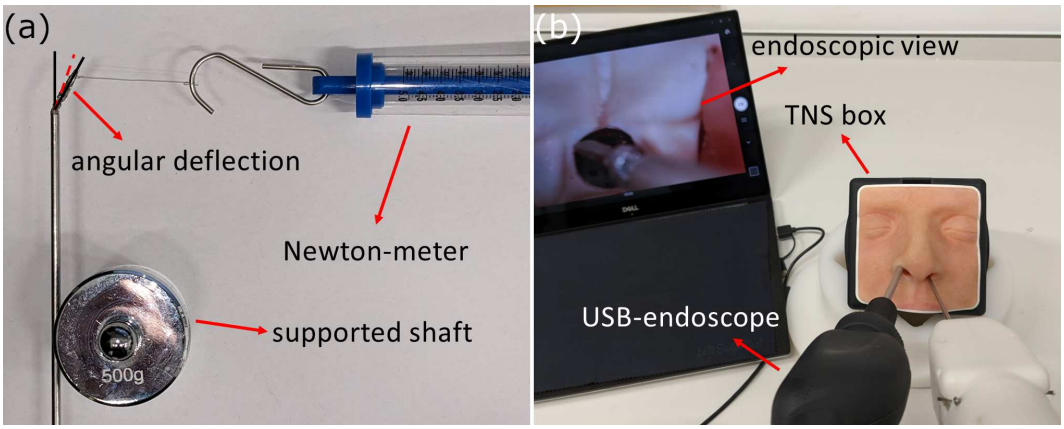

Figure 5.3: (a). Structural integrity test experimental setup, and (b). Phantom feasibility test experimental setup.

5.3.3 Cadaver pilot study

The scope of the second pre-clinical study was also exploratory, relying on qualitative surgeon feedback. During this study, the feasibility of the robotic device was investigated in terms of workspace exploration and tissue interaction. Additionally, its introduction into the surgical workflow was observed, alongside the device robustness and durability. The added articulation and dexterity required to perform the first portion of the experiment, using the ring-curette could be linked to operative steps 9., and 11.-13. as presented in Section 2.2, whereas the second portion of the experiment, where the articulated endoscope is used is mostly relating to operative steps 10. and 14.

The novel instruments that were brought into the operating theatre for this study are found in Fig. 5.4. Additionally, the standard equipment consisted of a 0^o neuroendoscope accompanied with its tele-pack stack (Karl Storz SE & Co. KG, Tuttlingen, Germany), and an endoscopic pituitary instrument set (B.Braun, Melsungen, Germany).

One expert neurosurgeon, one intermediate-level neurosurgical trainee, as well as four novices with no dedicated pituitary surgery experience, were recruited from a single UK neurosurgical unit (National Hospital for Neurology and Neurosurgery, London, UK). A pre-clinical study design was adopted to evaluate the robotic instrument alongside the use of standard endoscopic instruments on a single cadaver. A fresh and frozen cadaver was procured from The Griffin Institute (Northwick Park Hospital, London, UK). The cadaver was placed supine. The head was positioned in the 'conversational' position with the neck flexed and turned to the right, facing the surgeon. The head was draped and the nares were exposed.

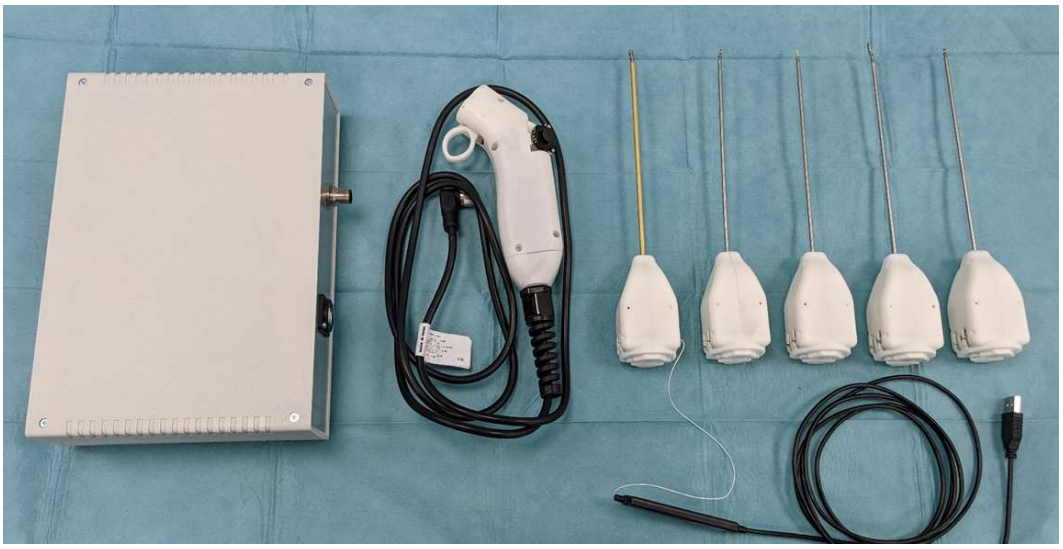

Figure 5.4: The novel robotic instruments that were tested during the cadaver pilot study. Left to right: control box, handheld controller, and articulated tools.

The EEA including the durotomy was performed pre-task. The participants were instructed to navigate through the nasal passage in order to reach the sphenoid sinus with the use of standard endoscopic instruments and expose the pituitary gland. This was followed by the introduction of the robotic instrument, with the participants being instructed to enter and explore the pituitary fossa using the articulated robotic instrument and interact with soft tissue and bony structures.

Finally, after all 6 participants tried the robotic instrument, the expert and intermediate neurosurgeons tried the robotic endoscope end-effector, alongside the robotic instrument, both with and without the guidance of the standard rigid endoscope. The goal of this part of the experiment was to visualize areas that were previously challenging to access with the standard rigid endoscope.

5.3.4 Comparative phantom study

The aim of this study was to compare the robotic device to standard endoscopic instruments during a tumour resection task [148]. This time, the operative task could be linked to operative steps 9.-14. as presented in Section 2.2. Participants were recruited from a single university teaching hospital and were defined as a) expert: if they had completed neurosurgical training or were neurosurgical registrars (residents) with experience specifically in pituitary surgery, and c) novices: if they did not meet either of the previous criteria. Participants included six males and two females. There were four expert and four novice

participants, of which seven were right-handed, and one was left-handed.

To compare the handheld robotic device against a standard endoscopic instrument, a randomised cross-over study was conducted using once again the TNS box, a previously validated phantom model for the eTSA [147]. The TNS Box was prepared by creating a surgical corridor such that the tumour was accessible. The silicone tumour that the participants were tasked to remove inside the phantom environment and when using the standard and robotic instruments is evident in Fig. 5.5.

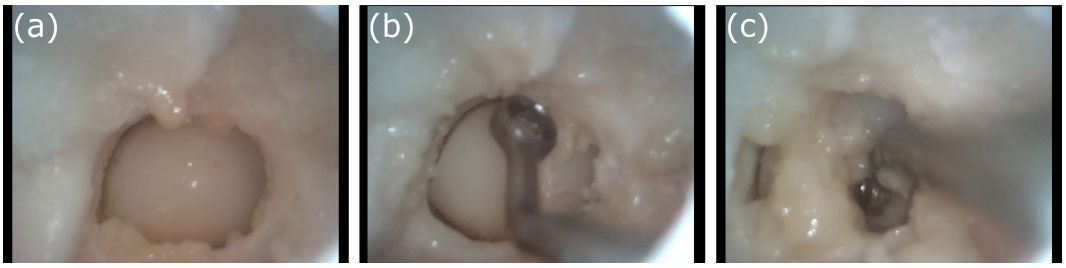

Figure 5.5: a) The eTSA phantom tumour, b) the standard instrument inside the phantom environment, and c) the articulated end-effector inside the phantom environment.

Participants were tasked with performing a durotomy and tumour resection after a short standardised induction to the robotic and standard instruments [21]. This was performed using either the standard instrument, a bayonet-shaped, 30° angled, ring-curette, or the robotic device. The end effector for the robotic device consisted of a ring-curette with similar dimensions to the standard instrument. Participants performed the resection task 5 times using each instrument for a total duration of 3 minutes per attempt. The tumour and dura were replaced for each iteration, but the rest of the model remained the same. Tumours were weighed before and after the resection task to calculate the percentage resection by mass. Fig. 5.6(a) and (b) showcase the operative setup during this experiment when using the standard and robotic instruments respectively.

Following the resection tasks, participants completed a validated, surgery-specific task load index (SURG-TLX), which prompted them to consider various intraoperative workload domains, and rate the extent to which they experienced these during the resection task. Intraoperative workload domains included: mental demands, physical demands, temporal demands, task complexity, situational stress, and distractions. The SURG-TLX evaluation involves performing weighted comparisons of different domains and rating each on a 20-point scale (0 = low, 20 = high). The domain specific workload score is calculated by determining the product of these numbers (range 0-100). The total workload score is calculated

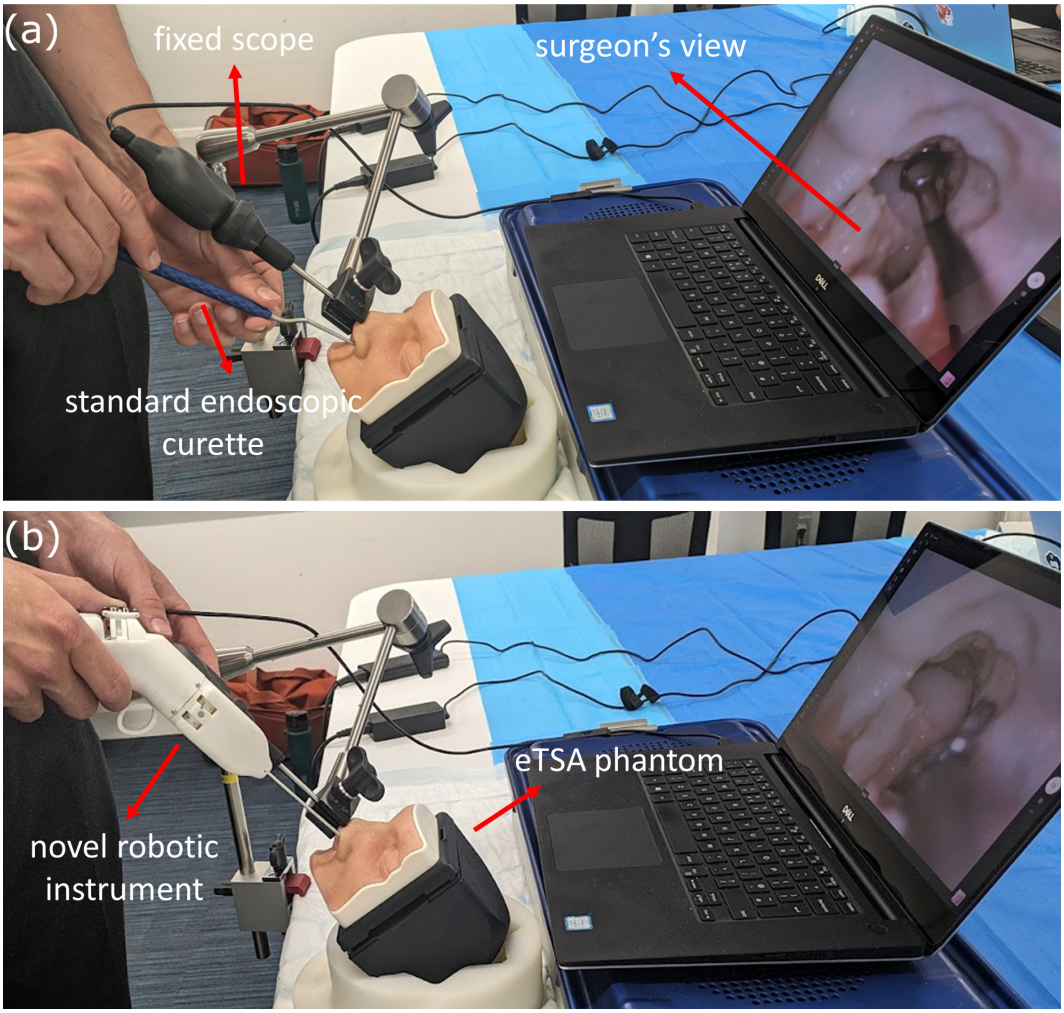

Figure 5.6: The operative setup during the comparison phantom study when using (a) the standard instrument, and (b) the novel handheld robotic instrument.

by adding the scores from the six workload domains.

Finally, participants completed a post-task questionnaire to score each instrument in terms of ease of use, comfort, precision, and integrity. The scores ranged from 1 to 5 points (1 = poor, 5 = excellent). Personal preference was assessed and qualitative feedback for each instrument was obtained.

The primary outcome was the median extent of resection (EOR) achieved on the final (5th) attempt. The final attempt was used as the comparative metrics to account for potential learning curve effects. Secondary outcomes included the median EOR on first attempt, the composite SURG-TLX workload scores and post-task questionnaire outcomes.

R Studio (2022.07.2) and Excel (Microsoft, version 16.6.1) were used for data analysis and data representation. Outcome measures including the EOR, and SURG-TLX were

expressed as median (IQR) and statistical differences were assessed using nonparametric tests (paired, Mann-Whitney U test). For parametric data distributions (e.g. post task questionnaire), paired t-tests were performed. Categorical variables, such as the favoured instrument, were evaluated using a chi squared test. P¡0.05 was deemed statistically significant.

5.4 Results

5.4.1 Workspace, structural integrity, and force delivery

The joint limits of the grasper and ring-curette end-effectors when each DoF was actuated individually can be seen in Fig. 5.7(a). and Fig. 5.7(b). respectively.

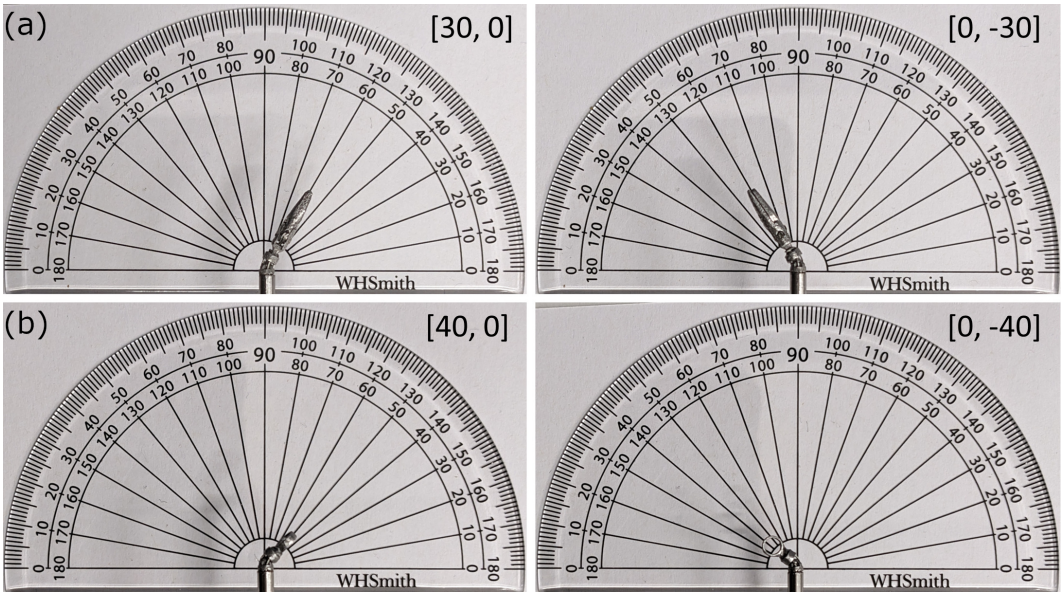

Figure 5.7: (a). The grasper end-effector at two different joint-space limits, (b). The ring-curette end-effector at two different joint-space limits.

For the grasper end-effector, when each DoF was actuated individually with the other DoF staying locked at 0^o, the joint limits were $\pm 30^o$ for both DoF. In the case of the ring-curette, however, the same joint-limits were $\pm 40^o$. In all end-effectors, when both DoF were actuated simultaneously, the joint limits were reduced. The overall joint-spaces of the end-effectors are evident in Fig. 5.8.

The maximum forces that the grasper and ring-curette end-effectors could withstand in a wide range of joint-spaces without noticeable angular deflection, maintaining, thus, their pose, are laid out in Table 5.1.

The grasper end-effector could withstand a maximum force of $2N$ when both joints were actuated to their joint-limits and this force was applied on the Z axis. The minimum

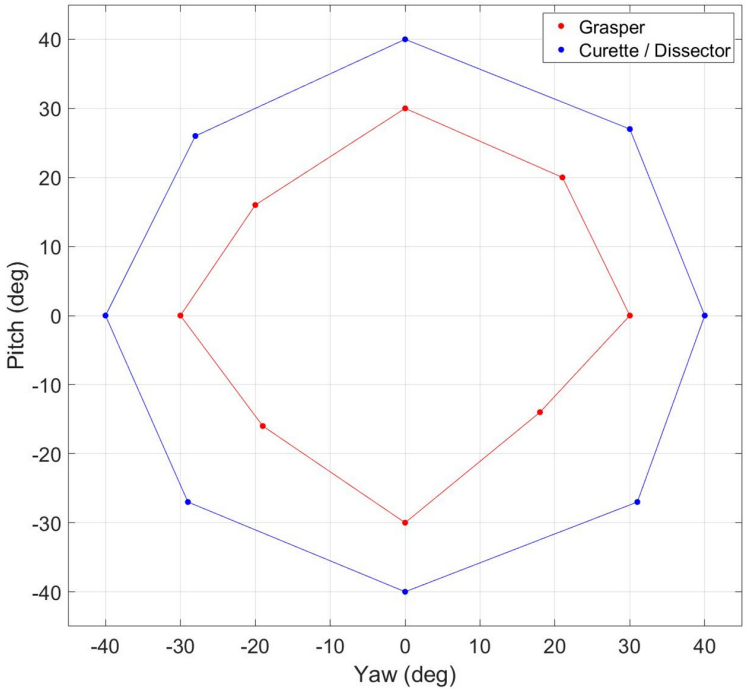

Figure 5.8: The overall joint-spaces of both end-effectors.

Table 5.1: The measured forces applied at the tip of the end-effectors in the ZZ' and YY' directions while at discrete joint-spaces, at which angular deflection was noticeable. These forces represent the maximum forces each end-effector can withstand at its tip when applied in that particular direction.

Robotic grasper													
Joint-space (yaw,pitch)	**(-30,0)**	**(-15,0)**	**(0,0)**	**(15,0)**	**(30,0)**	**(0,-30)**	**(0,-15)**	**(0,15)**	**(0,30)**	**(21,20)**	**(18,-14)**	**(-19,-16)**	**(-20,16)**
$F_Z(N)$	0.9	0.8	1	0.8	0.8	1.5	0.8	1	1.7	2	1.5	0.6	1.1
$F_{Z'}(N)$	1.2	0.6	0.9	0.6	0.7	1.3	1	0.8	1.5	1.5	1.7	0.8	1.2
$F_Y(N)$	1.3	0.5	0.7	0.7	1.5	1	0.6	0.8	1.1	1.6	1.4	1.1	0.9
$F_{Y'}(N)$	1.2	0.7	0.5	0.7	1.2	0.8	0.6	0.6	1	1.4	1.2	1.2	1.4
Robotic curette													
Joint-space (yaw,pitch)	**(-40,0)**	**(-20,0)**	**(0,0)**	**(20,0)**	**(40,0)**	**(0,-40)**	**(0,-20)**	**(0,20)**	**(0,40)**	**(31,27)**	**(31,-27)**	**(-29,-27)**	**(-28,26)**
$F_Z(N)$	2.5	2	1.6	1.4	2.5	3.5	1.3	3.5	5	1.8	2.5	1.5	1.8
$F_{Z'}(N)$	2.3	1.5	1.6	1.2	3	3	1.6	1.8	5	2	2.2	2	2.3
$F_Y(N)$	2	1	1.5	1	2	1.8	1.1	1.7	2.5	1.1	1.3	2	2
$F_{Y'}(N)$	1.5	1.2	1.5	1.2	1.8	1.9	1.2	2	2	1.3	1.6	2.2	1.6

force, $0.5N$ in the Y' direction, was recorded at the end-effector's neutral position. The maximum force withstood by the ring-curette was $5N$ in either $Z-Z'$ direction when the pitch joint was individually actuated and the minimum was $1N$ in the Y direction, both at the $(-20^o, 0^o)$ joint-space, as well as at the $(20^o, 0^o)$. The maximum force of $5N$ achieved during this experimental procedure is replicated in Fig. 5.9, where the ring-curette end-effector maintains a $500g$ weight.

Figure 5.9: The ring-curette end-effector maintaining its pose holding a 500g weight.

Finally, and regarding the force delivery capability of the end-effectors, the measured forces when the end-effectors were moved to the individual DoF limit joint-spaces are shown in Table 5.2. Both end-effectors showcased similar force-delivery capabilities in all different directions, with the grasper end-effector having the lower force thresholds between the two. The grasping-force recorded with the force-sensitive sensor for the grasper end-effector had a maximum value of $2N$.

5.4.2 Phantom feasibility test

The participant managed to remove the tumor with all three end-effectors in $14sec$ with the grasper, $33sec$ with the ring-curette, and $26sec$ with the dissector. Endoscopic view frames extracted from the USB-endocope during the tumor removal experiment are depicted in Fig. 5.10.

5.4.3 Cadaver pilot study

Fig. 5.11(a). presents the robotic tool used in the cadaveric specimen, with Fig. 5.11(b). showing the standard endoscope view of the novel robotic curette interacting with the sellar

Table 5.2: The forces measured by the F/T sensor when the end-effectors were moved to discrete joint-spaces.

Robotic grasper				
Joint-space (yaw,pitch)	**(-30,0)**	**(30,0)**	**(0,-30)**	**(0,30)**
$F(N)$	0.78	0.66	0.86	0.79
Robotic curette				
Joint-space (yaw,pitch)	**(-40,0)**	**(40,0)**	**(0,-40)**	**(0,40)**
$F(N)$	1.34	1.27	1.24	1.29

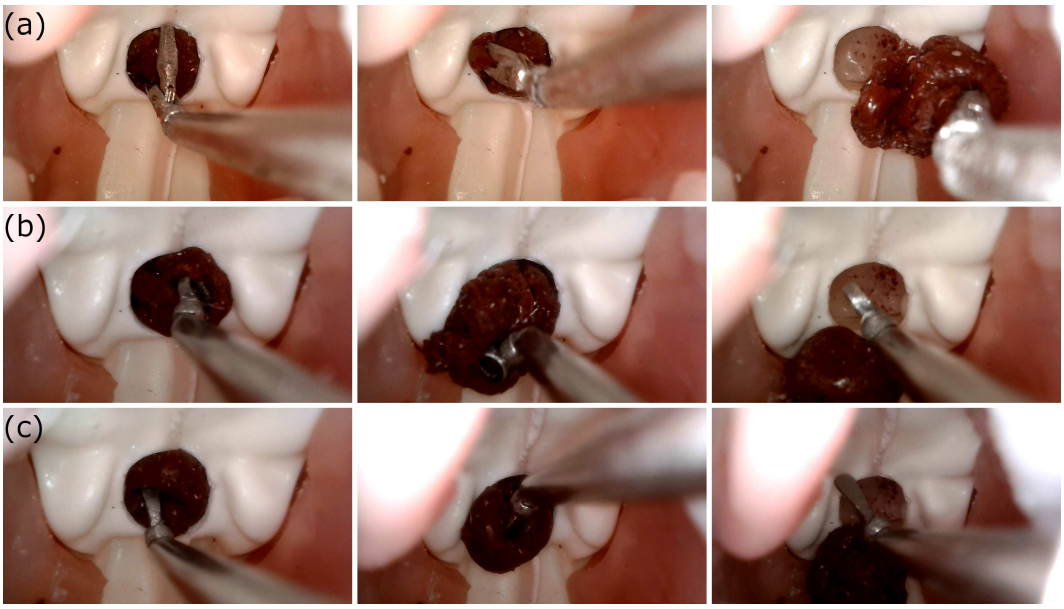

Figure 5.10: The view from the USB-endoscope during the phantom feasibility study where the silicone tumor at the pituitary gland region was removed with the use of (a). The robotic grasper, (b). The robotic ring-curette, and (c). The robotic dissector.

anatomy. To qualitatively evaluate the feasibility of the device, feedback regarding the dexterity, force delivery, structural integrity of the robotic device, and overall user experience was obtained through a post-task questionnaire.

All participants reported the articulated robotic instrument provided greater dexterity than existing tools and maintained its structural integrity during the task. The instrument maintained its robustness throughout the experiment and for the entire duration it was used by the surgeon cohort. Other than some the untangling or snapping of single tendon strands, which however were not concerning, it did not show any signs of significant wear or breakages. The state of the miniature end-effector after the completion of the experiment can be

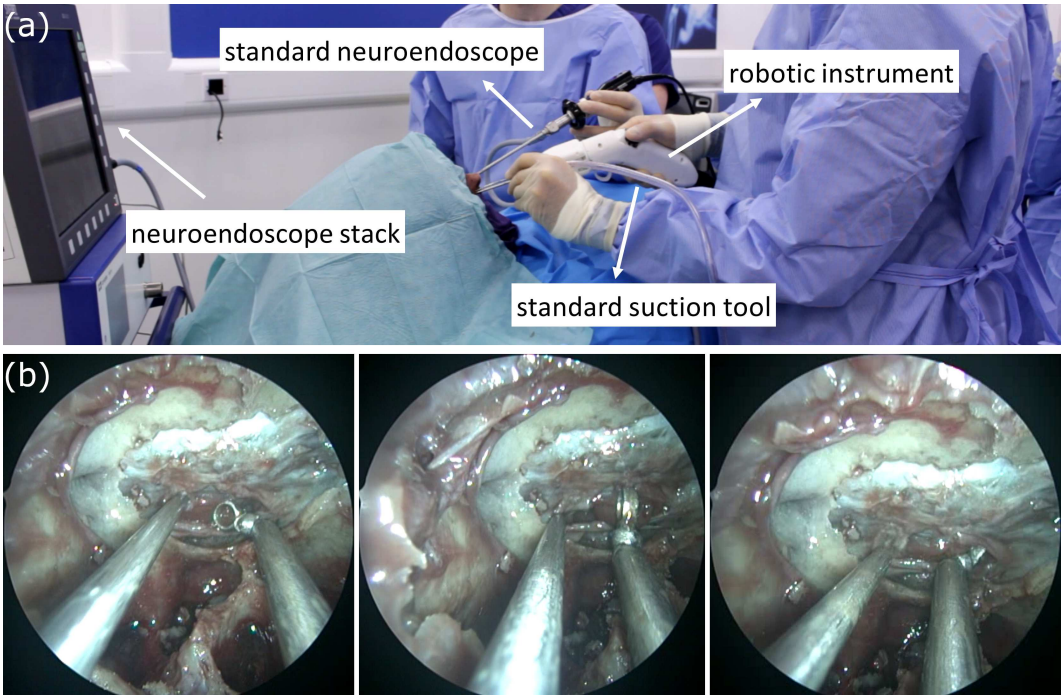

Figure 5.11: (a). The surgical setup with the introduction of the novel robotic instrument, and (b). (left to right) A standard suction tool, and the robotic curette in different poses interacting with soft tissue.

seen in Fig. 5.12.

Figure 5.12: The miniature end-effector after the completion of the cadaver pilot study. In this figure, a snapped tendon strand can be seen.

All six participants also felt the instrument applied sufficient force when pre-positioned at an angle in free space. However, the inability of sufficient forces to be applied during the movement of the instrument and the lack of precise movements were noted by all participants. In terms of user experience, all six participants reported the instrument was intuitive and comfortable to use, with the noise and wires not having an impact on workflow. Further

minor comments included that while the participants were satisfied with the robot articulation when each DoF was actuated individually, the movement felt constrained when the end-effector was moving diagonally when both DoF were actuated. The questions and surgeon replies are presented in Table 5.3.

Table 5.3: The post-cadaver study questionnaire, and the surgeon replies

Question	Yes	No
Does the robot maintain its pose when pressing against soft and boney tissue?	6	0
Does the robot allow for precise movements?	0	6
Does the robot allow for increased dexterity?	6	0
Does the robot apply sufficient forces when already articulated?	6	0
Does the robot apply sufficient forces while in motion?	0	6
Is the robot easy to use?	6	0
Is the robot comfortable to use?	6	0

Finally, the articulated endoscope experiment was conducted. The surgical setup with the introduction of the robotic endoscope can be seen in Fig. 5.13. One surgeon was manipulating the robotic curette, and afterwards the robotic curette and the standard neuroendoscope, while a second surgeon was manipulating the robotic endoscope. Concurrent views from both endoscopes can be seen in the same figure.

Regarding the concurrent usage of an articulated instrument and articulated endoscope, the takeaway was that while promising, this work was preliminary. The camera quality was not sufficient, the depth perception of the articulated visual elements is challenging and, the best usage of such a device would most likely be alongside a standard endoscope that would ensure the articulated endoscope elements don't collide with soft tissue. The concurrent usage of the two robotic tools is shown in Fig. 5.14(a)., with Fig. 5.14(b). and (c). depicting two views from the articulated endoscope.

5.4.4 Comparative phantom study

Fig. 5.15 depicts primary outcome measures. On the first attempt, participants using the standard instrument and robotic instruments achieved a median EOR of 84% (IQR $65\% - 91\%$) and 58.6% (IQR $52\% - 77\%$), respectively ($p = 0.055$). On the final attempt, the median EOR with the standard instrument and robotic device were 80% (IQR $70\% - 89\%$) and 83% (IQR $61\% - 94\%$), respectively ($p = 0.76$). The EOR improved across attempts

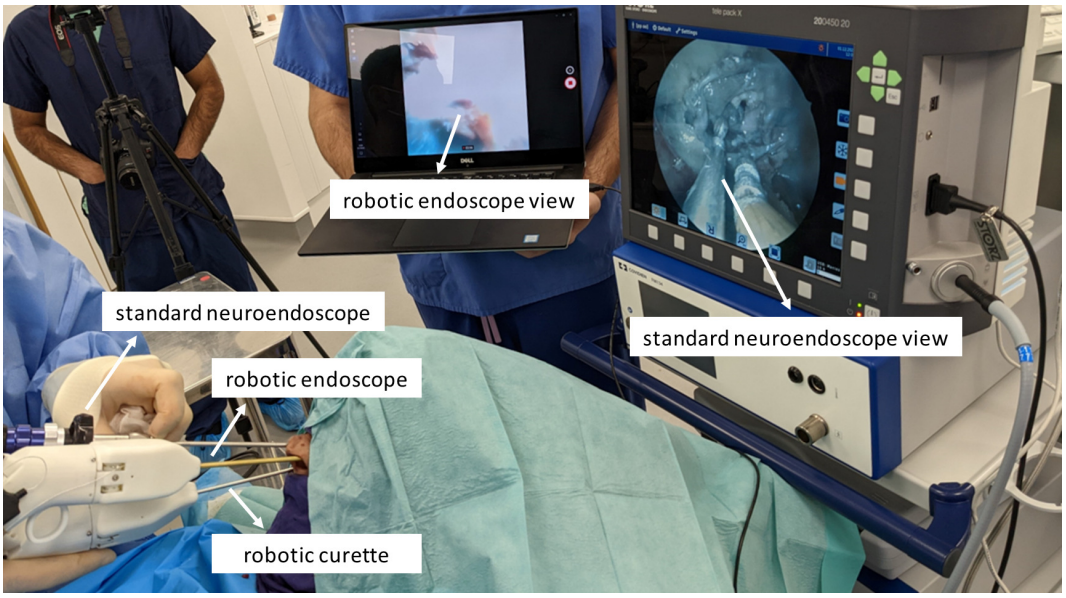

Figure 5.13: The surgical setup with the introduction of the robotic endoscope, alongside endoscopic views. Concurrently with this instrument, a robotic curette as well as a standard neuroendoscope were used.

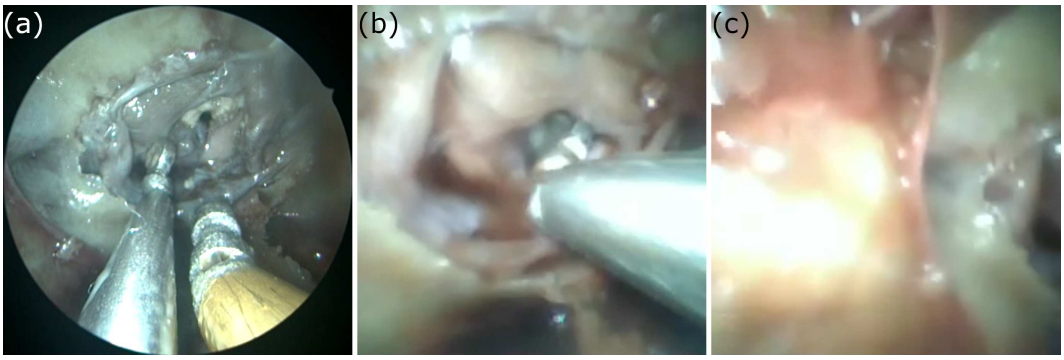

Figure 5.14: (a). Concurrent usage of the robotic ring-curette and the robotic endoscope, while in visual guidance from the standard neuroendoscope, (b). View of the sellar anatomy using the articulated endoscope, in its initial pose, and (c). View of the sellar anatomy using the articulated endoscope, having it actuated on the yaw axis.

with the robotic device ($p = 0.38$), and decreased with the standard instrument ($p = 0.95$), as seen in Fig. 5.16.

Fig. 5.17 depicts the EOR on first and final attempts, across the levels of experience with each instrument. Novices achieved a first attempt EOR of 76% (IQR $60\% - 86\%$) with the standard instrument, and 55% (IQR $52\% - 91\%$) with the robotic instrument ($p = 0.62$). On their final attempt, novices resected 80% (IQR $70\% - 84\%$) with the standard instrument, and 83% (IQR $64\% - 91\%$) with the robotic device ($p = 1.0$). Considering the intermediate and expert surgeon's first attempt, a greater EOR was achieved with the

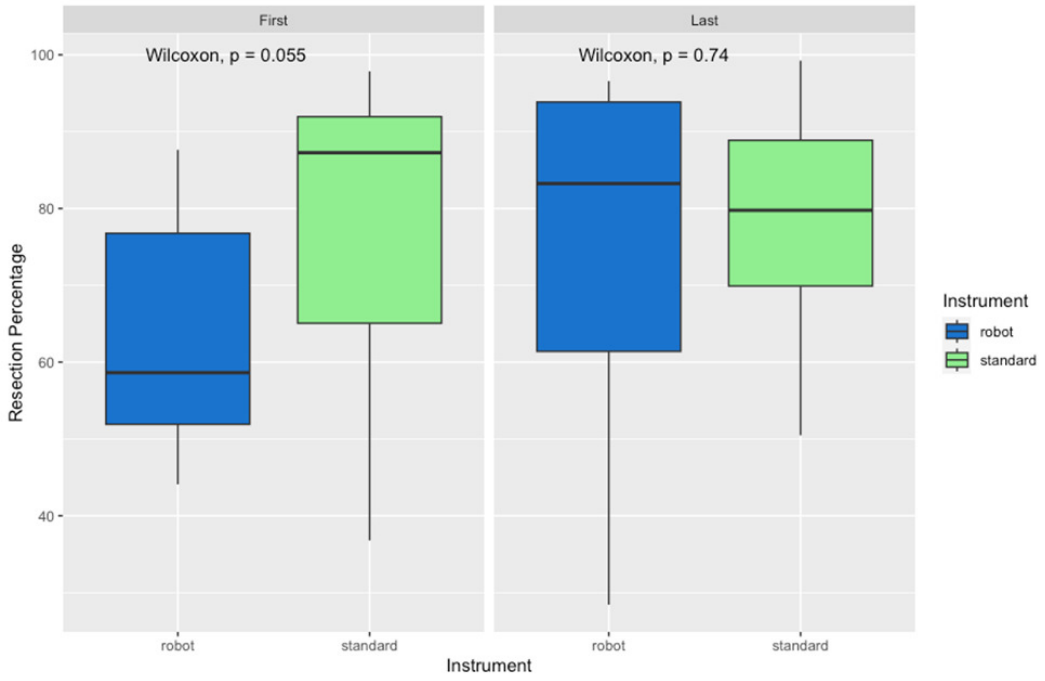

Figure 5.15: Primary outcome measure represented by participant performance, grouped by attempt.

standard instrument compared to the robotic device (87% (IQR $77\% - 92\%$) versus 71% (IQR $56\% - 85\%$) ($p = 0.12$)). On their final attempt, intermediates and experts achieved an EOR of 80% (IQR $70\% - 91\%$) with the standard instrument and 80% (IQR $61\% - 94\%$) with the robotic device ($p = 0.88$).

Regarding the SURG-TLX evaluation, compared to the standard instrument, the robotic device was associated with a lower mean total workload score (standard total workload score=156, robotic total workload score=118, $p = 0.006$). Considering subdomains, the only subdomain that individually demonstrated a significant difference between devices was the reduced perceived physical demands with the robotic device (Robotic device = 5.4, Standard instrument = 42, $p = 0.03$).

Finally, the post task questionnaire found participants to favour the robotic device in terms of comfort ($3.9/5$ versus $3.0/5$, $p = 0.28$), ease of use ($4.0/5$ versus $3.5/5$, $p = 0.46$), precision ($4.1/5$ versus $3.6/5$ $p = 0.46$). Participants favoured the standard device in terms of stability ($4.1/5$ versus $3.9/5$, $p = 0.58$). All but one participant ($7/8$) favoured the robotic device to the standard instrument overall ($p = 0.0027$). The reported justifications for favouring the robotic device included that it had a "better range of movement", "required fewer wrist movements", "was more comfortable", and "more precise". Reported drawbacks and suggested improvements of the robotic device included that it was "uncom-

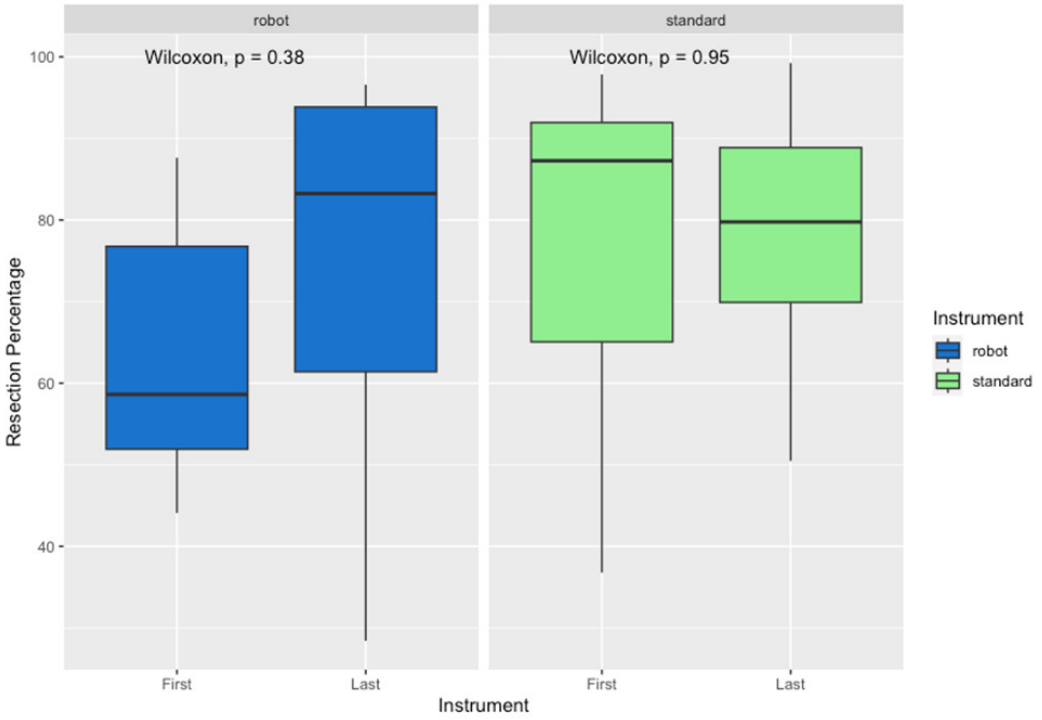

Figure 5.16: Extent of resection on the first and fifth attempts, grouped by instrument.

fortable to hold the thumb on the joystick", "(it) clashed with the endoscope", " would benefit from a longer curette" and required "haptic feedback".

5.5 Discussion

In this chapter, a novel handheld robotic system for endoscopic neurosurgery comprised was evaluated during a series of engineering tests as well as pre-clinical cadaveric and phantom multi-participant user-studies.

The spherical-joint design and routing-mechanism of this system allowed for significant workspace increase compared to rigid instruments with a $\pm 30^0$ joint-limit for the articulated grasper, and $\pm 40^0$ for the ring-curette and dissector. This difference in joint-space is a result of the wider middle segment of the grasper, still within the 3*mm* diameter, that allows a path for the gripper DoF tendons. These limits are smaller than other similar-sized end-effectors, such as the ones presented in [128] and [149]. However, a number of advantages this design offers, namely the miniature size of the 3*mm* robots, the concentration of both DoF on the same point, and the handheld nature of the device, suggest significantly increased dexterity and ability to navigate within the confined spaces of the EEEA.

In [150], it is recorded that average forces during soft tissue excision of pituitary lesions

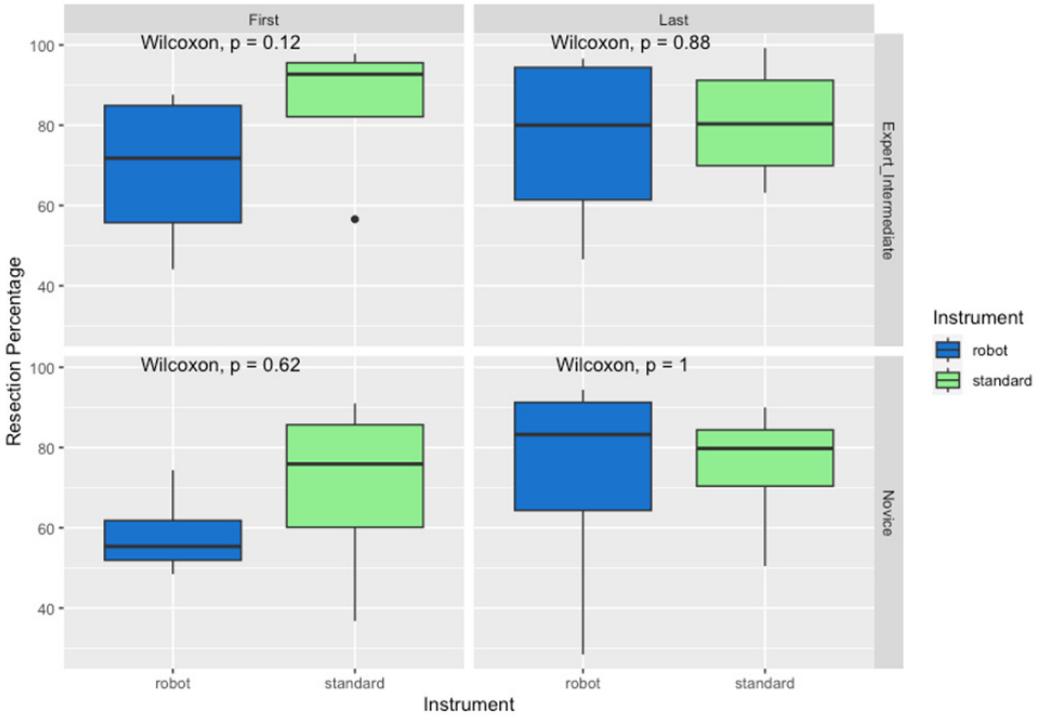

Figure 5.17: Extent of resection, grouped by attempt and experience.

are in the $0.1N$ to $0.5N$ range in the X, Y, and Z directions. Maximal forces tended to occur in the Z direction, especially with bony collisions, and peaked at $2.12N$. Both end-effectors could comfortably withstand the maximum force of $0.5N$ associated with the soft-tissue excision phase of the operation, as showcased during the structural-integrity tests, with the ring-curette having the better capability to withstand even the maximum force associated with bony collisions. The grasper would not be able to withstand $2N$ of force in most poses and needs further development. The structural-integrity discrepancy between the two end-effectors, as well as the clear limitation of the grasper in that front, is believed to be a result of the tendon pre-tensioning value of the two end-effectors. It is possible that using the same pre-tensioning methodology and value for both designs was not a sufficient approach, and in future work, the most appropriate pre-tensioning values for the grasper end-effector will be investigated.

During this engineering test-set, the end-effectors showcased the least capability in terms of force-delivery. While there are anticipated limitations due to the miniature size of the robot-joint, there is a number of suggestions that could increase force-delivery capability. The mechanical backlash and friction in the end-effector housing will be reduced by replacing current materials with better surface-finish materials, the motors and their gear-

boxes will be replaced with higher continuous torque motor assemblies, and the coupling gear-ratio will be investigated to maximize the torque transferred from the motor-end, to the joint-end.

The pre-clinical evaluation re-iterated these findings. The phantom feasibility test suggested increased dexterity and adequate robustness for tumor extraction, with the limitation that the silicone tumor was conveniently located in the skull-base cavity, and thus, workspace exploration could not be adequately investigated. For future validation, the phantom physiology could be customised to allow for an operative workspace increase, more similar to the expanded endoscopic endonasal approach.

During the cadaver pilot study, the received surgeon feedback lead to the understanding of the current development stage of the robotic system. The favorable results on workspace exploration, dexterity, structural integrity when interacting with soft-tissue, and ease-of-use, suggest that future development should focus on the study limitations, namely the imprecise control, and the force-delivery capabilities. The current control methodology, which is open-loop velocity domain control, will be replaced with a more sophisticated position-domain closed-loop control in future work that will map the robot joints movements to the joystick and trigger interfaces.

Finally, in the comparative phantom study, we observed a learning curve effect, as the robotic device was inferior to the standard instrument on the first attempt at tumour resection (84% vs 59%, $p = 0.055$), but equivalent on the 5th attempt (80% vs 83%, $p = 0.76$). This was observed for both novices and experts. Separately, participants scored the robotic device higher in terms of range of movement, ergonomic manipulation, comfort, ease of use, and precision. Indeed, the robot was the overall favoured instrument by $7/8$ participants ($p = 0.0021$). The robotic device was associated with a lower total cognitive workload ($p = 0.003$).

Due to the need for pragmatic constraints to the trial design, our study has limitations. Firstly, there was a small number of participants, which limits the statistical significance of our results. Also, participants were not blinded to the intent of the trial, and thus may have been biased in their subjective interviews.

Chapter 6

Discussion

6.1 Conclusions

The Endoscopic Endonasal Approach, one of the best examples of keyhole brain-surgery, allows surgeons to access the pituitary gland through the natural orifice of the nose. Recently, surgeons have also described an Expanded Endoscopic Endonasal Approach for the treatment of tumours around a broader area at the base of the brain. Operating in this way, however, with standard tools which are lacking articulation, is technically very difficult and not widely adopted. Thus, these operations are only performed by few surgeons, in highly-specialised centres, limiting access to most patients. While detection rates have increased due to recent advances in medical imaging, clinical outcome has not improved in the last 20 years. Resultantly, it is widely recognised by patient groups and healthcare institutions that there is an urgent need for surgical innovation to advance clinical outcomes in patients with brain tumours.

Robotic technology can be the solution to the constrained operative workspaces and limited dexterity. However, the surge in surgical robots in recent years is mainly focused on general laparoscopy and is unsuitable for the constrained spaces and the delicate nature of brain surgery. Additionally, these robotic solutions are often associated with high costs that would hinder their deployment in most hospitals around the world. A further solution to this problem that has been recently explored, could be offered by handheld robotic devices. These smart instruments offer robotic capability, while also being smaller, simpler, less expensive, and more easily incorporated into the existing workflow.

The focus of this thesis is to develop a handheld robotic instrument for neurosurgical approaches that can expand the surgeon's capabilities. The enhanced robotic articulation aims to increase the surgeon's dexterity, and thus, the surgical efficacy. Additionally, the er-

gonomic design of the device, combined with the absence of a trocar-port, can decrease the surgeon's physical fatigue and strain associated with these demanding operations. Deploying these instrument in the operating theatre will make more surgeons capable of performing these highly specialized keyhole approaches, and can potentially cut down referral costs with more hospitals being able to offer them. Simultaneously, repeat-procedures occurrence due to complications or incomplete tumour resection will be reduced.

In this thesis, the system shown in Fig. 6.1 is presented, comprised of a series of handheld robotic insturments for the EEEA. The development started with the fabrication of a miniature robotic end-effector which expanded the operative workspace of current standard instruments, followed by two ergonomic handle prototypes intended for its control. To understand surgical device ergonomics, a review chapter was produced that was investigating ergonomic considerations in pre-existing robotic devices. The two handle designs were collectively covering a large set of ergonomic literature guidelines and were compared for their efficacy and ergonomics. The superior handle design in terms of this comparison was then paired with the pre-existing miniature end-effector to develop a set of handheld robotic instruments that was tested during a pre-cinical cadaver pilot study and a multi-surgeon comparative phantom experiment.

Figure 6.1: Renderings of the handheld controller and the articulated instruments.

Concluding, preliminary results from all experimental procedures evaluating the robotic instruments presented in this thesis, including laboratory and pre-clinical testing, suggested improvement over current neurosurgical instruments, as well as feasibility within a clinical context.

6.2 Contributions

In Chapter 3, a novel end-effector design for the EEEA was introduced. A kinematic and workspace analysis was presented, accompanied by repeatability and structural integrity tests. At the time of publication and intellectual property protection filing (2020) no other

robotic end-effector was using the spherical-joint as the focal point of development to concentrate both pitch and yaw DoF in a single moving point. Other research robotic devices were using ball-joints as part of larger continuum structures that would be unsuitable for the constrained spaces of the EEEA. Rather than having an articulated or continuum body, this end-effector utilizes the spherical-joint concept modifying it with specific design considerations, such as parts-coupling and tendons placement, to concentrate all movement in a single point and allow for articulation at a minimum size.

In Chapter 4, an ergonomic handle design is presented aimed for the handheld controller that would control the end-effector presented in the previous chapter. The handle is forearm-mounted and maps the surgeon's wrist directly to the robot-joints. This work investigated a popular but yet unanswered research question, that of using an intuitive control scheme for robotics control in endonasal surgery. To achieve direct wrist-to-joint motion mapping the design needed to provide the surgeon with a stable platform around which they can control the robot joint. While during a preliminary study this design showcased short learning curves and improved surgeon performance, its ergonomics needed to be further explored.

To cater to a larger set of ergonomic literature guidelines, and to identify the most suitable handheld controller design for robotic neurosurgery, another handle was developed in the same chapter. This prototype was finger-operated and employed a rotating joystick-body which could be placed at the position where the operator would feel most comfortable. This position most often would be the pose where the surgeon would keep their hand at a resting pose. A randomised crossover user study took place where novice clinicians used the two novel prototypes, as well as a traditional non-articulated tool, inside a custom virtual simulator. At the conclusion of this chapter, the most suitable ergonomic design for the handheld robotic instrument had been identified, and the research question set in the previous chapter was answered.

Finally, Chapter 5 evaluates the work that was the result of all the preliminary development of previous chapters. A first of its kind handheld robotic instrument with interchangeable end-effectors is presented. This ergonomically designed instrument does not require a remote-centre-of-motion around its shaft and deploys miniature end-effectors at a diameter of $3mm$. To the best of the author's knowledge, this diameter is equal to the diameter of the smallest commercial system with a wristed end-effector [151]. However, rather than

requiring a complex tele-operated system, this capability exists at the palm of the surgeon's hand.

In this thesis, the handheld robotic instruments were developed for endoscopic neurosurgery. However, the same design and functionality principles could be applied to neighbouring disciplines, such as Ear Nose and Throat (ENT) surgery, with Functional Endoscopic Sinus Surgery being especially relevant, as well as more disparate approaches, such as Transanal Endoscopic Microsurgery (TEM). These procedures are also burdened with difficult access areas, constrained workspaces, and lack of dexterity, and thus, could benefit from robotic articulation. These instruments have the potential to be used as the foundation for wider clinical adoption and cover a larger patient need. Finally, based on the modularity of the system and its exchangeable end-effectors, in the long-term, this device has the potential to be used in combination with pre-existing commercial systems to offer an even more complete platform for surgical innovation.

6.3 Limitations

One of the main challenges throughout the device development was miniaturization and fabrication. Incorporating robotic capability in such a small form-factor is associated with many mechanical engineering issues. While an array of those was solved, some mechanical limitations still remain today.

As with most modular electromechanical systems, mechanical components introduce backlash that leads to undesired motion. Here, backlash is introduced as a result of various different components. The device is tendon-driven, so tendon pre-tensioning, as well as tendon slack or slippage, can introduce undesired performance. Another factor that contributes to backlash can be from slight misalignment during the coupling of the end-effector with the handheld controller. Fig. 6.2 suggests some points on the design that might be contributing to this issue. Finally, producing the end-effectors with additive manufacturing, namely DMLS, leads to imperfect surface finishes that can in-turn increase the device backlash.

Other than backlash, another mechanical design limitation of this device is its force-delivery capabilities. As evident during the cadaver pilot study, while the device can maintain its structural integrity when a force is applied on its miniature body, the end-effector itself cannot always apply sufficient force to interact with the anatomy. This can be attributed to insufficient torque during the motor selection, as well as to the tendon-routing and tendon-termination.

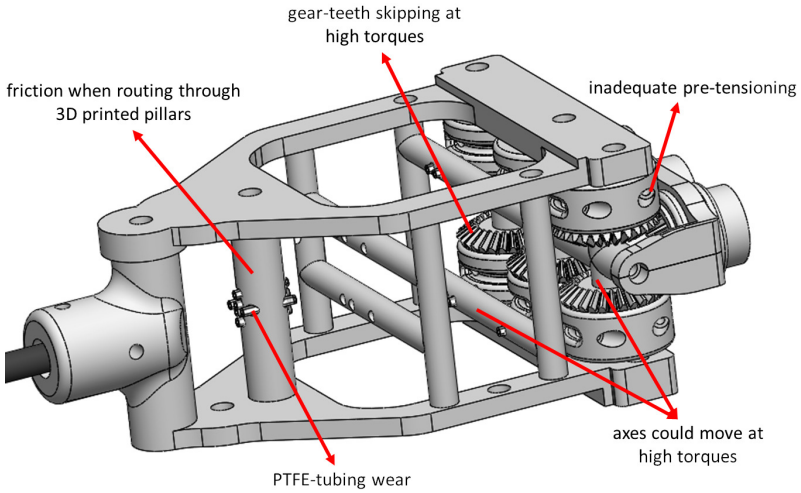

Figure 6.2: Design components that could be contributing to the mechanical backlash.

Mechanical limitations can have a big impact on the device performance and perception. Equally important, however, are software limitations which could affect both the performance and the clinical preference and adoption of the device. In this case, the major software limitation was the control methodology followed to actuate the end-effector. As evident in Chapter 4, the device is controlled in velocity-domain with a very simple open-loop control scheme that does not take into account the end-effector and device kinematics. It does not deploy any position encoders and thus, closed-loop position control is not possible. A surgical device needs to provide a more sophisticated control scheme with fail-safe alternatives to the standard control methodology in order to be used in the operating theatre.

Another software limitation is the absence of a user-friendly graphical user interface that could accompany the device and offer the operator options such as velocity scaling or position resets. The absence of such features could hinder clinical adoption, as surgeons might find the interaction with the device unintuitive.

Finally, and while the technical limitations are often the easiest to identify, there are also some clinical aspects that could further strengthen the potentiality of the presented instruments. For example, while the concept handle designs were run through an extensive user-study to identify the most suitable design, something crucial at that development stage, the final robotic prototype was not evaluated in-depth for its human factors and procedural ergonomics. Furthermore, while the device was tested in pre-clinical trials, it was not tested for tumor extraction. However understandable, since a commissioned cadaveric specimen will very rarely have a pituitary gland abnormality, the absence of a tumor during testing is

a limitation nonetheless. The final clinical limitation has to do with the system usage, and the fact that even though the main operative scenarios have been considered, more time is needed to identify catastrophic clinical scenarios and the possibility for misuse.

6.4 Future work

The continuation of this project is focusing on translating this preliminary technology into the operating theatre. To achieve that, the device performance and reliability will be improved. Increasing force delivery is a focal point of the development. To do that, appropriate motors and tendons will be sourced, and the joint-design, as well as the routing-design, will be analysed to find out the best tendon termination and routing physiology. This will serve both for force-transmission, as well as for backlash minimization. The handheld controller will be redesigned to allow for the new motors incorporation, and the coupling interface will be amended to not allow any misalignments.

Minimising the backlash and increasing the force delivery capability of the device are important features. Equally if not more important, however, is increasing the safety of the device, as well as its repeatability and accuracy. To do that, the usage of position-domain control will be investigated. Appropriate motor encoders will be sourced, and the device kinematics will be further explored. The joint-controller will incorporate forward and inverse kinematics, and a closed-loop control system will be developed to reliably actuate the end-effector to the desired position.

Evaluation studies will be held throughout this development, with the first one being a human-factors workshop where neurosurgeons of different surgical training experience will test the device in a comparison study alongside traditional tools. Additionally, multi-centre cadaveric studies will be regularly organised to evaluate the development progress and test all assumptions and research questions that will have yet to be answered. Clinicians from different centres have been involved and have shaped this research from an early stage, and the intention is to keep involving and expanding those groups to keep the development clinically relevant.

Post-development, all prototyping components that are aimed for sterilization will be replaced with autoclaveable materials, and custom draping with sterile adapters will be designed for the remaining components. The system will undertake all required testing and verification, with the overarching aim being a first-in-human series of testing.

Positive results from these clinical studies will position the system one step closer

towards clinical adoption. Smarter neurosurgical instrumentation will lead to improved surgical outcome, and as a result, more effective care for patients with brain tumours.

Bibliography

[1] Brian S Peters, Priscila R Armijo, Crystal Krause, Songita A Choudhury, and Dmitry Oleynikov. Review of emerging surgical robotic technology. *Surgical endoscopy*, 32(4):1636–1655, 2018.

[2] Hani J Marcus, Archie Hughes-Hallett, Thomas P Cundy, Dipankar Nandi, Guang-Zhong Yang, and Ara Darzi. Not everything that counts can be easily counted. *Bmj*, 346:f2461, 2013.

[3] Chris S Karas and E Antonio Chiocca. Neurosurgical robotics: a review of brain and spine applications. *Journal of robotic surgery*, 1(1):39–43, 2007.

[4] A L Benabid, P Cinquin, S Lavalle, J F Le Bas, J Demongeot, and J De Rougemont. Computer-driven robot for stereotactic surgery connected to CT scan and magnetic resonance imaging. *Stereotactic and Functional Neurosurgery*, 50(1-6):153–154, 1987.

[5] M S Eljamel. Validation of the PathFinder™ neurosurgical robot using a phantom. *The International Journal of Medical Robotics and Computer Assisted Surgery*, 3(4):372–377, 2007.

[6] Garnette R Sutherland, Isabelle Latour, Alexander D Greer, Tim Fielding, Georg Feil, and Perry Newhook. An image-guided magnetic resonance-compatible surgical robot. *Neurosurgery*, 62(2):286–293, 2008.

[7] James J Doulgeris, Sabrina A Gonzalez-Blohm, Andreas K Filis, Thomas M Shea, Kamran Aghayev, and Frank D Vrionis. Robotics in neurosurgery: evolution, current challenges, and compromises. *Cancer Control*, 22(3):352–359, 2015.

[8] K Hongo, T Goto, T Miyahara, Y Kakizawa, J Koyama, and Y Tanaka. Telecontrolled micromanipulator system (NeuRobot) for minimally invasive neurosurgery. In *Medical Technologies in Neurosurgery*, pages 63–66. Springer, 2006.

[9] Hani J Marcus, Carlo A Seneci, Christopher J Payne, Dipankar Nandi, Ara Darzi, and Guang-Zhong Yang. Robotics in keyhole transcranial endoscope-assisted microsurgery: a critical review of existing systems and proposed specifications for new robotic platforms. *Operative Neurosurgery*, 10(1):84–96, 2013.

[10] Paolo Cappabianca, Luigi Maria Cavallo, and Enrico de Divitiis. Endoscopic endonasal transsphenoidal surgery. *Neurosurgery*, 55(4):933–941, 2004.

[11] Amir R Dehdashti, Ahmed Ganna, Ian Witterick, and Fred Gentili. Expanded endoscopic endonasal approach for anterior cranial base and suprasellar lesions: indications and limitations. *Neurosurgery*, 64(4):677–689, 2009.

[12] Hani J Marcus, Thomas P Cundy, Archie Hughes-Hallett, Guang-Zhong Yang, Ara Darzi, and Dipankar Nandi. Endoscopic and keyhole endoscope-assisted neurosurgical approaches: a qualitative survey on technical challenges and technological solutions. *British journal of neurosurgery*, 28(5):606–610, 2014.

[13] Hani Marcus, Dipankar Nandi, Ara Darzi, and Guang-Zhong Yang. Surgical robotics through a keyhole: From today's translational barriers to tomorrow's "disappearing" robots. *IEEE Transactions on Biomedical Engineering*, 60(3):674–681, 2013.

[14] Chan Hee Koh, Danyal Z Khan, Ronneil Digpal, Hugo Layard Horsfall, Ahmad Ali, Stephanie E Baldeweg, Pierre-Marc Bouloux, Neil L Dorward, William M Drake, Jane Evanson, et al. The clinical outcomes of imaging modalities for surgical management cushing's disease–a systematic review and meta-analysis. *Frontiers in Endocrinology*, 13:3591, 2023.

[15] Sameer Chopra, Abhishek Srivastava, and Ashutosh Tewari. Robotic radical prostatectomy: the new gold standard. *Arab journal of urology*, 10(1):23–31, 2012.

[16] Hani J Marcus, Archie Hughes-Hallett, Christopher J Payne, Thomas P Cundy, Dipankar Nandi, Guang-Zhong Yang, and Ara Darzi. Trends in the diffusion of robotic surgery: A retrospective observational study. *The International Journal of Medical Robotics and Computer Assisted Surgery*, 13(4):e1870, 2017.

[17] Hani J Marcus, Archie Hughes-Hallett, Thomas P Cundy, Guang-Zhong Yang, Ara Darzi, and Dipankar Nandi. da vinci robot-assisted keyhole neurosurgery: a cadaver study on feasibility and safety. *Neurosurgical review*, 38:367–371, 2015.

[18] Hani Joseph Marcus. The application of robotics to keyhole transcranial endoscopic microsurgery. 2015.

[19] Christopher J Payne and Guang-Zhong Yang. Hand-held medical robots. *Annals of biomedical engineering*, 42(8):1594–1605, 2014.

[20] Francisco M Sánchez-Margallo, Juan A Sánchez-Margallo, and Amir Szold. Hand-held devices for laparoscopic surgery. *New Horizons in Laparoscopic Surgery*, page 75, 2018.

[21] Hani J Marcus, Danyal Z Khan, Anouk Borg, Michael Buchfelder, Justin S Cetas, Justin W Collins, Neil L Dorward, Maria Fleseriu, Mark Gurnell, Mohsen Javadpour, et al. Pituitary society expert delphi consensus: operative workflow in endoscopic transsphenoidal pituitary adenoma resection. *Pituitary*, 24(6):839–853, 2021.

[22] Sorayouth Chumnanvej, Suwiphat Chalongwongse, Branesh M Pillai, and Jackrit Suthakorn. Pathway and workspace study of Endonasal Endoscopic Transsphenoidal (EET) approach in 80 cadavers. *International Journal of Surgery Open*, 16:22–28, 2019.

[23] Christos Bergeles, Andrew H Gosline, Nikolay V Vasilyev, Patrick J Codd, J Pedro, and Pierre E Dupont. Concentric tube robot design and optimization based on task and anatomical constraints. *IEEE Transactions on Robotics*, 31(1):67–84, 2015.

[24] Jessica Burgner, Philip J Swaney, D Caleb Rucker, Hunter B Gilbert, Scott T Nill, Paul T Russell, Kyle D Weaver, and Robert J Webster. A bimanual teleoperated system for endonasal skull base surgery. In *2011 IEEE/RSJ international conference on intelligent robots and systems*, pages 2517–2523. IEEE, 2011.

[25] Jessica Burgner, D Caleb Rucker, Hunter B Gilbert, Philip J Swaney, Paul T Russell, Kyle D Weaver, and Robert J Webster. A telerobotic system for transnasal surgery. *IEEE/ASME Transactions on Mechatronics*, 19(3):996–1006, 2013.

[26] Philip J Swaney, Jordan M Croom, Jessica Burgner, Hunter B Gilbert, D Caleb Rucker, Robert J Webster, Kyle D Weaver, and Paul T Russell. Design of a quadramanual robot for single-nostril skull base surgery. In *ASME 2012 5th Annual Dynamic Systems and Control Conference joint with the JSME 2012 11th Motion and Vibration Conference*, pages 387–393. American Society of Mechanical Engineers, 2012.

[27] Philip J Swaney, Hunter B Gilbert, Robert J Webster III, Paul T Russell III, and Kyle D Weaver. Endonasal skull base tumor removal using concentric tube continuum robots: a phantom study. *Journal of Neurological Surgery Part B: Skull Base*, 76(02):145–149, 2015.

[28] Jumpei Arata, Yasunori Tada, Hiroaki Kozuka, Tomohiro Wada, Yoshitaka Saito, Norio Ikedo, Yuichiro Hayashi, Masazumi Fujii, Yasukazu Kajita, and Masaaki Mizuno. Neurosurgical robotic system for brain tumor removal. *International journal of computer assisted radiology and surgery*, 6(3):375–385, 2011.

[29] Jumpei Arata, Yosuke Fujisawa, Ryu Nakadate, Kazuo Kiguchi, Kanako Harada, Mamoru Mitsuishi, and Makoto Hashizume. Compliant four degree-of-freedom manipulator with locally deformable elastic elements for minimally invasive surgery. In *2019 International Conference on Robotics and Automation (ICRA)*, pages 2663–2669. IEEE, 2019.

[30] Giada Gerboni, Paul W J Henselmans, Ewout A Arkenbout, Wouter R van Furth, and Paul Breedveld. HelixFlex: bioinspired maneuverable instrument for skull base surgery. *Bioinspiration & biomimetics*, 10(6):66013, 2015.

[31] Ch Nimsky, J Rachinger, H Iro, and R Fahlbusch. Adaptation of a hexapod-based robotic system for extended endoscope-assisted transsphenoidal skull base surgery. *min-Minimally Invasive Neurosurgery*, 47(01):41–46, 2004.

[32] Suwiphat Chalongwongse and Jackrit Suthakorn. Workspace determination and robot design of a prototyped surgical robotic system based on a cadaveric study in Endonasal transsphenoidal surgery. In *2014 IEEE International Conference on Robotics and Biomimetics (ROBIO 2014)*, pages 241–246. IEEE, 2014.

[33] Chao He, Kevin Olds, Iulian Iordachita, and Russell Taylor. A new ENT microsurgery robot: error analysis and implementation. In *2013 IEEE International Conference on Robotics and Automation*, pages 1221–1227. IEEE, 2013.

[34] Lannie Liu, Sarah Giulia Mariani, Emmanuel De Schlichting, Sylvie Grand, Michel Lefranc, Eric Seigneuret, and Stéphan Chabardès. Frameless rosa® robot-assisted lead implantation for deep brain stimulation: technique and accuracy. *Operative Neurosurgery*, 19(1):57–64, 2020.

[35] Reid Hoshide, Mark Calayag, Hal Meltzer, Michael L Levy, and David Gonda. Robot-assisted endoscopic third ventriculostomy: institutional experience in 9 patients. *Journal of Neurosurgery: Pediatrics*, 20(2):125–133, 2017.

[36] Alessandro De Benedictis, Andrea Trezza, Andrea Carai, Elisabetta Genovese, Emidio Procaccini, Raffaella Messina, Franco Randi, Silvia Cossu, Giacomo Esposito, Paolo Palma, et al. Robot-assisted procedures in pediatric neurosurgery. *Neurosurgical focus*, 42(5):E7, 2017.

[37] Shigeo Hirose and Shugen Ma. Coupled tendon-driven multijoint manipulator. In *Proceedings. 1991 IEEE International Conference on Robotics and Automation*, pages 1268–1269. IEEE Computer Society, 1991.

[38] Zheng Li, Liao Wu, Hongliang Ren, and Haoyong Yu. Kinematic comparison of surgical tendon-driven manipulators and concentric tube manipulators. *Mechanism and machine theory*, 107:148–165, 2017.

[39] David P Noonan, Valentina Vitiello, Jianzhong Shang, Christopher J Payne, and Guang-Zhong Yang. A modular, mechatronic joint design for a flexible access platform for mis. In *2011 IEEE/RSJ International Conference on Intelligent Robots and Systems*, pages 949–954. IEEE, 2011.

[40] Pierre Berthet-Rayne, Gauthier Gras, Konrad Leibrandt, Piyamate Wisanuvej, Andreas Schmitz, Carlo A Seneci, and Guang-Zhong Yang. The i 2 snake robotic platform for endoscopic surgery. *Annals of biomedical engineering*, 46(10):1663–1675, 2018.

[41] Jianzhong Shang, Konrad Leibrandt, Petros Giataganas, Valentina Vitiello, Carlo A Seneci, Piyamate Wisanuvej, Jindong Liu, Gauthier Gras, James Clark, and Ara

Darzi. A single-port robotic system for transanal microsurgery—design and validation. *IEEE robotics and automation letters*, 2(3):1510–1517, 2017.

[42] Karthik Chandrasekaran and Asokan Thondiyath. Design of a tether-driven minimally invasive robotic surgical tool with decoupled degree-of-freedom wrist. *The International Journal of Medical Robotics and Computer Assisted Surgery*, 16(3):e2084, 2020.

[43] David B Camarillo, Christopher F Milne, Christopher R Carlson, Michael R Zinn, and J Kenneth Salisbury. Mechanics modeling of tendon-driven continuum manipulators. *IEEE transactions on robotics*, 24(6):1262–1273, 2008.

[44] Takahisa Kato, Ichiro Okumura, Sang-Eun Song, Alexandra J Golby, and Nobuhiko Hata. Tendon-driven continuum robot for endoscopic surgery: Preclinical development and validation of a tension propagation model. *IEEE/ASME Transactions on Mechatronics*, 20(5):2252–2263, 2014.

[45] G Vachtsevanos, Kent Davey, and Kok-Meng Lee. Development of a novel intelligent robotic manipulator. *IEEE Control Systems Magazine*, 7(3):9–15, 1987.

[46] Kok-Meng Lee, George Vachtsevanos, and Chikong Kwan. Development of a spherical stepper wrist motor. *Journal of Intelligent and Robotic Systems*, 1(3):225–242, 1988.

[47] Mark L Guckert and Michael D Naish. A compact 3 degree of freedom spherical joint. *Journal of Mechanisms and Robotics*, 3(3), 2011.

[48] Andreas Schmitz, Shen Treratanakulchai, Pierre Berthet-Rayne, and Guang-Zhong Yang. A Rolling-Tip Flexible Instrument for Minimally Invasive Surgery. In *2019 International Conference on Robotics and Automation (ICRA)*, pages 379–385. IEEE, 2019.

[49] Kanako Harada, Kota Tsubouchi, Masakatsu G Fujie, and Toshio Chiba. Micro manipulators for intrauterine fetal surgery in an open MRI. In *Proceedings of the 2005 IEEE International Conference on Robotics and Automation*, pages 502–507. IEEE, 2005.

[50] Peter Berkelman and Ji Ma. A compact modular teleoperated robotic system for laparoscopic surgery. *The International journal of robotics research*, 28(9):1198–1215, 2009.

[51] Andrew T Schlussel and Justin A Maykel. Ergonomics and musculoskeletal health of the surgeon. *Clinics in colon and rectal surgery*, 32(06):424–434, 2019.

[52] Pavel Stoklasek, Ales Mizera, Miroslav Manas, and David Manas. Improvement of handle grip using reverse engineering, cae and rapid prototyping. In *MATEC Web of Conferences*, volume 76, page 02029. EDP Sciences, 2016.

[53] AK Hemal, M Srinivas, and AR Charles. Ergonomic problems associated with laparoscopy. *Journal of endourology*, 15(5):499–503, 2001.

[54] Allison DiMartino, Kathryn Doné, Timothy Judkins, Jonathan Morse, Jennifer Melander, Dmitry Oleynikov, and M Susan Hallbeck. Ergonomic laparoscopic tool handle design. In *Proceedings of the Human Factors and Ergonomics Society Annual Meeting*, volume 48, pages 1354–1358. SAGE Publications Sage CA: Los Angeles, CA, 2004.

[55] A G González, D R Rodríguez, and J García Sanz-Calcedo. Ergonomic analysis of the dimension of a precision tool handle: a case study. *Procedia Manufacturing*, 13:1336–1343, 2017.

[56] Ali Hassan Zahraee, Jamie Kyujin Paik, Jerome Szewczyk, and Guillaume Morel. Toward the development of a hand-held surgical robot for laparoscopy. *IEEE/ASME Transactions on mechatronics*, 15(6):853–861, 2010.

[57] Laura Santos-Carreras, Monika Hagen, Roger Gassert, and Hannes Bleuler. Survey on surgical instrument handle design: ergonomics and acceptance. *Surgical innovation*, 19(1):50–59, 2012.

[58] M A Van Veelen, D W Meijer, R H M Goossens, and C J Snijders. New ergonomic design criteria for handles of laparoscopic dissection forceps. *Journal of Laparoendoscopic & Advanced Surgical Techniques*, 11(1):17–26, 2001.

[59] Vijay R Ramakrishnan and Paul N Montero. Ergonomic considerations in endoscopic sinus surgery: lessons learned from laparoscopic surgeons. *American journal of rhinology & allergy*, 27(3):245–250, 2013.

[60] Hui Dong, Peter Loomer, Alan Barr, Charles LaRoche, Ed Young, and David Rempel. The effect of tool handle shape on hand muscle load and pinch force in a simulated dental scaling task. *Applied ergonomics*, 38(5):525–531, 2007.

[61] Hyung-Taeg Han, Seong-il Kwon, and Chunwoo Kim. Ergonomic Design Process of Minimally Invasive Surgery Instrument hand-held manipulator with kinematic, psychologic analysis. In *2019 16th International Conference on Ubiquitous Robots (UR)*, pages 306–312. IEEE, 2019.

[62] Alfonso González González, David Rodríguez Salgado, Lorenzo García Moruno, and Alonso Sánchez Ríos. An ergonomic customized-tool handle design for precision tools using additive manufacturing: a case study. *Applied Sciences*, 8(7):1200, 2018.

[63] Thierry Bensignor, Guillaume Morel, David Reversat, David Fuks, and Brice Gayet. Evaluation of the effect of a laparoscopic robotized needle holder on ergonomics and skills. *Surgical endoscopy*, 30(2):446–454, 2016.

[64] Zhuoqi Cheng, Brian L Davies, Darwin G Caldwell, Giacinto Barresi, Qinqi Xu, and Leonardo S Mattos. A hand-held robotic device for peripheral intravenous catheterization. *Proceedings of the Institution of Mechanical Engineers, Part H: Journal of Engineering in Medicine*, 231(12):1165–1177, 2017.

[65] Yash Chitalia, Seokhwan Jeong, Nancy Deaton, Joshua J Chern, and Jaydev P Desai. Design and kinematics analysis of a robotic pediatric neuroendoscope tool body. *IEEE/ASME Transactions on Mechatronics*, 25(2):985–995, 2020.

[66] Paolo Dario, Maria Chiarra Carrozza, Maurilio Marcacci, Simona D'Attanasio, Bernardo Magnami, Oliver Tonet, and Giuseppe Megali. A novel mechatronic tool for computer-assisted arthroscopy. *IEEE transactions on information technology in biomedicine*, 4(1):15–29, 2000.

[67] Emmanouil Dimitrakakis, George Dwyer, Lukas Lindenroth, Petros Giataganas, Neil L Dorward, Hani J Marcus, and Danail Stoyanov. A spherical joint robotic

end-effector for the expanded endoscopic endonasal approach. *Journal of Medical Robotics Research*, 5(03n04):2150002, 2020.

[68] Emmanouil Dimitrakakis, Lukas Lindenroth, George Dwyer, Holly Aylmore, Neil L Dorward, Hani J Marcus, and Danail Stoyanov. An intuitive surgical handle design for robotic neurosurgery. *International Journal of Computer Assisted Radiology and Surgery*, pages 1–9, 2021.

[69] Emmanouil Dimitrakakis, Holly Aylmore, Lukas Lindenroth, George Dwyer, Joshua Carmichael, Danyal Z Khan, Neil L Dorward, Hani J Marcus, and Danail Stoyanov. Robotic handle prototypes for endoscopic endonasal skull base surgery: Pre-clinical randomised controlled trial of performance and ergonomics. *Annals of biomedical engineering*, 50(5):549–563, 2022.

[70] Richelle Ebrahimi, S Okazawa, Robert Rohling, and Septimiu E Salcudean. Handheld steerable needle device. In *Medical Image Computing and Computer-Assisted Intervention-MICCAI 2003: 6th International Conference, Montréal, Canada, November 15-18, 2003. Proceedings 6*, pages 223–230. Springer, 2003.

[71] Jing Feng, Zhiyuan Yan, Man Li, Zhang Zhang, XiaoJia Chen, Zhijiang Du, and Kun Yang. Handheld robotic needle holder training: slower but better. *Surgical Endoscopy*, 35:1667–1674, 2021.

[72] Francesco Focacci, Marco Piccigallo, Oliver Tonet, Giuseppe Megali, Andrea Pietrabissa, and Paolo Dario. Lightweight hand-held robot for laparoscopic surgery. In *Proceedings 2007 IEEE International Conference on Robotics and Automation*, pages 599–604. IEEE, 2007.

[73] Cédric Girerd and Tania K Morimoto. Design and control of a hand-held concentric tube robot for minimally invasive surgery. *IEEE Transactions on Robotics*, 2020.

[74] A Hackethal, M Koppan, K Eskef, and H-R Tinneberg. Handheld articulating laparoscopic instruments driven by robotic technology. first clinical experience in gynecological surgery. *Gynecological Surgery*, 9(2):203–206, 2012.

[75] Richard J Hendrick, Christopher R Mitchell, S Duke Herrell, and Robert J Webster III. Hand-held transendoscopic robotic manipulators: A transurethral laser

prostate surgery case study. *The International journal of robotics research*, 34(13):1559–1572, 2015.

[76] Kenji Kawashima, Takahiro Kanno, and Kotaro Tadano. Robots in laparoscopic surgery: current and future status. *BMC Biomedical Engineering*, 1:1–6, 2019.

[77] Julie Legrand, Mouloud Ourak, Laura Van Gerven, Vincent Vander Poorten, and Emmanuel Vander Poorten. A miniature robotic steerable endoscope for maxillary sinus surgery called plient. *Scientific Reports*, 12(1):2299, 2022.

[78] Mariana Leite, Ana F Carvalho, Patrício Costa, Ricardo Pereira, Antonio Moreira, Nuno Rodrigues, Sara Laureano, Jorge Correia-Pinto, João L Vilaça, and Pedro Leão. Assessment of laparoscopic skills performance: 2d versus 3d vision and classic instrument versus new hand-held robotic device for laparoscopy. *Surgical innovation*, 23(1):52–61, 2016.

[79] Juan A Sánchez-Margallo and Francisco M Sánchez-Margallo. Initial experience using a robotic-driven laparoscopic needle holder with ergonomic handle: assessment of surgeons' task performance and ergonomics. *International journal of computer assisted radiology and surgery*, 12(12):2069–2077, 2017.

[80] Nobuto Matsuhira, Makoto Jinno, Toyomi Miyagawa, Takamitsu Sunaoshi, Takehiro Hato, Yasuhide Morikawa, Toshiharu Furukawa, Soji Ozawa, Masaki Kitajima, and Kazuo Nakazawa. Development of a functional model for a master–slave combined manipulator for laparoscopic surgery. *Advanced Robotics*, 17(6):523–539, 2003.

[81] Ryoken Miyazaki, Kohei Hirose, Yoshiya Ishikawa, Takahiro Kanno, and Kenji Kawashima. A master–slave integrated surgical robot with active motion transformation using wrist axis. *IEEE/ASME Transactions on Mechatronics*, 23(3):1215–1225, 2018.

[82] Stephen Okazawa, Richelle Ebrahimi, Jason Chuang, Septimiu E Salcudean, and Robert Rohling. Hand-held steerable needle device. *IEEE/ASME Transactions on Mechatronics*, 10(3):285–296, 2005.

[83] Christopher J Payne, Gauthier Gras, Michael Hughes, Dinesh Nathwani, and Guang-Zhong Yang. A hand-held flexible mechatronic device for arthroscopy. In *2015*

IEEE/RSJ International Conference on Intelligent Robots and Systems (IROS), pages 817–823. IEEE, 2015.

[84] Ricardo Pereira, António HJ Moreira, Mariana Leite, Pedro L Rodrigues, Sandro Queirós, Nuno F Rodrigues, Pedro Leão, and João L Vilaça. Hand-held robotic device for laparoscopic surgery and training. In *2014 IEEE 3nd International Conference on Serious Games and Applications for Health (SeGAH)*, pages 1–8. IEEE, 2014.

[85] Marco Piccigallo, Francesco Focacci, Oliver Tonet, Giuseppe Megali, Claudio Quaglia, and Paolo Dario. Hand-held robotic instrument for dextrous laparoscopic interventions. *The International Journal of Medical Robotics and Computer Assisted Surgery*, 4(4):331–338, 2008.

[86] Francisco Miguel Sánchez-Margallo and Juan A Sánchez-Margallo. Assessment of postural ergonomics and surgical performance in laparoendoscopic single-site surgery using a handheld robotic device. *Surgical innovation*, 25(3):208–217, 2018.

[87] Jianzhong Shang, David P Noonan, Christopher Payne, James Clark, Mikael Hans Sodergren, Ara Darzi, and G-Z Yang. An articulated universal joint based flexible access robot for minimally invasive surgery. In *2011 IEEE international conference on robotics and automation*, pages 1147–1152. IEEE, 2011.

[88] Victor Gabriel Hernández-Valderrama, Ricardo Manuel Ordorica-Flores, Salvador Montoya-Alvarez, Daniel Haro-Mendoza, Luis Ochoa-Toledo, Daniel Lorias-Espinoza, José L Ortiz-Simón, and Fernando Pérez-Escamirosa. Steerable surgical instrument for conventional and single-site minimally invasive surgery. *Surgical Innovation*, page 15533506211037091, 2021.

[89] Hiromasa Yamashita, Nobuhiko Hata, Makoto Hashizume, and Takeyoshi Dohi. Handheld laparoscopic forceps manipulator using multi-slider linkage mechanisms. In *Medical Image Computing and Computer-Assisted Intervention–MICCAI 2004: 7th International Conference, Saint-Malo, France, September 26-29, 2004. Proceedings, Part II 7*, pages 121–128. Springer, 2004.

[90] Yingkan Yang, Kang Kong, Jianmin Li, Shuxin Wang, and Jinhua Li. Design and evaluation of a dexterous and modular hand-held surgical robot for minimally invasive surgery. *Journal of Medical Devices*, 13(4), 2019.

[91] Yingkan Yang, Kang Kong, Jianmin Li, and Shuxin Wang. Design and implementation of a hand-held robot-assisted minimally invasive surgical device with enhanced intuitive manipulability and stable grip force. *The International Journal of Medical Robotics and Computer Assisted Surgery*, page e2286, 2021.

[92] Russell Taylor, Pat Jensen, Louis Whitcomb, Aaron Barnes, Rajesh Kumar, Dan Stoianovici, Puneet Gupta, ZhengXian Wang, Eugene Dejuan, and Louis Kavoussi. A steady-hand robotic system for microsurgical augmentation. *The International Journal of Robotics Research*, 18(12):1201–1210, 1999.

[93] Wei Tech Ang, PK Pradeep, and CN Riviere. Active tremor compensation in microsurgery. In *The 26th Annual International Conference of the IEEE Engineering in Medicine and Biology Society*, volume 1, pages 2738–2741. IEEE, 2004.

[94] Yan Naing Aye, Su Zhao, Cheng Yap Shee, and Wei Tech Ang. Vision aided active error canceling in handheld microsurgical instrument. *Procedia Engineering*, 41:729–736, 2012.

[95] Dongjune Chang, Gwang Min Gu, and Jung Kim. Design of a novel tremor suppression device using a linear delta manipulator for micromanipulation. In *2013 IEEE/RSJ International Conference on Intelligent Robots and Systems*, pages 413–418. IEEE, 2013.

[96] Berk Gonenc, Ellen Feldman, Peter Gehlbach, James Handa, Russell H Taylor, and Iulian Iordachita. Towards robot-assisted vitreoretinal surgery: Force-sensing microforceps integrated with a handheld micromanipulator. In *2014 IEEE International Conference on Robotics and Automation (ICRA)*, pages 1399–1404. IEEE, 2014.

[97] Win Tun Latt, Richard C Newton, Marco Visentini-Scarzanella, Christopher J Payne, David P Noonan, Jianzhong Shang, and Guang-Zhong Yang. A hand-held instrument to maintain steady tissue contact during probe-based confocal laser endomicroscopy. *IEEE transactions on biomedical engineering*, 58(9):2694–2703, 2011.

[98] Robert A MacLachlan, Brian C Becker, Jaime Cuevas Tabarés, Gregg W Podnar, Louis A Lobes, and Cameron N Riviere. Micron: an actively stabilized handheld tool for microsurgery. *IEEE transactions on robotics*, 28(1):195–212, 2011.

[99] Sara Moccia, Simone Foti, Arpita Routray, Francesca Prudente, Alessandro Perin, Raymond F Sekula, Leonardo S Mattos, Jeffrey R Balzer, Wendy Fellows-Mayle, Elena De Momi, et al. Toward improving safety in neurosurgery with an active handheld instrument. *Annals of biomedical engineering*, 46:1450–1464, 2018.

[100] Cheol Song, Dong Yong Park, Peter L Gehlbach, Seong Jin Park, and Jin U Kang. Fiber-optic oct sensor guided "smart" micro-forceps for microsurgery. *Biomedical optics express*, 4(7):1045–1050, 2013.

[101] Chantal CJ Alleblas, Michel PH Vleugels, Sjors FPJ Coppus, and Theodoor E Nieboer. The effects of laparoscopic graspers with enhanced haptic feedback on applied forces: a randomized comparison with conventional graspers. *Surgical endoscopy*, 31:5411–5417, 2017.

[102] Francesco Amato, Marco Carbone, Carlo Cosentino, Alessio Merola, Michele Morelli, and Fulvio Zullo. A versatile mechatronic tool for minimally invasive surgery. In *The First IEEE/RAS-EMBS International Conference on Biomedical Robotics and Biomechatronics, 2006. BioRob 2006.*, pages 192–197. IEEE, 2006.

[103] Matthew W Gilbertson and Brian W Anthony. Ergonomic control strategies for a handheld force-controlled ultrasound probe. In *2012 IEEE/RSJ International Conference on Intelligent Robots and Systems*, pages 1284–1291. IEEE, 2012.

[104] Takuya Iwai, Takahiro Kanno, Tetsuro Miyazaki, Daisuke Haraguchi, and Kenji Kawashima. Pneumatically driven surgical forceps displaying a magnified grasping torque. *The International Journal of Medical Robotics and Computer Assisted Surgery*, 16(2):e2051, 2020.

[105] Choonghan Lee, Uikyum Kim, Dong-Hyuk Lee, Canh Toan Nguyen, Dat Tien Nguyen, Hoa Phung, Joonwoo Park, Hosang Jung, and Hyouk Ryeol Choi. Development of a smart handheld surgical tool with tactile feedback. *Intelligent Service Robotics*, 10(2):149–158, 2017.

[106] Christopher J Payne, Hani J Marcus, and Guang-Zhong Yang. A smart haptic hand-held device for neurosurgical microdissection. *Annals of biomedical engineering*, 43(9):2185–2195, 2015.

[107] George Stetten, Bing Wu, Roberta Klatzky, John Galeotti, Mel Siegel, Randy Lee, Francis Mah, Andrew Eller, Joel Schuman, and Ralph Hollis. Hand-held force magnifier for surgical instruments. In *Information Processing in Computer-Assisted Interventions: Second International Conference, IPCAI 2011, Berlin, Germany, June 22, 2011. Proceedings 2*, pages 90–100. Springer, 2011.

[108] Zhen Wang, Shuxin Wang, and Siyang Zuo. A hand-held device with 3-dof haptic feedback mechanism for microsurgery. *The International Journal of Medical Robotics and Computer Assisted Surgery*, 15(5):e2025, 2019.

[109] Hsin-Yun Yao, Vincent Hayward, and Randy E Ellis. A tactile enhancement instrument for minimally invasive surgery. *Computer Aided Surgery*, 10(4):233–239, 2005.

[110] Andrew K Battenberg, Nathan A Netravali, and Jess H Lonner. A novel handheld robotic-assisted system for unicompartmental knee arthroplasty: surgical technique and early survivorship. *Journal of robotic surgery*, 14(1):55–60, 2020.

[111] Axel Follmann, Alexander Korff, Tobias Fuertjes, Sandra C Kunze, Kirsten Schmieder, and Klaus Radermacher. A novel concept for smart trepanation. *Journal of Craniofacial Surgery*, 23(1):309–314, 2012.

[112] Markus Hessinger, Jürgen Hielscher, Peter P Pott, and Roland Werthschützky. Hand-held surgical drill with integrated thrust force recognition. In *2013 E-Health and Bioengineering Conference (EHB)*, pages 1–4. IEEE, 2013.

[113] Gavin Kane, Georg Eggers, Robert Boesecke, Jörg Raczkowsky, Heinz Wörn, Rüdiger Marmulla, and Joachim Mühling. System design of a hand-held mobile robot for craniotomy. In *Medical Image Computing and Computer-Assisted Intervention–MICCAI 2009: 12th International Conference, London, UK, September 20-24, 2009, Proceedings, Part I 12*, pages 402–409. Springer, 2009.

[114] Vladimir Kotev, George Boiadjiev, Haruhisa Kawasaki, Tetsuya Mouri, Kamen Delchev, and Tony Boiadjiev. Design of a hand-held robotized module for bone

drilling and cutting in orthopedic surgery. In *2012 IEEE/SICE International Symposium on System Integration (SII)*, pages 504–509. IEEE, 2012.

[115] Justin H Ma, Shahriar Sefati, Russell H Taylor, and Mehran Armand. An active steering hand-held robotic system for minimally invasive orthopaedic surgery using a continuum manipulator. *IEEE Robotics and Automation Letters*, 6(2):1622–1629, 2021.

[116] Yan Wang, Hao Zheng, Russell H Taylor, and Kwok Wai Samuel Au. A handheld steerable surgical drill with a novel miniaturized articulated joint module for dexterous confined-space bone work. *IEEE Transactions on Biomedical Engineering*, 69(9):2926–2934, 2022.

[117] Yingkan Yang, Kang Kong, Jianmin Li, Shuxin Wang, and Jinhua Li. Design and Evaluation of a Dexterous and Modular Hand-Held Surgical Robot for Minimally Invasive Surgery. *Journal of Medical Devices*, 13(4), 2019.

[118] Ali Hassan-Zahraee, Benoît Herman, and Jérôme Szewczyk. Mechatronic design of a hand-held instrument with active trocar for laparoscopy. In *2011 IEEE International Conference on Robotics and Automation*, pages 1890–1895. IEEE, 2011.

[119] Jing Feng, Kun Yang, Zhang Zhang, Man Li, XiaoJia Chen, Zhiyuan Yan, Zhijiang Du, and XingHuan Wang. Handheld laparoscopic robotized instrument: progress or challenge? *Surgical Endoscopy*, 34(2):719–727, 2020.

[120] Deepika Sareen, A K Agarwal, J M Kaul, and Ashwani Sethi. Study of sphenoid sinus anatomy in relation to endoscopic surgery. *Int J Morphol*, 23(3):261–266, 2005.

[121] KARL STORZ S E & Co. KG. All instruments for Endonasal Skull Base Surgery, Endoscopy and Microscopy. *Oral and Maxillofacial Surgery*, 2012.

[122] F Conti, F Barbagli, R Balaniuk, M Halg, C Lu, D Morris, L Sentis, J Warren, O Khatib, and K Salisbury. The CHAI libraries. In *Proceedings of Eurohaptics 2003*, pages 496–500, Dublin, Ireland, 2003.

[123] E. Rohmer, S. P. N. Singh, and M. Freese. Coppeliasim (formerly v-rep): a versatile and scalable robot simulation framework. *Proc. of The International Conference on Intelligent Robots and Systems (IROS)*, 2013. www.coppeliarobotics.com.

[124] Nikolaos Evangeliou, Emmanouil Dimitrakakis, and Anthony Tzes. Design and experimental evaluation of a tendon-driven minimally invasive surgical robotic tool with antagonistic control. In *2017 IEEE Conference on Control Technology and Applications (CCTA)*, pages 463–467. IEEE, 2017.

[125] Morgan Quigley, Ken Conley, Brian Gerkey, Josh Faust, Tully Foote, Jeremy Leibs, Rob Wheeler, and Andrew Y Ng. Ros: an open-source robot operating system. In *ICRA workshop on open source software*, volume 3, page 5. Kobe, Japan, 2009.

[126] B KS. 7082: 1999 (iso 9283: 1998) robot peformance criteria. *Association of Korean Standard*, 1999.

[127] James R Bekeny, Philip J Swaney, Robert J Webster III, Paul T Russell, and Kyle D Weaver. Forces applied at the skull base during transnasal endoscopic transsphenoidal pituitary tumor excision. *Journal of Neurological Surgery Part B: Skull Base*, 74(06):337–341, 2013.

[128] Seong-il Kwon, Geunwoong Ryu, Sungchul Kang, and Keri Kim. A steerable endoscope for transnasal skull base surgery. In *2018 40th Annual International Conference of the IEEE Engineering in Medicine and Biology Society (EMBC)*, pages 4158–4161. IEEE, 2018.

[129] TN Do, T Tjahjowidodo, MWS Lau, T Yamamoto, and SJ Phee. Hysteresis modeling and position control of tendon-sheath mechanism in flexible endoscopic systems. *Mechatronics*, 24(1):12–22, 2014.

[130] Kaitlin Oliver-Butler, John Till, and Caleb Rucker. Continuum robot stiffness under external loads and prescribed tendon displacements. *IEEE Transactions on Robotics*, 35(2):403–419, 2019.

[131] L Don Lehmkuhl and Laura K Smith. Brunnstrom's clinical kinesiology. 1984.

[132] Patrick L Anderson, Ray A Lathrop, and Robert J Webster III. Robot-like dexterity without computers and motors: a review of hand-held laparoscopic instruments with wrist-like tip articulation. *Expert review of medical devices*, 13(7):661–672, 2016.

[133] Anna M Derossis, Gerald M Fried, Harvey H Sigman, Jeffrey S Barkun, and Jonathan L Meakins. Development of a model for training and evaluation of laparoscopic skills. *The American journal of surgery*, 175(6):482–487, 1998.

[134] Hani J Marcus, Carlo A Seneci, Archie Hughes-Hallett, Thomas P Cundy, Dipankar Nandi, Guang-Zhong Yang, and Ara Darzi. Comparative performance in single-port versus multiport minimally invasive surgery, and small versus large operative working spaces: a preclinical randomized crossover trial. *Surgical innovation*, 23(2):148–155, 2016.

[135] Lynn McAtamney and Nigel Corlett. Rapid upper limb assessment (RULA). In *Handbook of human factors and ergonomics methods*, pages 86–96. CRC Press, 2004.

[136] Mark R Wilson, Jamie M Poolton, Neha Malhotra, Karen Ngo, Elizabeth Bright, and Rich S W Masters. Development and validation of a surgical workload measure: the surgery task load index (SURG-TLX). *World journal of surgery*, 35(9):1961, 2011.

[137] Nuzhath Khan, Hamid Abboudi, Mohammed Shamim Khan, Prokar Dasgupta, and Kamran Ahmed. Measuring the surgical 'learning curve': methods, variables and competency. *BJU international*, 113(3):504–508, 2014.

[138] Byron F Santos, Taylor J Reif, Nathaniel J Soper, and Eric S Hungness. Effect of training and instrument type on performance in single-incision laparoscopy: results of a randomized comparison using a surgical simulator. *Surgical endoscopy*, 25(12):3798–3804, 2011.

[139] Harry P Corker, Pritam Singh, Mikael H Sodergren, Sathyan Balaji, Richard M Kwasnicki, Ara W Darzi, and Paraskevas Paraskeva. A randomized controlled study to establish the effect of articulating instruments on performance in single-incision laparoscopic surgery. *Journal of surgical education*, 72(1):1–7, 2015.

[140] Thomas M Greiner. Hand anthropometry of us army personnel. united states army natick research. *Development and Engineering Center. Natick, MA*, 1991.

[141] AG González, J García Sanz-Calcedo, O López, DR Salgado, I Cambero, and JM Herrera. Guide design of precision tool handle based on ergonomics criteria using parametric cad software. *Procedia engineering*, 132:1014–1020, 2015.

[142] Lynn McAtamney and E Nigel Corlett. Rula: a survey method for the investigation of work-related upper limb disorders. *Applied ergonomics*, 24(2):91–99, 1993.

[143] Danyal Z Khan, Imanol Luengo, Santiago Barbarisi, Carole Addis, Lucy Culshaw, Neil L Dorward, Pinja Haikka, Abhiney Jain, Karen Kerr, Chan Hee Koh, et al. Automated operative workflow analysis of endoscopic pituitary surgery using machine learning: development and preclinical evaluation (ideal stage 0). *Journal of Neurosurgery*, 1(aop):1–8, 2021.

[144] Joseph Brunworth, Vikram Padhye, Ahmed Bassiouni, Alkis Psaltis, Stephen Floreani, Simon Robinson, Stephen Santoreneos, Nick Vrodos, Andrew Parker, Agadha Wickremesekera, et al. Update on endoscopic endonasal resection of skull base meningiomas. *International forum of allergy & rhinology*, 5(4):344–352, 2015.

[145] Paolo Cappabianca, Luigi Maria Cavallo, and Enrico De Divitiis. Endoscopic endonasal transsphenoidal surgery. *Neurosurgery*, 55(4):933–941, 2004.

[146] Emmanouil Dimitrakakis, George Dwyer, Nicola Newall, Danyal Z Khan, Hani J Marcus, and Danail Stoyanov. Handheld robotic system for endoscopic neurosurgery. *IEEE Robotics and Automation Letters (under review)*, 2023.

[147] Nicola Newall, Danyal Z Khan, John G Hanrahan, James Booker, Anouk Borg, Joseph Davids, Federico Nicolosi, Siddharth Sinha, Neil Dorward, and Hani J Marcus. High fidelity simulation of the endoscopic transsphenoidal approach: Validation of the upsurgeon tns box. *Frontiers in Surgery*, page 1945.

[148] Emmanouil Dimitrakakis, Joachim Starup-Hansen, Nicola Newall, Danyal Z Khan, George Dwyer, Danail Stoyanov, and Hani J Marcus. A handheld robotic device for endoscopic endonasal skull base surgery: An updated preclinical validation study (ideal-d stage 0). *Journal of Neurosurgery, (to be submitted)*, 2023.

[149] Jumpei Arata, Yosuke Fujisawa, Ryu Nakadate, Kazuo Kiguchi, Kanako Harada, Mamoru Mitsuishi, and Makoto Hashizume. Compliant four degree-of-freedom manipulator with locally deformable elastic elements for minimally invasive surgery.

In *2019 International Conference on Robotics and Automation (ICRA)*, pages 2663–2669. IEEE, 2019.

[150] James R Bekeny, Philip J Swaney, Robert J Webster III, Paul T Russell, and Kyle D Weaver. Forces applied at the skull base during transnasal endoscopic transsphenoidal pituitary tumor excision. *Journal of Neurological Surgery Part B: Skull Base*, 74(06):337–341, 2013.

[151] Alberto Ballestín, Gerardo Malzone, Giulio Menichini, Elena Lucattelli, and Marco Innocenti. New robotic system with wristed microinstruments allows precise reconstructive microsurgery: Preclinical study. *Annals of Surgical Oncology*, 29(12):7859–7867, 2022.